THE UNIVERSITY OF TURKISH AERONAUTICAL ASSOCIATION
INSTITUTE OF SCIENCE AND TECHNOLOGY

WIND ENERGY ASSESSMENT AT ELSPIAA TRIPOLI LIBYA – DESIGN AND PERFORMANCE OF HORIZONTAL AXIS WIND TURBINE USING BLADE ELEMENT MOMENTUM THEORY (BEMT)

Master Thesis

HAMZA ABO NAMA

Mechanical and Aeronautical Engineering Department

Master Thesis Program

November, 2017

THE UNIVERSITY OF TURKISH AERONAUTICAL ASSOCIATION
INSTITUTE OF SCIENCE AND TECHNOLOGY

WIND ENERGY ASSESSMENT AT ELSPIAA TRIPOLI LIBYA – DESIGN AND PERFORMANCE OF HORIZONTAL AXIS WIND TURBINE USING BLADE ELEMENT MOMENTUM THEORY (BEMT)

MASTER THESIS

Hamza Abo Nama

1606080011

Mechanical and Aeronautical Engineering Department

Master Thesis Program

Supervisor: Asst. Prof. Dr. Mohamed Salem Elmnefi

Hamza Abo Nama, having student number 1606080011and enrolled in the Master Program at the Institute of Science and Technology at the University of Turkish Aeronautical Association, after meeting all of the required conditions contained in the related regulations, has successfully accomplished, in front of the jury, the presentation of the thesis prepared with the title of : wind energy assessment at Elspiaa Tripoli Libya – design and performance of horizontal axis wind turbine using blade element momentum theory (BEMT)

Supervisor: Asst. Prof. Dr. **Mohamed Salem ELMNEFI**
The University of Turkish Aeronautical Association

Jury Members: Assoc. Prof. Dr. **Çetin ŞENTÜRK**
The University of Turkish Aeronautical Association

Asst. Prof. Dr. **Mohamed Salem ELMNEFI**
The University of Turkish Aeronautical Association

Asst. Prof. Dr. **Monier ELFARRA**
Ankara Yildirim Beyazit University

Thesis Defense Date: 23.11.2017

THE UNIVERSITY OF TURKISH AERONAUTICAL ASSOCIATION
INSTITUTE OF SCIENCE AND TECHNOLOGY

I hereby declare that all the information in this study I presented as my Master's Thesis, called "Wind Energy Assessment at Elspiaa Tripoli Libya – Design and Performance of Horizontal Axis Wind Turbine Using Blade Element Momentum Theory (BEMT)" has been presented in accordance with the academic rules and ethical conduct. I also declare and certify on my honor that I have fully cited and referenced all the sources I made use of in this present study.

Date 23/ 11/2017

Hamza Abo Nama

ACKNOWLEDGEMENTS

First of all, I am grateful to The Almighty Allah for helping me to complete this thesis.

I would like to express gratitude to my supervisor, Asst. Prof. Dr. Mohamed Salem Elmnefi, for his patience, encouragement, useful advice, discussion, comments and understanding my situation. He gave me opportunities to present my work in front of experts in the field.

I am forever profoundly indebted to my parents, for their supports, without their prayers the completion of this thesis would not have been possible.

Thanks to my sister, brothers, family and friends.

I would like to express my profound gratitude to my daughter Razan, to whom this work is dedicated, for every time she needed me but I wasn't there. For missing me throughout my study.

The most of all my sincere love and infinite appreciation goes to my wife, for being everything in my life, for his patience, supporting, invaluable assistance, for every time she listened to me when reviewing the thesis.

Hamza Abo Nama

CONTENTS

LIST OF TABLES

LIST OF FIGURES

ABBREVIATIONS

CF	Capacity Factor
WTG	Wind Turbine Generators
WPD	Wind Power Density
AMSL	Above Mean Sea Level
AGL	Above Grand Level
BEM	Blade Element Momentum Theory
HAWT	Horizontal Axis Wind Turbine
VAWT	Vertical Axis Wind Turbine
CFD	Computational Fluid Dynamics
NREL	National Renewable Energy Laboratory
UIUC	University Of Illinois Urbana-Champaign
LSWT	Large-Scale Wind Turbine
SSWT	Small-Scale Wind Turbine
Re	Reynolds Number
RPM	Revolution Per Minute
TSR	Tip-Speed Ratio

LIST OF SYMBOLS

A : Area of wind turbine rotor

A_s : Airflow cross sectional area

a : Axial induction factor at rotor plane

a' : Angular induction factor

a_1 : Corresponding axial induction factor at $\lambda_r = \lambda_h$

a_2 : Corresponding axial induction factor at $\lambda_r = \lambda$

B : Number of blade

C_D : Drag force coefficient of an airfoil

C_L : Lift force coefficient of an airfoil

$C_{L,design}$: Lift force coefficient of an airfoil

C_P : Power coefficient

C_{Pd} : Design power coefficient

$C_{P,max}$: Maximum rotor power coefficient

C_Q : Torque coefficient

C_T : Thrust coefficient

C_{Tr} : Local thrust coefficient for each annular rotor section

c : Chord length

$c(r)$: Local chord length

F_D : Drag force

F_L : Lift force

dF_T : Force on an annular element tangential to the circle swept by the rotor

dF_N : Force on an annular element tangential to the circle swept by the rotor

k : Weibull Shape parameter

F : Tip-loss correction factor

$\dot{m}$: Air mass flow rate through rotor plane

P : Power output from wind turbine

C : Weibull Scale parameter

P_d : Required power output (design power)

P_w : Available power

P_c : Cumulative Weibull function

Q : Rotor torque

p_d : Downwind pressure of rotor

p_0 : Pressure of undisturbed air

p_u : Upwind pressure of rotor

Δp : Pressure drop across rotor plane

R : Radius of wind turbine rotor

r : Local radius

r_h : Rotor radius at hub of the blade

T : Rotor thrust

U_d : Rated wind speed

U_{in} : Input velocity

U_{out} : Output velocity

U_m : Mean wind speed

U_R : Uniform wind velocity at rotor plane

U_r : Wind speed at reference height

U_{rel} : Relative wind velocity

U_w : Uniform wind velocity at far wake

$U(10)$: Wind speed at 10 m height above ground level

U_∞ : Free stream velocity of wind

WPD : Wind power density

w : Angular wind velocity at rotor plane

Z : Height above ground level

Z_0 : Roughness length

Z_r : Reference height

GREEK SYMBOLS

α	: Angle of attack
α_{design}	: Design angle of attack
η_g	: Generator efficiency
η_t	: Gear-train efficiency
θ_P	: Section pitch angle
$\theta_{P,0}$	: Blade pitch angle at the tip
θ_T	: Blade twist angle
$\theta_P(r)$	: Local section pitch angle
$\theta_T(r)$	: Local blade twist angle
λ	: Tip-speed ratio
λ_d	: Design tip-speed ratio
λ_h	: Local tip-speed ratio at the hub
λ_r	: Local tip-speed ratio
ν	: Kinematic viscosity of air
ρ	: Air density
σ	: Solidity
φ	: Angle of relative wind velocity with rotor plane
φ_{opt}	: Optimum relative wind angle
$\varphi_{opt}(r)$	: Local optimum relative wind angle
Ω	: Angular velocity of wind turbine rotor
ω	: Rotational speed.
β	: Twist angle.

ABSTRACT

WIND ENERGY ASSESSMENT AT ELSPIAA TRIPOLI LIBYA – DESIGN AND PERFORMANCE OF HORIZONTAL AXIS WIND TURBINE USING BLADE ELEMENT MOMENTUM THEORY (BEMT)

Abo Nama, Hamza

Master, Department of Mechanical and Aeronautical Engineering

Thesis Supervisor: Asst. Prof. Dr. Mohamed Salem Elmnefi

November – 2017, 121 pages

Estimation of wind characteristics is considered as the first essential step to evaluate a wind energy project based on information about all aspects of the implementation and operation of the project. It's therefore necessary to have detailed knowledge of the wind to design a suitable wind turbine for a certain zone, also to estimate its performance accurately. The first step in this thesis is study the wind energy and wind assessment in the selected site (Elspiaa, Tripoli _Libya) based on the available wind data, which are obtained from the representative meteorological station. It is found that, the maximum wind speed was U =11.97 m/s for data of year 2014 at height of 40m, which has the maximum probability (10. 25%).The wind power density, E, (W/m²) was expressed in terms of the Weibull shape and scale parameters, (k and c). It is found that , the yearly wind power density of year 2013 at both heights of 10 and 40 m are (651.02 W/m²) and (814.61W/m²) respectively. And the yearly wind power density for year 2014 at 10 and 40 m are (715.85W/m²) and (980.41 W/m²) respectively. The second step in this thesis is to design a suitable horizontal axis wind turbine. Design (HAWT) to achieve satisfactory levels of performance starts with knowledge of the aerodynamic forces acting on the blades. The blade element momentum theory (BEM) is applied for HAWT blade design to predict the performance of the rotor. A computer program (FORTRAN and MATLAB cod) for HAWT blade design and its performance analysis is belt. The input of this program was the power required from a turbine, number of blades, design wind velocity, design tip-speed ratio and properties of the selected airfoil,

while the outputs are the blade geometry parameters (chord and twist distribution), power, torque and thrust coefficients versus tip-speed ratios. As a result of that, it is possible for the designed wind turbine to extract the power from the wind with satisfactory levels of performance in the selected site. The modified twist effects on power coefficient, while the optimum chord linearized twist angle reduced the power output by approximately 8.3 % compared with the power output of the optimum blade. Moreover, the effect of tip losses factor reduced power output approximately 2.23 % the power output in the case of optimum blade.

Keywords: (BEM) theory, wind energy assessment, Rotor design.

ÖZET

ELSPIAA TRIPOLI LIBYA'DAKİ RÜZGAR ENERJİ DEĞERLENDİRMESİ - BLADE ELEMENT MOMENTÜS TEORİSİNİ (BEMT) KULLANARAK YÜKSEK AKSAM RÜZGAR TÜRBİNİNİN TASARIMI VE PERFORMANSI

Abo Nama, Hamza

Yüksek lisans, Makine ve Uçak Mühendisliği Bölümü

Tez Danışmanı, Yardımcı Doç. Dr. Mohamed Salem ELMNEFI

Kasım - 2017, 121 sayfa

Rüzgar özelliklerinin tahmini, bir rüzgar enerjisi projesinin değerlendirilmesi için projenin uygulanması ve işletilmesi ile ilgili tüm hususlara dayalı ilk adım olarak kabul edilir. Bu nedenle, belirli bir bölge için uygun bir rüzgar türbini tasarlamak ve performansını doğru bir şekilde tahmin etmek için rüzgar hakkında ayrıntılı bilgi sahibi olmak gereklidir. Bu tezin ilk adımı, temsili meteoroloji istasyonundan elde edilen rüzgar verilerine dayanarak seçilen yerde (El-Spiaa, Tripoli _Libya) rüzgar enerjisi ve rüzgar değerlendirmesinin incelenmesi. Maksimum rüzgar hızı, 2014 yılının 40m yüksekliğindeki maksimum olasılık (% 10. 25) verileri için U = 11.97 m / dk, Rüzgar gücü yoğunluğu E, (vat /mertekare), Weibull şekil ve skala parametreleri, (k ve c). 2013 yılının yıllık rüzgar enerjisi yoğunluğunun sırasıyla 10 ve 40 m yüksekliklerde (651.02 W / m²) ve (814.61W / m²) olduğu tespit edilmiştir. 2014 yılı için 10 ve 40 m'de yıllık rüzgar enerjisi yoğunluğu sırasıyla (715.85W / m²) ve (980.41 W / m²) 'dir. Bu tezin ikinci basamağı, uygun bir yatay eksen rüzgar türbini tasarlamaktır. Tatmin edici düzeyde performans elde etmek için Tasarım (HAWT), kanatlara etki eden aerodinamik kuvvetlerin bilgisi ile başlar. Bıçak elemanı momentum teorisi (BEM), HAWT bıçak tasarımı için ve rotorun performansını öngörmek için uygulanır. HAWT bıçak tasarımı ve performans analizi için bir bilgisayar programı (FORTRAN ve MATLAB cod) kemerlidir. Bu programın girdileri türbinlerden gelen güç, bıçak sayısı, tasarım rüzgar hızı, tasarım ucu-hız oranı ve seçilen kanadın özellikleri. Çıktılar: bıçak geometri parametreleri (akor ve büküm dağılımı), güç, tork ve itme katsayıları ile ucu-hız oranları. Bunun bir sonucu olarak, rüzgar türbini, seçilen yerde tatmin edici düzeyde performans ile

rüzgardan çekilmek üzere tasarlanabilir. Modifiye bükülme açısı güç katsayısı üzerine etki ederken, optimum kord lineerleştirilmiş büküm açısı optimum bıçağın güç çıkışı ile karşılaştırıldığında güç çıktısını yaklaşık% 8 oranında düşürdü. Üstelik, uç kayıp faktörünün etkisi, optimum bıçak durumunda güç çıkışını yaklaşık% 2.23 güç çıkışını azalttı.

Anahtar Kelimeler: (BEM) teorisi, rüzgar enerjisi değerlendirmesi, rotor tasarımı.

Chapter One

INTRODUCTION TO WIND TURBINE APPLICATION

1.1. Background and Historical Review of Wind Energy

There are many factors that are driving the development and use of renewable energy technologies. Starting from the global warming, scarcity in energy, increase in fossil fuel costs, and ending by the ecological balance of the earth. However, the main reason behind this movement is the increasing use of fossil fuels. Therefore, the nations of the world have signed a mutual agreement in order to reduce emissions under the Kyoto protocol prepared by the UN Framework Convention on Climate Change (UNFCCC) [1].

Furthermore, there is consensus on the time wind energy got invented or used for the first time. While a group of scientists claims its origin is Egyptian around 3000 years ago, another group of scientists believe that the first windmill was built in the 7^{th} century in Afghanistan [2] [3]. As decrypted in travelers' notes in the 10^{th} century, the windmill consisted of a vertical axis rotation, which was used to mill grains, presented below in the Fig. 1.1.

Fig. 1.1 Afghanistan windmill, the old vertical axis [3]

Furthermore, the usage of wind energy was an ancient idea by using it for several other applications. From using it as a thrusting power for boats and ships by the Egyptians since the 5th millennium BC to pulling water from wills in China since the 2nd century BC. In addition to that, several applications for wind energy were in use in the Middle East region, including using a vertical axis windmills for grinding purposes. During the crusade campaigns on the region, the Europeans brought the technology back to their homelands and developed it. The first application for electricity generation was known in America in the 19th century, which was used in local scales for houses and factories, while the use of windmills was reduced due to its replacement by the steam engine.

Fig. 1.2 A windmill for water pumping with steel-bladed [4]

In the 3rd decade of the 20th century, the American government worked to bring electric power to all the regions of the country. Due to the increasing demand, the engineers developed the windmill to what became known as the wind turbine. The wind turbine earliest conception was established in Denmark about same time period, by building the largest unit known as Grandpa's Knob, with a rating of 1.25 MW at 48 Km per hour. This first unit was used to substitute the reduction in Electric power production from fossil fuels during the World War II.

The concept of wind energy from wind turbines was not always a hot topic since then, especially when fossil fuels became more competitive and available after the war. Nevertheless, the increase in oil prices in the 70s drove that interest back for economic reasons, which eventually increased the research and development efforts

resulting into the introduction of more efficient wind turbines. Since that time, many wind power generation plants and farms have been constructed and connected the power grids in the Western world.

Nowadays, the many research and development efforts that were invested over the years have brought wind energy to an efficiency point that competes with the conventional methods of generating electricity, making wind energy the most developed and grown renewable energy source [5].

1.2. Types of Wind Turbines

The wind turbine application is to converting the wind energy of kinetic to electrical power by transporting the wind through the turbine turning its blades, which result into an initial mechanical torque, which then turns into the electric power. The lifting force of the wind drives the blades, which turns the rotor of the turbine. The wind turbine type mostly influenced by the axis positioning. Therefore, the wind turbines types can be divided to [6]:

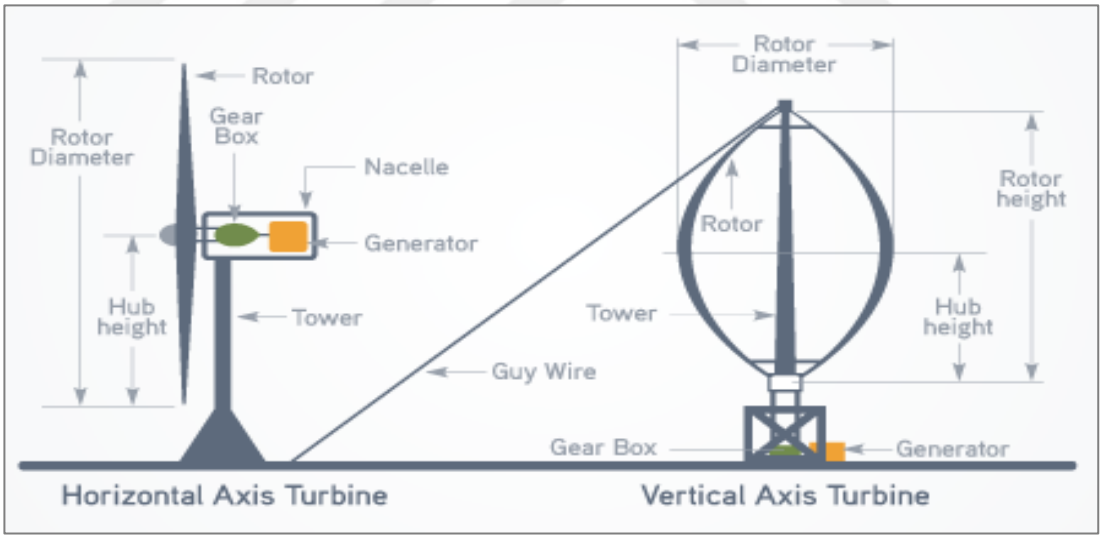

Fig. 1.3 The types of wind turbine systems; HAWT and VAWT systems [7]

1.2.1. Vertical wind turbines

The vertical-axis wind turbine rotor shaft is installed vertically eliminating the need to orient it towards the effective wind direction, especially in areas where wind direction is constantly changing. Moreover, this assembly allows for the generator and the gearbox placement on the ground level, easing the maintenance operations and lowering the bearing load on the tower. Nonetheless, the disadvantages of such an assembly is the generated drag and pulsating torque during the rotation of the blade [7]. Types of the VAWT are illustrated in Fig. 1.4.

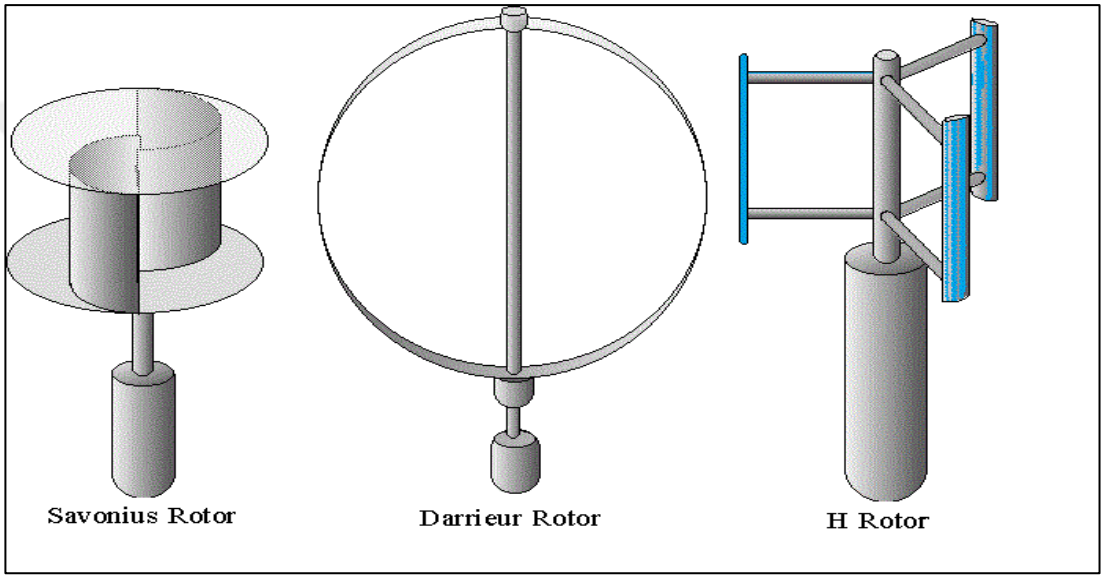

Fig. 1.4 Vertical Axis wind turbines types [8]

1.2.2. Horizontal Axis Wind Turbines

The horizontal axis wind turbine concept is similar to the conventional windmill, in terms of the blades and shaft direction. Contrary to the VAWT, the rotor and the generator are placed at the tower in top to be in the wind direction. Directing the component to the wind direction according to the turbine size is performed through a wind vane or wind sensor and a motor.

Additionally, the wind turbine gearbox works to accelerate the rotational movement of the rotor generating a higher rotational speed to cope up with the electric generator. Due to the turbulence behind the tower, this factor can be eliminated through directing the turbine to the upwind. The blades have to be made of rigid

material to sustain its place and prevent its collision with the tower during the rotations, placing them at a sufficient distance depending on their maximum flexibility calculations.

However, downwind turbines are still used as they do not require a wind alignment mechanism and regardless of the created turbulence. Moreover, this assembly allows the blades to bend reducing the swept area and resistance to wind at high wind speeds. The disadvantages of this downwind assembly results into the use of upwind in HAWT in most of the case due to the reliability factor [7].

Nonetheless, the use of a yaw system, which direct the turbine towards the wind, is an old, developed and common system. In small HAWTs, a passive yaw system can put between the nacelle and the tower a roller bearing. At the back of the finned tail the nacelle generates a moment that keeps the rotor in the same direction of the wind. In larger HAWTs, an active yaw system consisting of a wind sensor and a motor generates the needed torque to rotate the tower. Thus, this study is mainly focused on the HAWT type of wind turbines, which is further elaborated in the next sections and chapters.

1.2.2.1. Upwind and Downwind Turbine

At the upwind assembly, the rotor faces the wind, resulting into the wind going through the rotor first, while the downwind assembly have the rotor at the protected part of the tower, making the wind face the nacelle first. Both assemblies are presented in Fig. 1.5.

a. Upwind Turbines

Turbine wind outlines have the benefit of maintaining a strategic distance from the wind drapery behind the tower. Most by far of wind turbines have this plan. Then again, there is likewise some shade of wind before the tower, i.e. the wind starts to tilt far from the tower before it achieves the tower, regardless of the possibility that the tower is smooth and round. In this way, every time the rotor goes through the tower, the energy of wind turbines diminishes a little. The fundamental burden of outlines against the wind is that the rotor must be set some separation from the tower.

What's more, the machine against the wind needs a Yao instrument to keep the rotor confronting the wind. [9].

b. Downwind Turbines

They have the hypothetical favorable position that they might be worked without a yaw instrument, if the rotor and nacelle have a reasonable plan that influences the nacelle to take after the wind inactively. For extensive wind turbines this is a fairly uncertain advantage, since for ideal vitality effectiveness of wind vitality converters, the yaw power must be connected precisely. Another favorable position of the downwind plan is that the rotor might be made more adaptable. This is favorable position both with respect to weight and the basic elements of the machine, i.e. the edges will twist at high wind speeds, therefore remove a portion of the heap off the tower. The fundamental disadvantage is the change in the wind power because of the rotor going through the wind shade of the tower. This may give more exhaustion stacks on the turbine than with an upwind outline. [9]

Beside the two choices, machines of upwind are all the more usually utilized because of an expanded vitality yield and thus their being more practical.

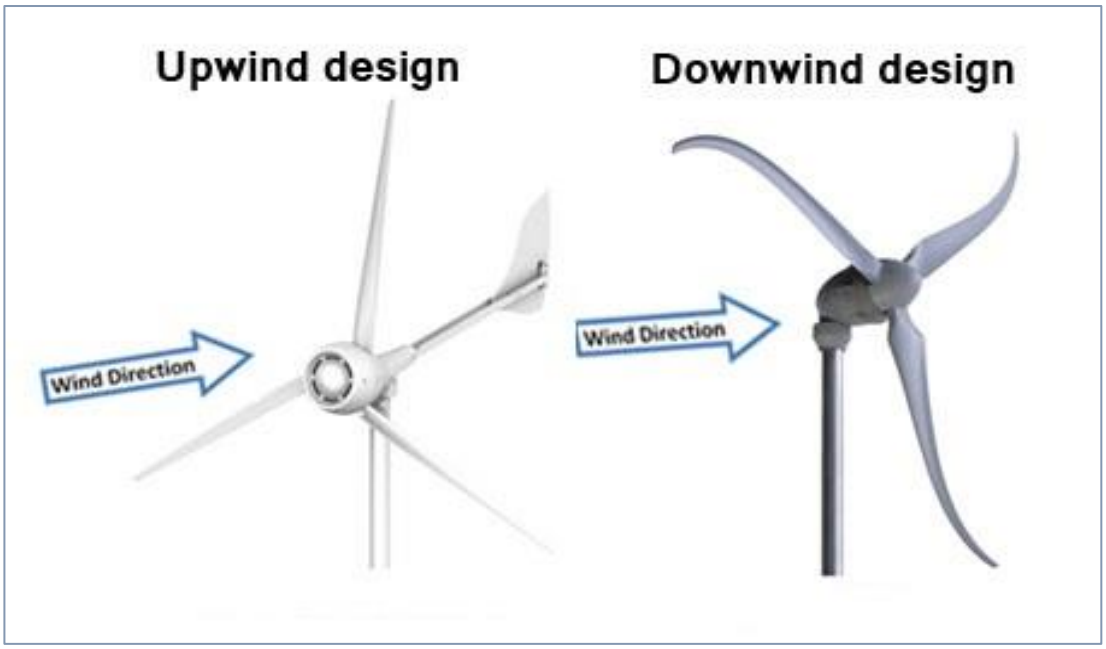

Fig. 1.5 The design of rotor of horizontal axis wind turbines [8]

1.3. Components of Horizontal Axis Wind Turbine

1.3.1. Tower and Foundation

This piece of the gathering incorporates the tower itself and the establishment of support. The important part of tower design right now being used are the free standing. Types utilizing steel tubes, cross section towers, and towers of concrete. For small turbines, towers of guyed are additionally utilized. Tower tallness is ordinarily 1 to 1.5 times the rotor measurement, however regardless is typically no less than 20 m. The establishments are necessary for helping the wind turbine different parts and tower which ponders in tones. Tower choice is enormously impacted for site potentials. Tower firmness is main consideration in framework flow of wind turbine on account of the likelihood of combined vibration flanked by the tower and rotor. Tower are underpinning at top of the rotor center and nacelle point. This is produced using steel tubular, cement, or grid. Height of the tower is important in design of HWAT. Since speed of wind increments and tallness, towers which is taller empower turbine to catch extra vitality with produce greater power. For the most part, yield energy of the wind framework increment with increment in tallness and furthermore lessens the wind turbulence. The tower stature hypothetical perspective vs power-out is appeared as Fig. 1.6 [9].

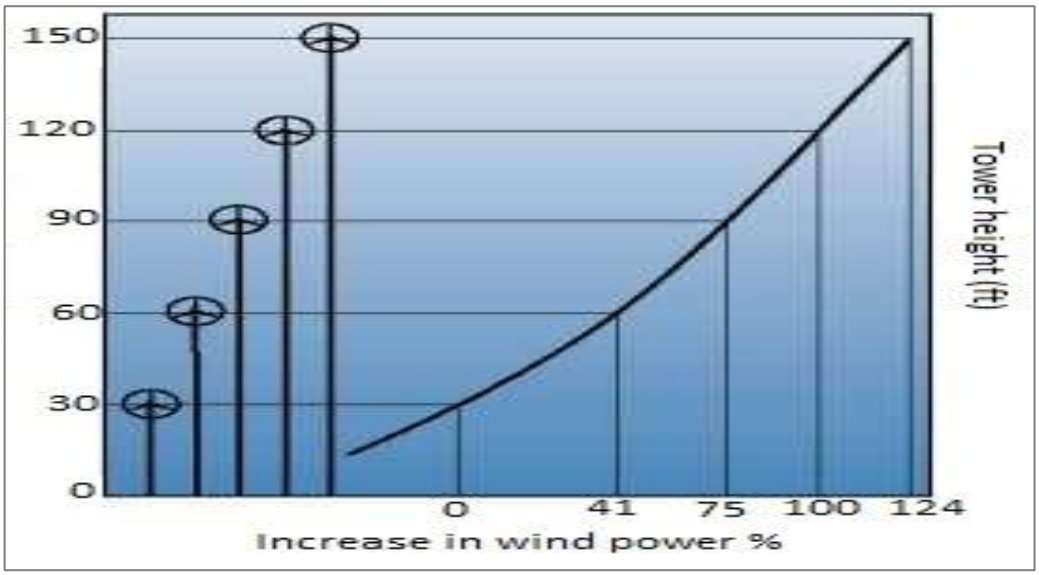

Fig. 1.6 Tower height Vs Power output [10]

1.3.2. Blades

Wind turbine blades are used to eliminate wind energy and switch to mechanical energy. These sheets are made of polyester reinforced with fiberglass or epoxy wood. Wind turbine has maybe a three or different blade construct with respect to development. The greater part of the HAWT have three blades. These are associated with rotor center point. Various cutting angle idea is utilized as a part of prior days for pumping water and pounding. Reduction the changes of the wind turbines. Some wind turbine with small size that create only a few watt energy though 5MW tremendous wind turbines are introduced moreover. In Fig. 1.7 examination of energy creation and measurements of wind turbines are characterized [9]. Today, wind turbine rotor breadth measurements are contrasted and biggest aircraft spans.

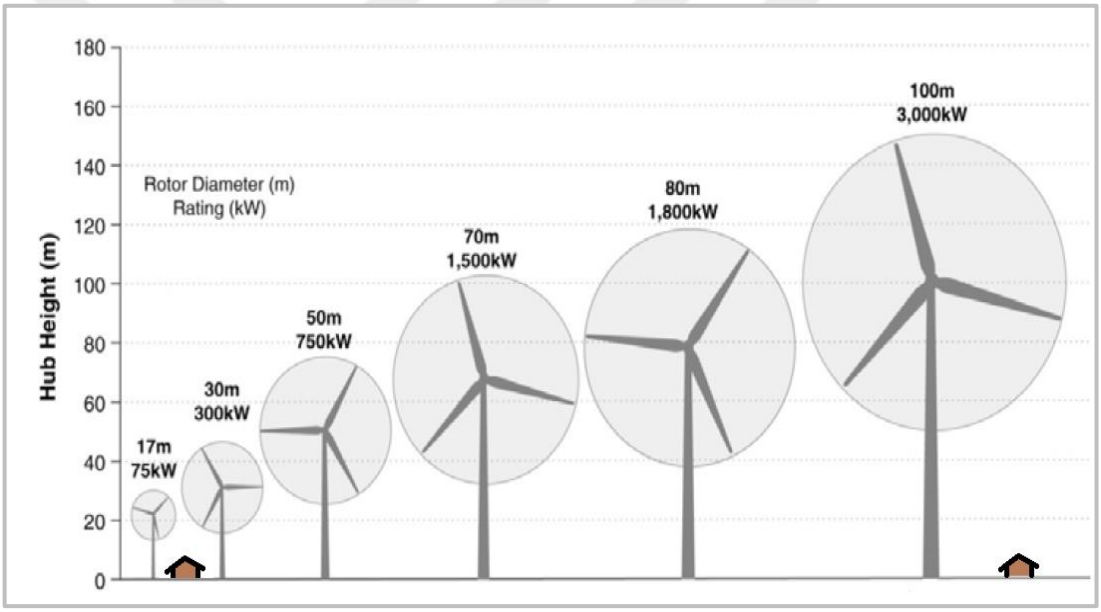

Fig. 1.7 Size of wind turbines and power production comparison [11]

1.3.3. Nacelle

A housing which contains all the components is essential to operate the turbine efficiently. It is installed on the top of the tower and includes gearbox, low and high speed axles, brakes, generator control. The wind is related to wind speed and winds wind to nacelle.

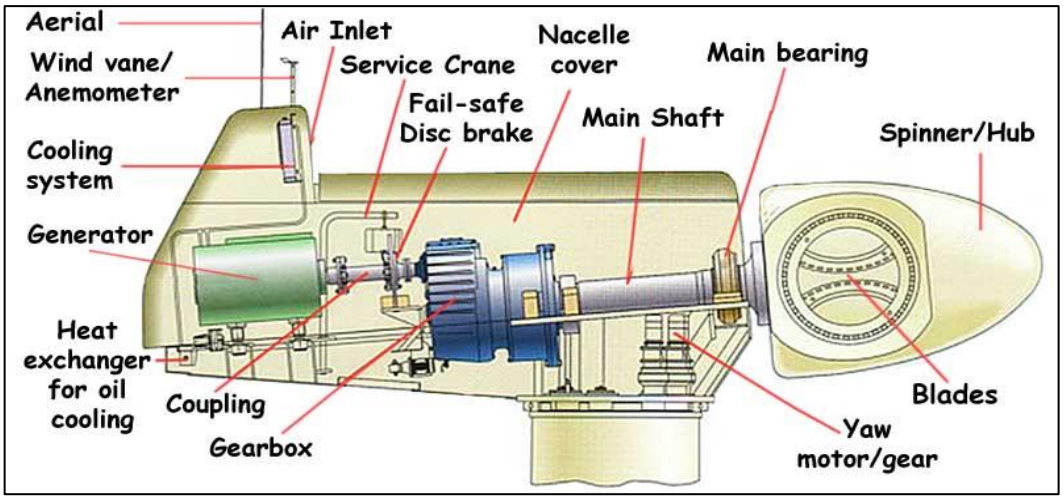

Fig. 1.8 Structure of Internal nacelle [12]

1.3.3.1. Hub

The central point of the rotor is absorbed by coupling the rotor blade of the wind turbine and the shaft. The center of the meeting consists of hub, bearings of blade, bolts, internals and pitch system. The hub of the rotor is made of welded steel plate, casting press and steel fabricated. There are two of hub. Center axis and stumbling.

1.3.3.2. Drive shaft

This shaft part is reinforced by blank or strong steel under large loads and wide torque. Transport shafts are used to exchange the mechanical energy of the rotation center of the sharpening blade of the generator to generate power. Wind turbines usually consist of two axes.

1.3.3.3. Main shaft

This part is introduced to interface the blade hub and contribution to the gearbox, turning at low speed; low speeds shafts.

1.3.3.4. Generator shaft

Connect the gearbox output to the generator input. It spins at a very high speed equal to generator rating. It is also called "high-speed shaft.

It associates the gearbox yield to the input of generator. It turns at rapid equivalents to the generator rating. It is likewise called 'rapid shaft.

Fig. 1.9 Horizontal Axis wind turbine shaft system [8]

1.3.4. Gear box

The gearbox used as part of the wind power structures to change power under a high speed connection stems from a rotor blade to a force that uses a low torque fast for the generator. This is connected to the center of the primary shaft and the shaft generator to increase the rotational speeds from about 30 to 60 turns per minute (rpm) at about 1000 to 1800 rpm. The gearbox used for wind turbines is produced using predominant fittings of quality aluminum, stainless steel, and molding press.

The various gear boxes used in wind turbines are:

1. Worm Gearbox.
2. Helical Gearbox.
3. Planetary Gearbox

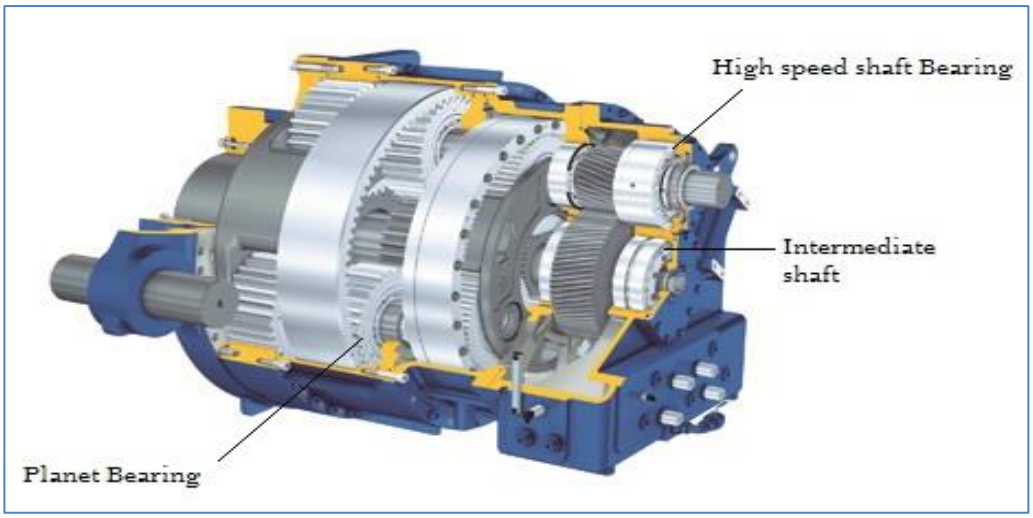

Fig. 1.10 Gearbox of Horizontal Axis wind turbine [8]

1.3.5. Generator

The output rotational mechanical energy of the gear box is connected to the generator through generator shaft. It works on the principle of "Faraday's law of electromagnetic induction." It converts mechanical energy into electrical energy.

1.3.6. Yaw Mechanism

The yaw system converts the rotor in the wind against bearing as the wind turns. Electric motors and gearboxes are used to keep turbines against the wind. This control system can also be used in mid-high wind speed.

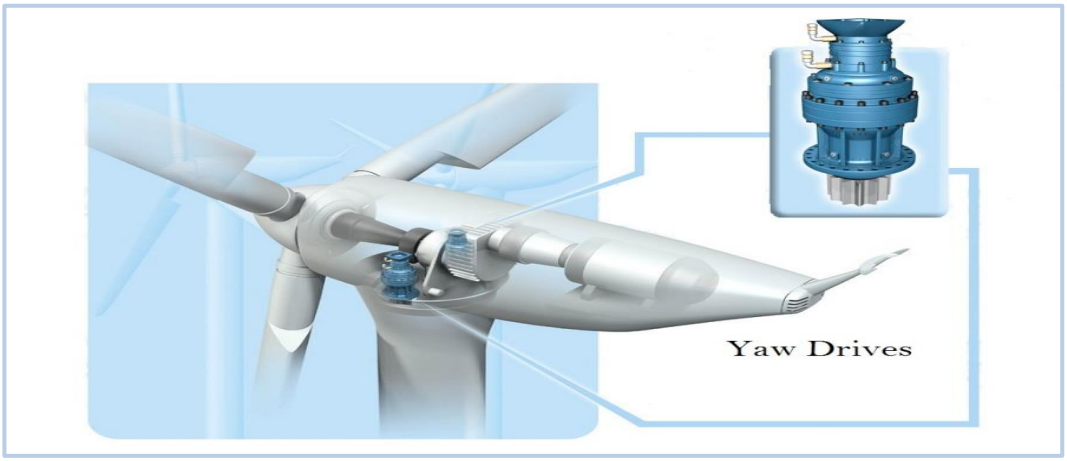

Fig. 1.11 Yaw Drives system [8]

1.4. Advantages of Horizontal Axis Wind Turbine

1. Variable blade pitch, which gives the turbine blades the ideal approach. Enabling the approach to be remotely balanced gives more noteworthy power, so the turbine gathers the most extreme measure of wind energy for the season of day and season.

2. The tall tower base enables access to more grounded wind in destinations with wind shear. In some wind shear destinations, each ten meters up, the wind speed can increment by 20% and the power yield by 34%.

3. High effectiveness, since the blades dependably move oppositely to the wind, accepting force through the entire pivot. Interestingly, all vertical pivot wind turbines, and most proposed airborne wind turbine designs, include different types of responding activities, requiring airfoil surfaces to backtrack against the wind for part of the cycle. Backtracking against the wind prompts inalienably bring down effectiveness.

1.5. Literature Review

Creating wind energy have been produced quickly finished the years because of its significance as a perfect energy source. In this way, many models have been made for its advancement, including the Blade Element Moment (BEM), which is known as an acknowledged technique in designing and examining the wind turbines.

1.5.1. Aerodynamic design of (HAWT) and optimization using BEM Theory and Genetic algorithm

An aerodynamic design and optimization process for of horizontal Axis Wind Turbines is progressing by using both of Genetic Algorithm and Theory of BEM (Blade Element Momentum). Turbines blade is advanced to outrageous generation to give speed of wind, a speed of rotational, blade range and various blades. The streamlining factor is use like a settled syllabic harmony lengths num22ber, contort points and airfoil profiles beside the traverse blade. Profiles of airfoil its streamlined information took from database airfoil of the drag coefficient and trial lift

information that is reachable. Blade Element Momentum examination device created is first approved with the test information for little wind speeds rate. A wind turbine, is then modified. The aftereffect of this enhancement, are the power creation is enhanced between 38 and 79 percentages. Enhancement procedures are next by designing 24m span and wind turbine of 1MW [13].

1.5.2. Small-scale Wind Energy Portable Turbine (SWEPT)

LSWTs (wind turbine with Large-scale) are widely inquired about for a considerable length of time, however there have been not very many investigations on small scale wind turbines (SSWTs) particularly for adjoining ground level applications where Wind is on the request of a couple of meters for every second. This examination gives the principal efficient thrust to the SSWTs improvement and design (the measurement of rotor <49 cm) proposed to work at blurring speed of wind (<4 m/s). We propose a converse design and streamlining device in light of the Momentum Theory of blade element. The utility and adequacy of the device was exhibited by the showing of a versatile wind turbine on a small scale 40 cm in distance across (SWEPT), which approved inside a speed scope of low wind of 1 m/s, 5 m/s with a greatly high power factor. Contrasted with the distributed writing, SWEPT is one of the small scale which are the most proficient and low wind speed with a 32% power factor and an aggregate effectiveness of 21% with an ostensible wind speed of four wind power plants. With short cutting pace of 1.6m/s. Burrow of Wind tests demonstrated the SWEPT has an ostensible yield 0.9W - 3.9m/s, equipped for delivering reach to 9.2W of energy at10 m/s speed of wind and it went to build up a wind speed piezoelectric footing of 1.9m/s. The wind piezo worldwide measurement of 105*77*60mm is fit for producing electrical energy pinnacle of around 450 microwaves at ostensible wind speed of 1.9 m/s. [14].

1.5.3. Computer-aided aerodynamic design of small scale horizontal axis wind turbine blades

In this study, aerodynamic design of 1, 5, 10, 25, 50, 100, 250 and 500 kW horizontal axis wind turbine generators have been performed. The design procedure starts with

the design and analysis of airfoils done by programs of PROFOIL and XFOIL, respectively through which the structural, aerodynamic and aeroacoustics principles have been taken into consideration. Then, the performance parameters of designed profiles were inputted to the constructed modified blade element momentum theory (BEM) code together with the main design parameters in order to obtain 3D blade geometry. The code is validated using MIE wind turbine with a rated power of 8 kW. The generated blade geometries are then analyzed using commercial computational fluid dynamics CFD code Numerical FINE™/Turbo and the velocity and pressure distributions around the blade have been visualized, separately. Moreover, the power coefficient Cp was calculated and the power curves of the designed wind turbine rotors were drawn [15].

1.6. Objectives and Scope of the Study

The Horizontal axis wind turbine is the dominant design principle in wind energy technology today due to many advantages compared with the other types of wind turbines. For example, the HAWT has no self-starting problem, also the rotor speed and the power output can be controlled by pitching the rotor blades. Moreover, the blade shape can be aerodynamically optimized to reach the maximum efficacy. Together, these advantages are the reason of why the HAWT is selected to be the subject of this study. The study will include the aerodynamic design and performance analysis of the HAWT using modified BEM theory and the correction factors as (Prandtl Tip Loss Corrections and Glauert corrections). In the following sections, the main objectives of this Thesis are:

1. The first stage in this thesis is to estimate the wind energy and wind assessment at El-Spiaa, Tripoli _Libya station based on the available wind data which obtained from the Center for new and renewable energies, and calculate the wind power density at both heights of 10 and 40m
2. The second stage will include the implementation modified BEM analysis with different existing correction factor as Prandtl Tip Loss, Glauert and Buhl Empirical, using iterative solution procedure with NACA 63(4)221 airfoil data. Then, validation the results it will be compared with experimental case which is (NLSE) Risoe wind turbine, because, they have the same airfoil

type. Also, for Additional procedure, the results will be compare with (NREL) Phase II, VI wind tunnel tested data.

3. The third stage in this dissertation, is to use BEM theory to design the rotor blade and to predict its aerodynamic performance. Also, design a suitable horizontal axis wind turbine based on the wind data available. Furthermore, few parameters influences relating to design of blade as effect of modified blade geometry, solidity, Tip-Losses and effect of pitch angle and chord length on wind rotor performance.

1.7. Organization of the Thesis

Chapter 1: This chapter is introducing background and historical review of wind energy, Types of wind Turbines, Components and Advantages of horizontal axis wind turbine, then presenting the summary of previous studies and finally its organization.

Chapter 2: Display the characteristics of the wind, wind Data Analysis, calculation of Weibull frequency using graphical method, Study Area and calculation of mean wind speed, Weibull probability and cumulative distribution. Finally, calculation the power density of El-Spiaa, Tripoli _Libya station.

Chapter 3: Express the aerodynamics of horizontal-axis Wind Turbines, Actuator disc model and rotating annular stream Tube Analysis, blade element momentum (BEM) theory analysis and prandtl tip loss correction factor and study flow states of horizontal Axis Wind Turbine.

Chapter 4: Showing the modified of (BEM) Analysis Tool, Airfoil families and experimental wind Turbine database, Aerodynamic analysis of NACA 63(4)221 airfoil using FLRX5 software and for validation the results of modified (BEM) will be compare with (experimental case which are Risoe wind Turbine). Additional procedure, the results will be also compare with (NREL) Phase II, VI wind tunnel tested data.

Chapter 5: A brief descriptions of rotor design and performance analysis, then Airfoil Terminology and Airfoil Classification and finally, blade design procedure (Input design data, rotor size and blade geometry).

Chapter 6: This chapter present the results and discussions of blade performance, and then display the few parameters influences relating to design of blade.

Chapter 7: Conclusion of the thesis, and highlighting for the future work.

Chapter Two

WIND ENERGY ASSESSMENT

2.1. Introduction

A legitimate examination of factual wind information is a vital advance when playing out a wind asset evaluation battle which bolsters a wind energy possibility activity. It's in this way important to have nitty gritty wind data to choose wind turbine appropriate for specific sector and furthermore for assessing the execution precisely. The WTG (wind turbine generators) execution on an especially place could be dictated to the site's likelihood wind speeds dispersion and relating wind turbine generators power bend. Therefore, since the wind turbine generators power bend is identified, likelihood wind speeds appropriation is the key data expected for wind energy evaluating yield at a chosen site for model of specific wind turbine generators. [16].

2.2. Characteristics of the Wind

Accessible wind energy are relative to solid shape of speed of wind $(p \ \alpha \ U_{\infty}^{3})$, and henceforth, it is accordingly important to have detail information of the wind and its trademark to evaluate execution of any wind turbine precisely. Different parameters should be known about the wind, including the mean wind speed, directional information, varieties about the mean for the time being (blasts), day by day, occasional and yearly varieties and variety with tallness. These parameters are profoundly site particular and must be resolved with adequate precision by estimations at specific site over an adequate long stretch. They are utilized to survey the execution and financial aspects of a wind plant. In this investigation we concentrate on gathering, assessment and examination of current information [17].

2.2.1. Variation in time

The wind speed varieties in time could be isolated to accompanying classifications [17]:

- **Inter-annual variations**

This type of varieties in wind speed happens after some time scale more noteworthy than one year. The capacity to evaluate between yearly at a chosen site are as critical to assessing the wind haul mean at sit.

- **Seasonal and monthly variation**

The level of occasional variety in the wind at a given site relies upon scope and position regarding particular topographic highlights, for example, arrive masses and water. By and large, mid-scope mainland areas are presented to high winds in winter and spring, mountain goes in beach front regions encounter solid winds in summer.

- **Diurnal variation**

This type of wind speed variety is because of respectful warming of the world's surface amid the day by day variety cycle. A run of the mill diurnal variety is an expansion wind speed amid the day, and is an abatement wind speed amid the time from midnight to dawn [17].

- **Short-term variations**

Here and now varieties normally mean varieties after some time interims of ten minutes or less. The wind speed is continually fluctuating, and in this manner the energy substance of the wind is continually evolving. Here and now wind speed varieties of intrigue incorporate turbulence and blasts. Turbulence can be thought of as irregular wind speed variances forced on the mean wind speed. These vacillations happen in every one of the three headings (longitudinal, horizontal and vertical) while a blast is a discrete occasion inside a turbulent wind field [17].

2.3. Wind Data Collection

In this venture, the wind speed information at once at regular intervals as an arrangement design for Elspiaa station has been measurably investigated. The wind speed information in time arrangement organize is typically masterminded in the recurrence conveyance design since it is more advantageous for factual investigation. The accessible time arrangement information was converted into recurrence conveyance design. The wind speed has been measured at stature of 10 m over the ground level utilizing 3 glass anemometers. Moreover, wind speed has been extracted to height of 40 at Elspiaa station.

2.4. Wind Data Analysis

The examination of wind information incorporates learning of wind bearing and wind speed information to assess wind power creation specifically site. Long haul wind information from the meteorological stations close to the applicant site can be utilized for making the estimation. This information which might be accessible for long stretches ought to be extrapolated to speak to the wind profile at the potential site.

2.4.1. Wind speed variation with height

Wind speed close to the ground changes with stature, at tallness around 2km over the ground the adjustment in the wind speed ends up plainly zero. The most widely recognized articulations for the variety of wind speed with hub stature depend on tests are given beneath.

- **Power law function**

$$U(z) = U(z_r)\left(\frac{Z}{Z_r}\right)^{\alpha} \quad (2.1)$$

Where $U(z)$ the wind speed at height (Z), $U(z_r)$ is the reference wind speed at Height Z_r, and α is the power law exponent which depends on the roughness of the terrain.

- **Logarithmic function (log law)**

$$U(z)/U(10) = \ln(\frac{Z}{z_0}) \div \ln(\frac{10}{z_0}) \quad (2.2)$$

Where U (10) is the wind speed at 10m above the ground level, and Z_0 is the roughness length. The parameters α and z_0 for different types of terrain are presented in table (2.1).

Table 2.1 wind speed parameters for calculating a vertical profile [18]

Type of terrain	**Roughness class**	**Roughness length z_0 (m)**	**Exponent α**
Water areas	0	0.001	0.01
Open country, few surface features	1	0.12	0.12
Farmland with buildings and hedges	2	0.05	0.16
Farmland with many trees, forests, villages	3	0.3	0.28

Both functions can be used for calculation of the mean wind velocity at certain height, if the mean wind velocity is known at the reference height. In this thesis, we use the second term which are open country, few surface features. Because, the site terrain requires that.

2.4.2. Weibull distribution

Wind speed dissemination can normally be depicted as far as the Weibull appropriation. The Weibull likelihood thickness work requires learning of two parameters a shape parameter K and scale parameter C. Together this parameter is capacity of normal mean wind speed U_m. The likelihood thickness capacity of Weibull appropriation is given by [1].

$$p(U) = \left(\frac{k}{C}\right)\left(\frac{U}{C}\right)^{k-1} \exp\left[-\left(\frac{U}{C}\right)^{k}\right] \tag{2.3}$$

Where $P(U)$ is the possibility of wind speed observing U, c is the parameter of the wobbler scale (m /s), and k is the parameter of the shape and urination (no dimensions), the parameter of the Weibull model, k, generally, varies from 1.5 to 3 for most wind conditions. [16].The Weibull function is commonly used because it gives a good fit to the observed wind speed data at the surface and the upper air [18].

The cumulative frequency distribution represents an essential part of the possibility density function Weibull, given by Eq. (2.4) [16].

$$P_C(U) = 1 - \exp\left[-\left(\frac{U}{C}\right)^{k}\right] \tag{2.4}$$

The probability of wind speeds between U_1 and U_2 is given by;

$$P_p(U_1 < U < U_2) = \exp\left[-\left(\frac{U_1}{C}\right)^{k}\right] - \exp\left[-\left(\frac{U_2}{C}\right)^{k}\right] \tag{2.5}$$

Numerical techniques were utilized to evaluate Weibull adoption parameters, for example, drawing strategy, most likely technique, energy design factor technology, moment technology, experimental technique, etc. [19]. In this test, the Weibull support parameters were resolved utilizing drawing technique.

2.4.3. Estimated of Weibull parameters by using graphical method

In the Method of Graphical, the distribution of cumulative purpose is converted to linear form, Eq. (2.4) can be [16]:

$$\ln[-\ln\ p\ (U)] = k\ \ln U - k\ \ln\ C \tag{2.6}$$

To find the parameters of the scale and shape of the wolves, a graphical method is displayed and used when planning or against $\ln[-\ln\ p\ (U)]$ where a straight line is obtained, as shown in Figs. 2.5 and 2.6, and the model parameter will be k [16]. And c is equal to $\exp \ln U$, where $\ln[-\ln\ p\ (U)]$ is zero.

2.4.4. Mean wind speed

The mean wind speed values and their standard deviations are calculated using the following Equations:

$$U_m = \frac{1}{M}\sum_{j=1}^{M} U_j \tag{2.7}$$

Where M is the sample size, U_j is the wind speed recorded for j^{th} observation.

2.4.5. Wind power density

Wind power density is a mount of wind power accessible per unit zone opposite to the wind stream. The Eq. for wind power density is essentially the accessible wind power isolated by the range.

$$P_w = \frac{1}{2}\rho U_\infty^3 A_s \tag{2.8}$$

$$WPD = \frac{1}{2}\rho . U_\infty^3 \tag{2.9}$$

Additionally, wind power density can be communicated regarding the Weibull shape and scale parameters, k and c, utilizing the relationship displayed by Eq. (2.10);

$$E = \frac{1}{2}\rho c^3\left(1+\frac{3}{k}\right) \tag{2.10}$$

2.5. Operational Characteristics

2.5.1. Power performance

The power curve of sample wind turbine is a chart that demonstrates how large the electrical power yield will be for wind turbine at various wind speeds. With such a curve the specialized points of interest of its different parts. The power curve gives the electrical power yield as an element of the hub stature wind speed [20]. The power curves are gotten from field tests utilizing government sanctioned testing techniques, it is additionally conceivable to appraise the power curve for a given machine by theoretical calculations. Fig. (2.1) shows a case of a power curve for run of the sample wind turbine, it is demonstrating the accompanying parameter.

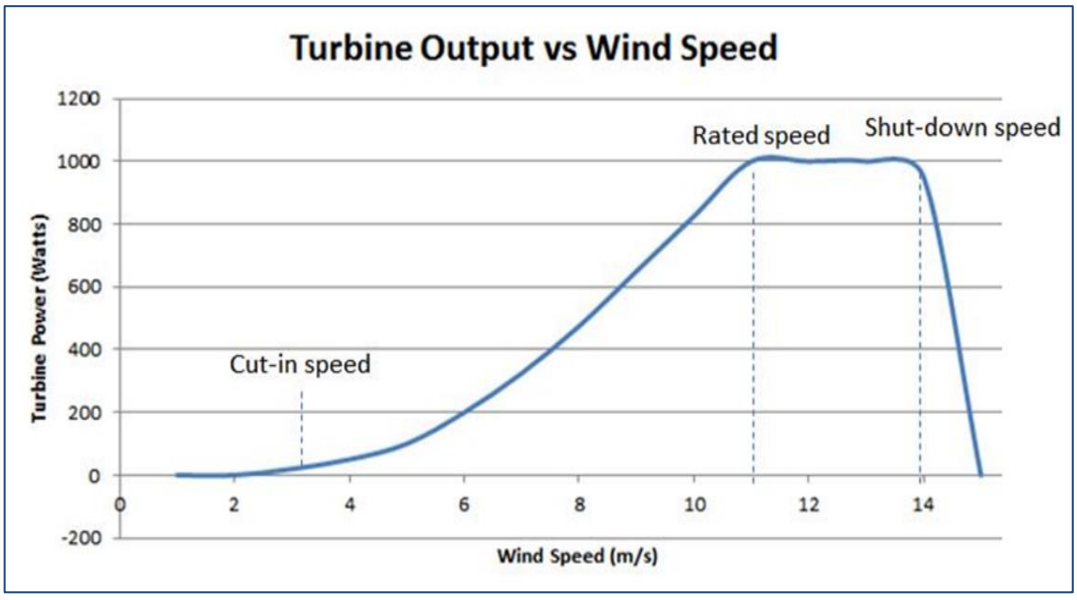

Fig. 2.1 The power output curve of a sample wind turbine [21]

- Cut in wind speed: This is the wind speed at which the wind turbine will begin creating power—ordinary cut-in wind speeds are 3 to 5 m/s.

- Cut out wind speed: This is the most minimal speed at which the wind turbine achieves its ostensible power yield. Over this speed, higher power yields are conceivable, however the rotor is controlled to keep up a consistent energy to restrain loads and weights on the blades.
- Cut-out wind speed: This is the most elevated wind speed which the turbine will work at. Over this speed, the turbine is ceased to avert harm to the blades. [22].

2.6. Study Area

The achievability of wind energy improvement relies upon the specific social, financial, and physical attributes of both investigation range and the wind asset. In this postulation one site is chosen, as case to demonstrate wind energy accessibility in shoreline of Libya and to design a reasonable by considering normal wind speed of ElSpiaa, Tripoli _Libya station, the areas of this site is introduced in Fig. (2.2).

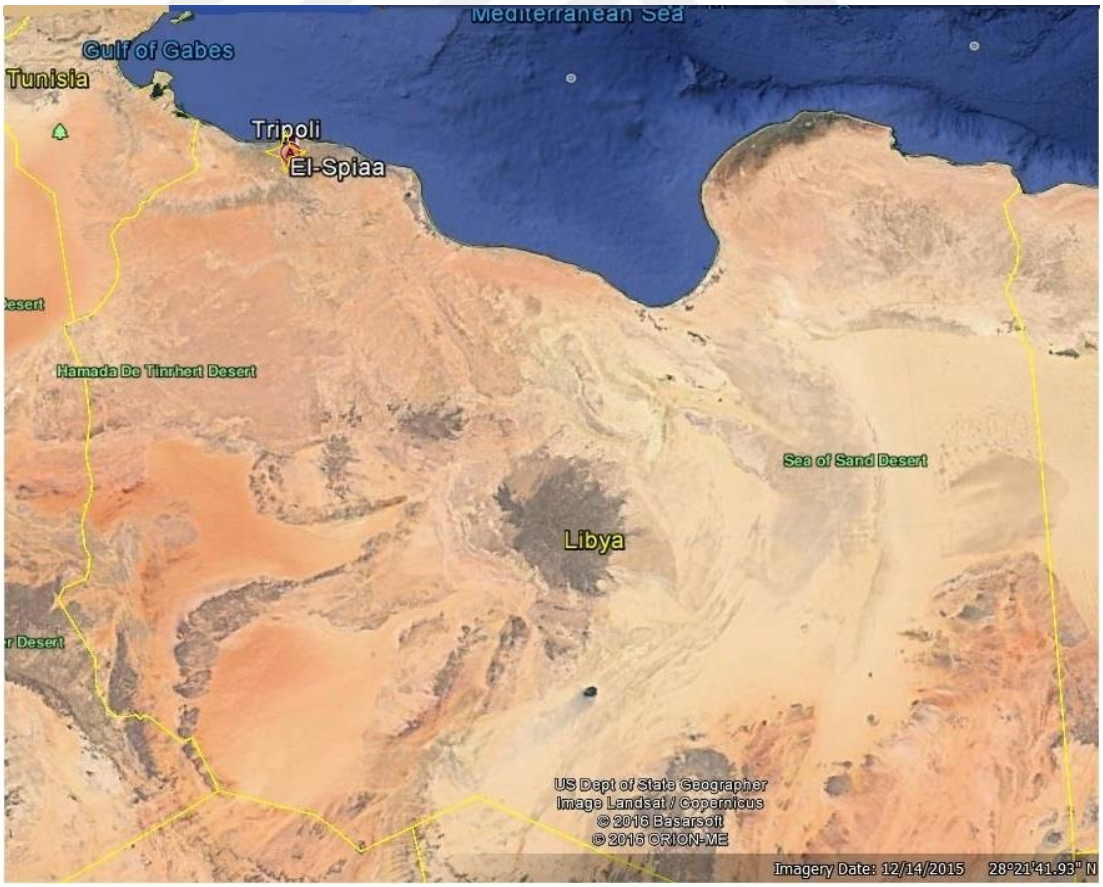

Fig. 2.2 Distribution of meteorological stations over Libya [23]

The Statistics of wind data obtained from measurements for two years (24-month) period. From January 2013 to December 2014.Furthermore, it is including daily wind speeds. Elspiaa has very important station which is located in North-west Libya, South of Tripoli about 30 km, the wind farm located one 25 kilometers away from the coast. The site coordinates are 32°32'24.66 (N°) and 13°10'13.31 Longitude (E°). The elevation of the site is 15 m above mean sea level (AMSL). The statistical wind data set was analyzed using Weibull distributions in order to investigate the Weibull shape and scale parameters. The location of the wind farm will be selected on the top of a plateau with a height around 50-100 m above mean sea level (AMSL), with a cliff terrain facing sea.

2.7. Analysis of Wind Data

2.7.1. Mean wind speed calculation

The wind speed has been measured at stature of 10 m over the ground level utilizing 3 container anemometers. Moreover, wind speed has been assessed at stature of 40 m by utilizing the most well-known articulations for the variety of wind speed which in light of Eq. (2.1). The mean wind speed rate at 10 and 40meters' tallness are ascertained for long stretch of year 2013 and 2014 at the chose station. It is normal that wind speed at ordinary turbine hub tallness of 10 meters or more would not higher distinction. The month to month normal wind speeds are calculated based on daily wind data for ElSpiaa, Tripoli _Libya station which measured by the station and acquired from the Center for new and sustainable power sources as exhibited in Table (2.2) and (2.3). The mean speed rate is displayed in Fig. (2.3) and (2.4) for the two statures.

Table 2.2 Mean monthly wind speed (m/s) for year 2013 at height of 10 and 40m

YEAR	JAN	FEB	MAR	APR	MAY	JUN	JUL	AUG	SEP	OCT	NOV	DEC
2013 At 10m	7.65	6.53	6.70	7.22	7.45	6.30	5.50	7.10	5.12	7.82	6.60	6.97
2013 At 40m	9.32	7.96	8.16	8.80	9.08	7.67	6.70	8.65	6.24	9.53	8.04	8.49

Table 2.3 Mean monthly wind speed (m/s) for year 2014 at height of 10 and 40m

YEAR	JAN	FEB	MAR	APR	MAY	JUN	JUL	AUG	SEP	OCT	NOV	DEC
2014 At 10m	5.93	7.12	6.23	6.68	8.10	7.15	6.34	5.75	6.27	5.97	7.70	5.39
2014 At 40m	7.22	8.67	7.59	8.14	9.87	8.71	7.72	7.00	7.64	7.27	9.38	6.57

Fig. (2.3) shows the monthly variation of the average wind speed for long period of year 2013 at height of 10 and 40m, the minimum value of average wind speed is in the SEP_2013 for both of the heights, and the maximum value is in the MAY_2014 for both of the heights.

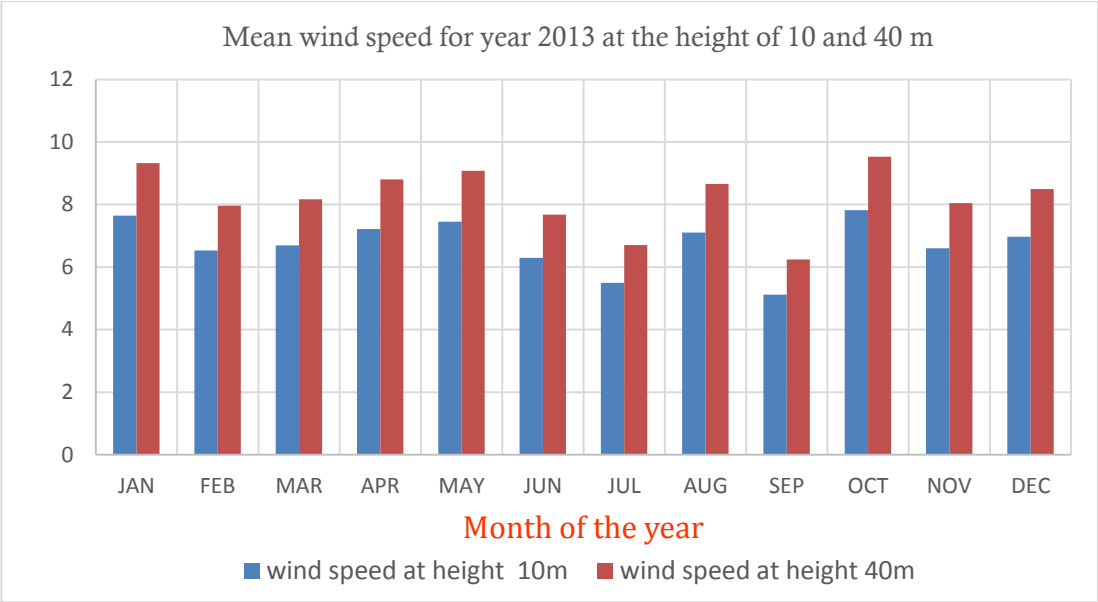

Fig. 2.3 Mean wind speed values for ElSpiaa, Tripoli – Libya

Fig (2.4) shows the monthly variation of the average wind speed for long period of year 2014 at height of 10 and 40m. The minimum value of average wind speed is in the DEC_2014 for both of the heights, and the maximum value is in the MAY_2014 for both of the heights.

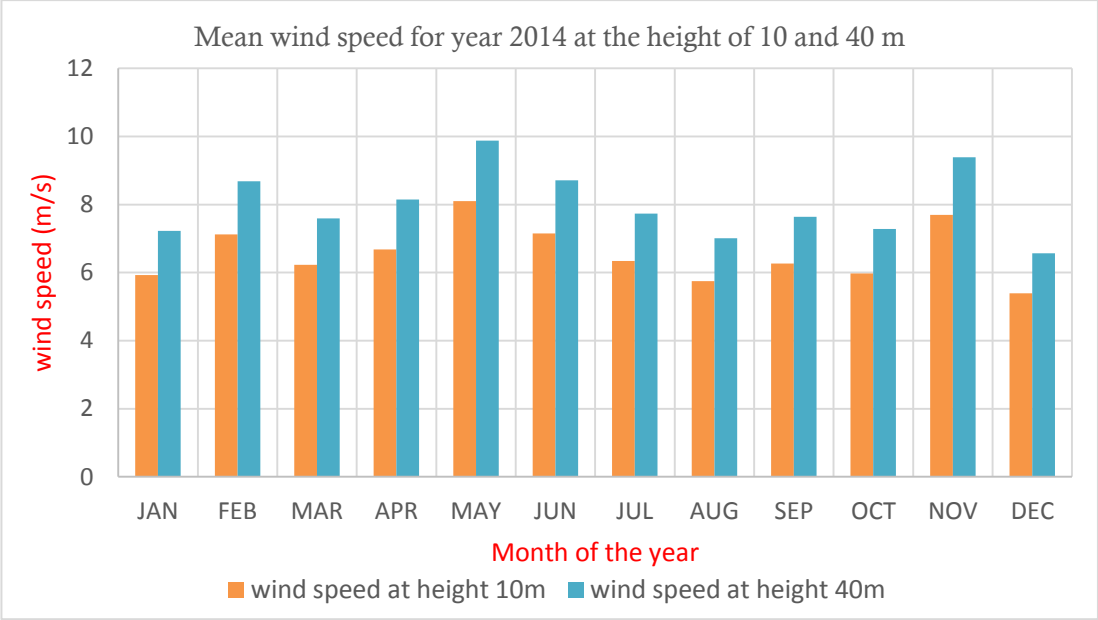

Fig. 2.4 Monthly variation of the average wind speed ElSpiaa, Tripoli – Libya

2.7.2. Calculation of Weibull frequency

There are a few works that arrangement with the utilization of likelihood thickness capacities to portray wind speed recurrence circulation. By and large, the Weibull likelihood thickness capacity can be utilized to gauge a site's likelihood appropriation of wind speeds. The dispersion system is widely known and used as part of the breeze industry as a preferred way to represent wind speed configurations at a given location; some claim that Weibull has extended as the best option for photographing configurations of wind speed at a given location. [16]. Be that as it may, a few scientists report that for destinations having low mean wind speeds, the Weibull dispersion does not speak to well the site's wind speed conveyance [16]. Aside from the Weibull appropriation, there are a few dispersions, for example, Gaussian disseminations, exponential circulations, gamma conveyances and coordination conveyances that can be utilized to demonstrate a site's wind speed variety [16]. To assurance of Weibull recurrence dispersion and Weibull aggregate conveyance required to decide first the scale parameter (c) and the shape parameter (k). The two parameters (c) and (k) the site information are ascertained by utilizing the realistic strategy as outlined in segment (2.7.3). The recurrence dispersion of wind speed at a site is given in Appendix A (Table A.1). At that point the total dispersion of the information is created in light of the given frequencies. Each class spoke to by its furthest breaking point as exhibited in Appendix A (Table A.2). By plotting (ln U) in the X pivot and (ln [-ln P (U)]) in the Y hub. Additionally, Table A-3 introduced the assurance of Weibull parameters for year 2013 and 2014 at 10m. The subsequent diagram for year of 2013 at tallness of 10 and 40m are introduced in Fig. (2.5) and (2.6). The subsequent chart for year of 2014 at stature of 10 and 40m are introduced in Fig. (2.7) and (2.8). The focuses are somewhat scattered. Fit a line through the focuses and find the best fit Eq.

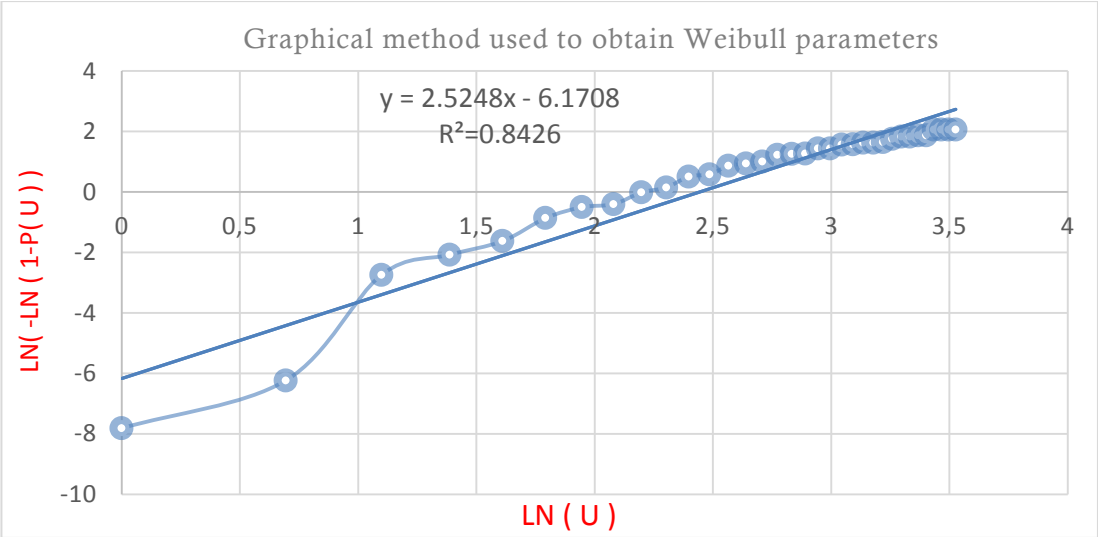

Fig. 2.5 Obtained of Weibull parameters (k) and (c), for year of 2013 at height of 10m

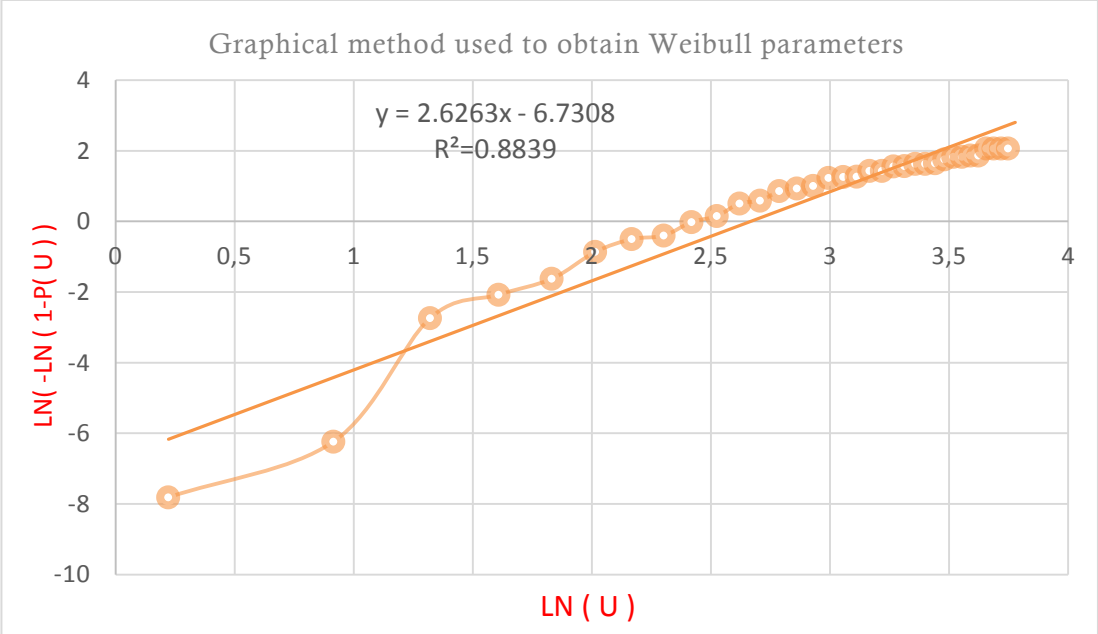

Fig. 2.6 Obtained of Weibull parameters (k) and (c), for year of 2013 at height of 40m

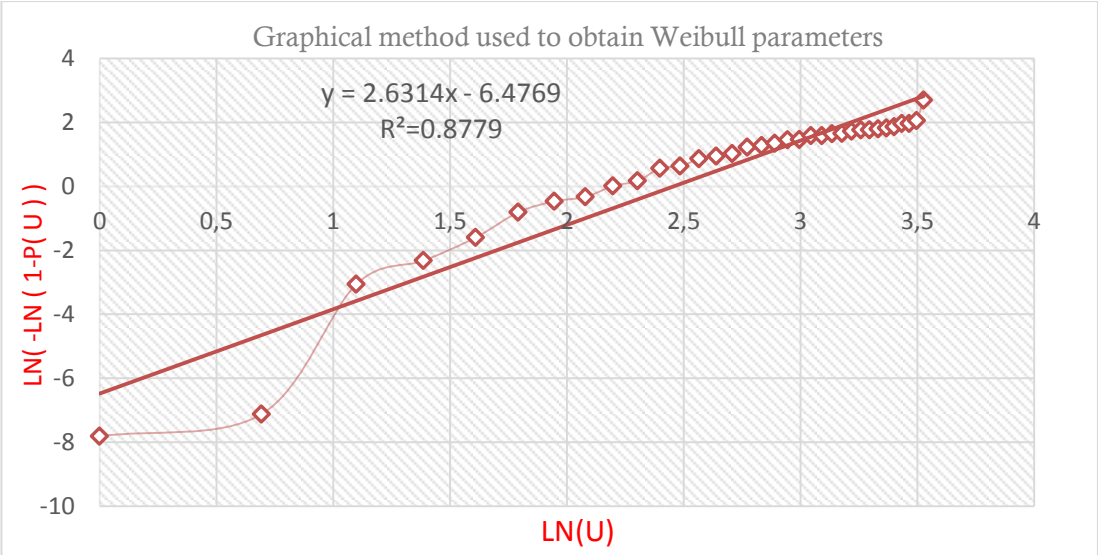

Fig. 2.7 Obtained of Weibull parameters (k) and (c), for year of 2014 at height of 10m

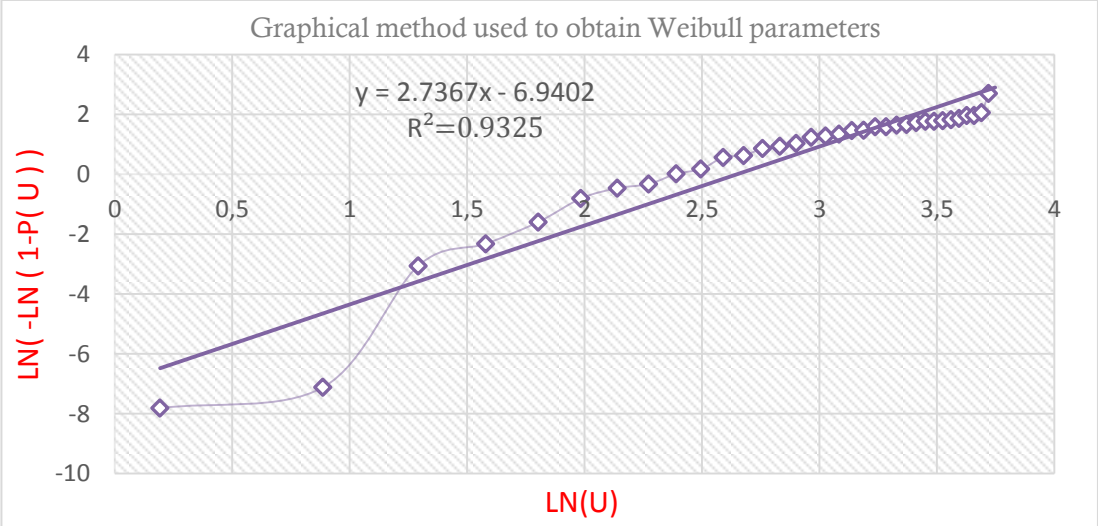

Fig. 2.8 Obtained of Weibull parameters (k) and (c), for year of 2014 at height of 40m

In addition to that, fig. (2.9) (2.10) shows the histogram of the wind velocity for year 2013 and 2014 respectively at height of 10 and 40m of the station. From these Figures it is clear that the wind speed U=11.97 m/s has the maximum probability (10.25%) for data of year 2014 at 40m. Moreover, fig. (2.11) shows the cumulative frequency distribution for year 2013 and 2014 respectively at height of 10m for the station.

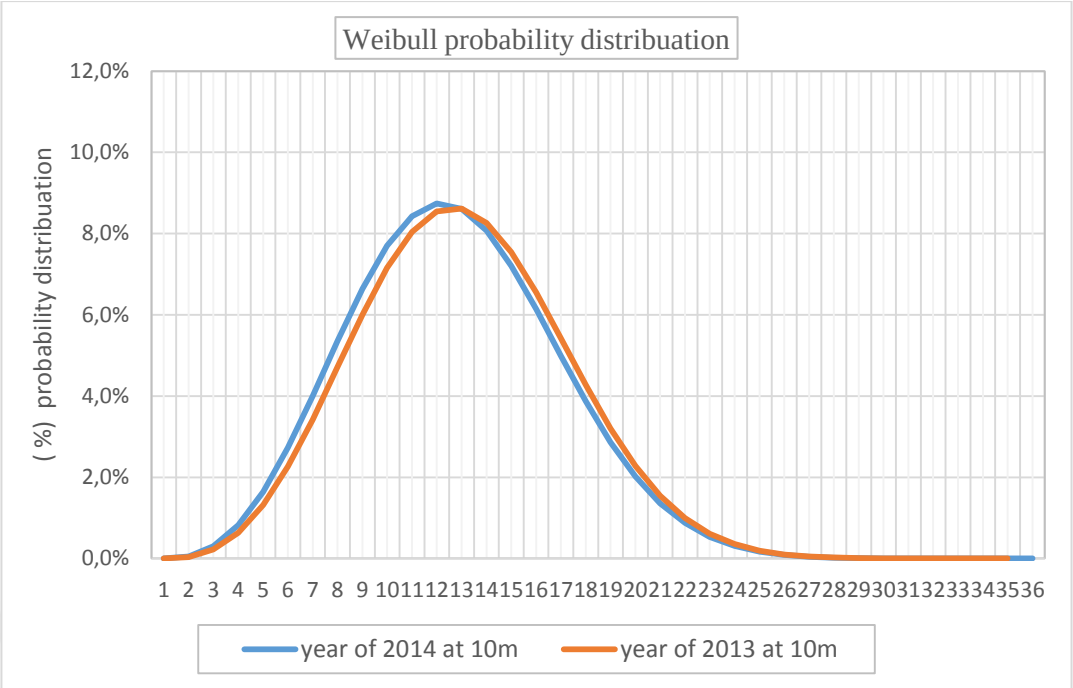

Fig. 2.9 Yearly Weibull distribution for ElSpiaa, Tripoli – Libya

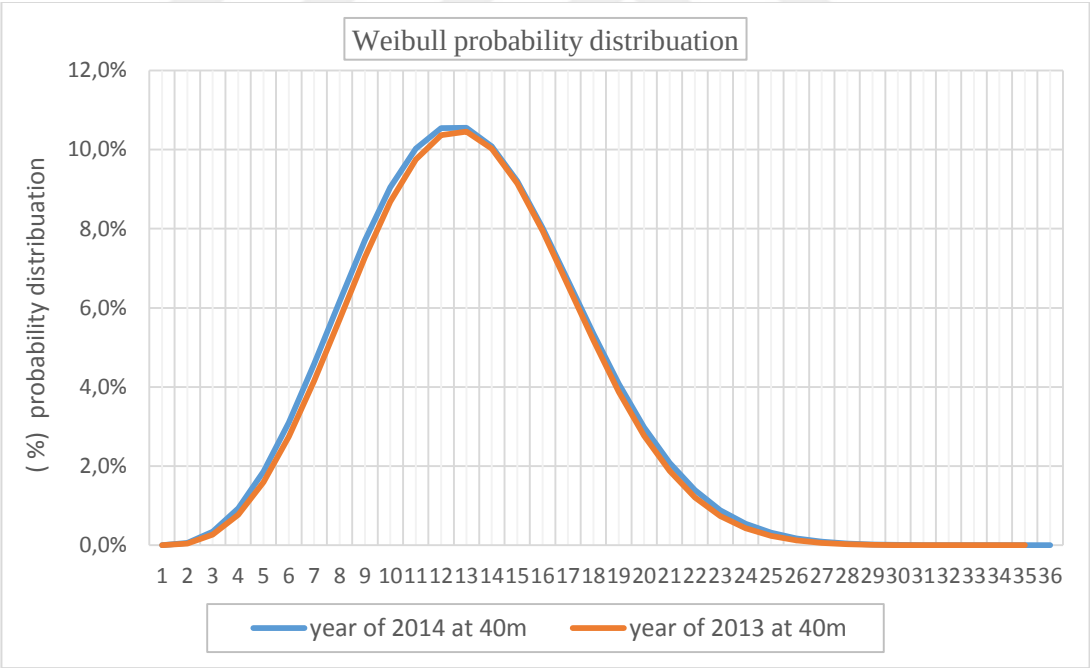

Fig. 2.10 Yearly Weibull distribution for ElSpiaa, Tripoli – Libya

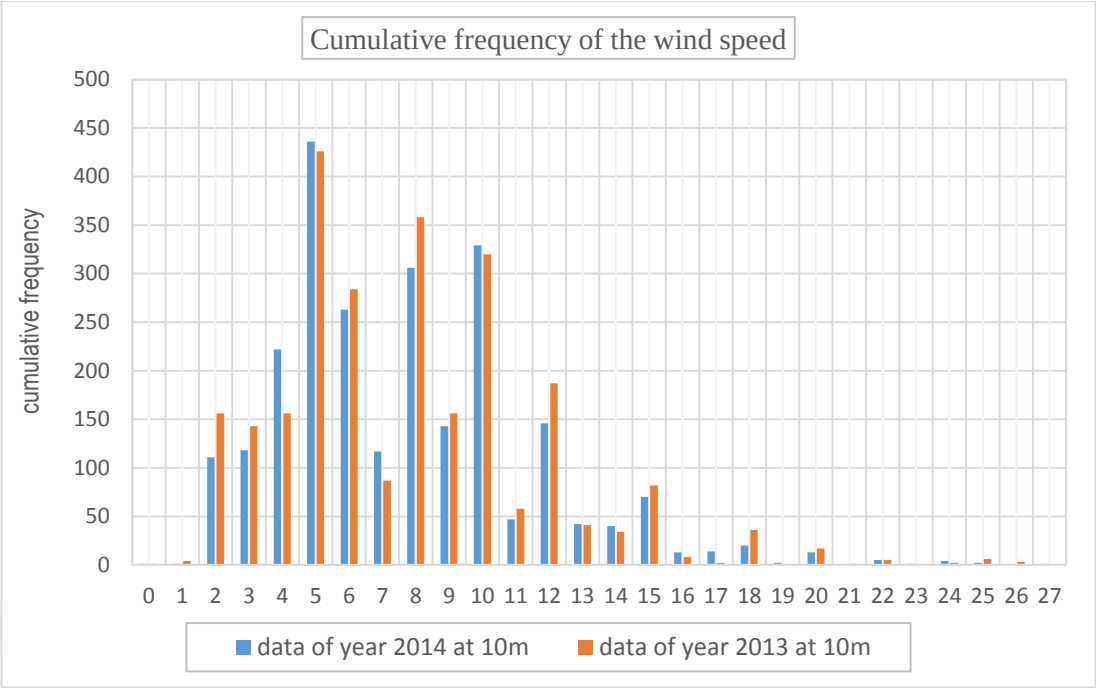

Fig. 2.11 Yearly cumulative frequency of wind speed for ElSpiaa, Tripoli – Libya

Beside, Fig. (2.12), (2.13), (2.14) and Fig. (2.15) shows the Weibull cumulative distribution for year 2013 and 2014 respectively at height of 10 and 40m, which gives the probability of the wind speeds exceeding the value of any given wind speed U.

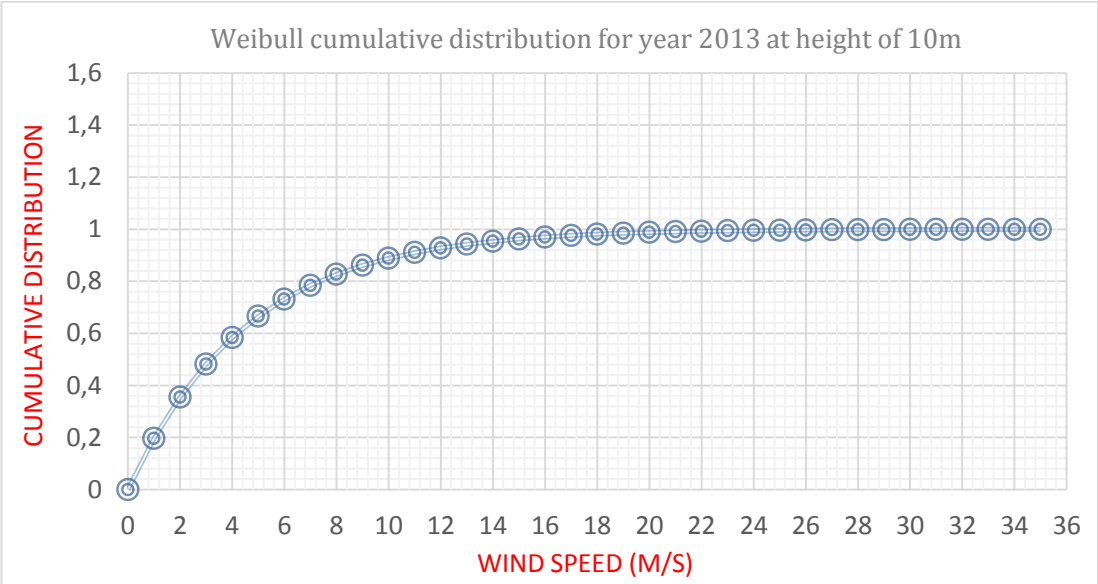

Fig. 2.12 Cumulative probability of year 2013 at height 10m (AGL)

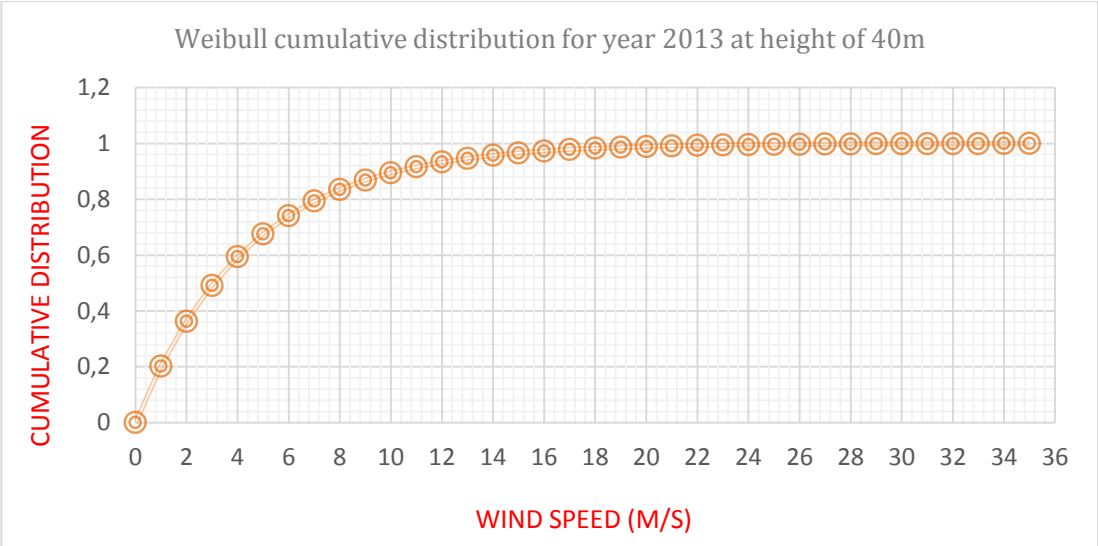

Fig. 2.13 Cumulative probability of year 2013 at height 40m (AGL)

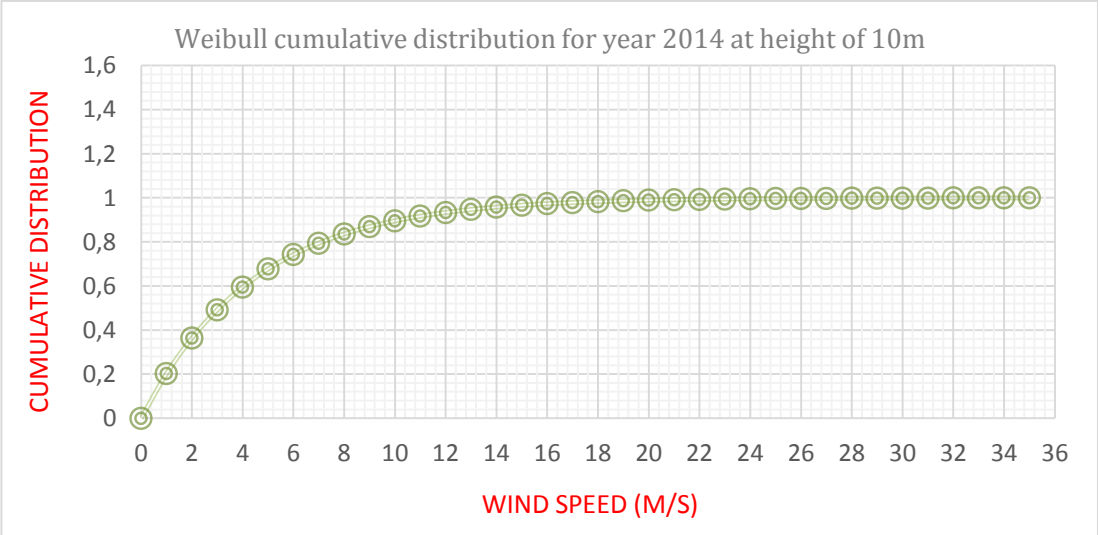

Fig. 2.14 Cumulative probability of year 2014 at height 10m (AGL)

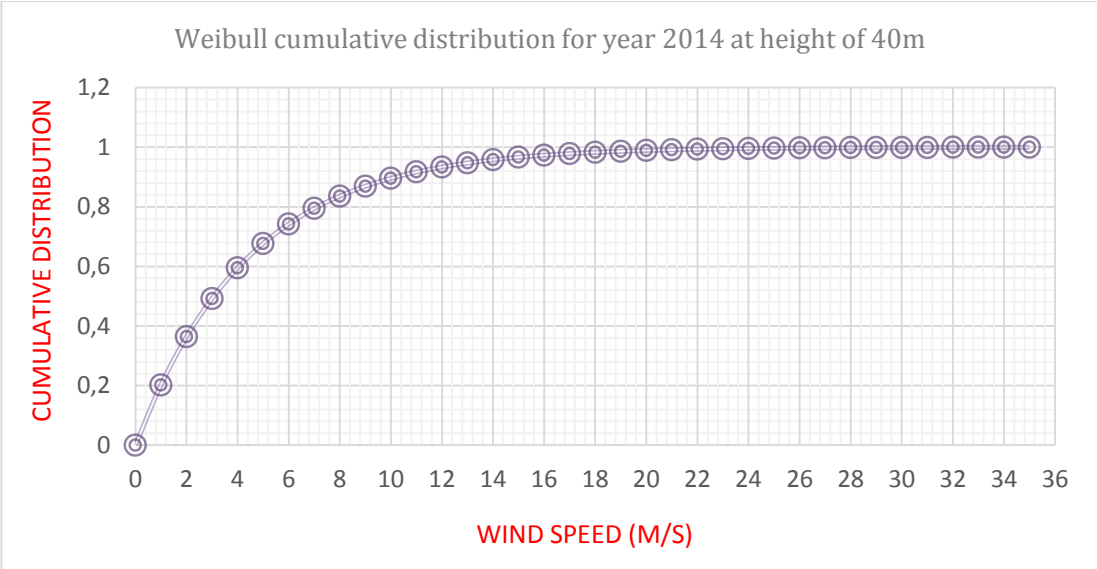

Fig. 2.15 Cumulative probability of year 2014 at height 40m (AGL)

The annual likelihood thickness capacities and the yearly total recurrence capacities are computed from the deliberate breeze speeds at 10 and 40m (AGL) at El-Spiaa, Tripoli _Libya which are presented in Fig. (2.5) to Fig. (2.15). The results are presented in the Table (2.4) corresponding to monthly mean wind speeds in the range of 5.12-9.87 m/s.

Table 2.4 The results of Weibull parameters (k) and (c), for year of 2013and 2014

years	Weibull shape at height of 10m	Weibull shape at height of 40m	Scale parameter at height of 10m	Scale parameter at height of 40m
2013	k = 2.5248	k = 2.6263	c = 7.8608 m/s	c = 8.5308 m/s
2014	k = 2.6314	k = 2.7367	c = 8.1739 m/s	c = 9.1402 m/s

2.7.3. Calculation of power density

The wind power density, E, (W/m²) can be expressed in terms of the Weibull shape and scale parameters, k and c, using Eq. (2.10) [1]. The yearly mean wind power densities for data of year 2013 and 2014 at height of 10 m and 40 at ElSpiaa, Tripoli _Libya are calculated based on the constant air density method at 1.225 kg/m³. It is found that the yearly wind power density of year 2013 at both heights of 10 and 40 m are (651.02 W/m²) and (814.61W/m²) respectively. What's more, the annual breeze control thickness for year 2014 at 10 and 40 m are (715.85W/m²) and (980.41 W/m²) individually. The reliable air thickness procedure can be used to overestimate the month to month mean breeze control densities by up to 5.5%, this overestimation is acceptable for resource assessment unless the variable air thickness is open [16].

Table 2.5 Wind power classification at 50 m [16]

Wind power class		Wind power Density (w/m²)	Mean wind speed (m/s)	Resource potential
1	1-	0-100	0-4.381	Very poor
	1+	100-200	4.381-5.588	
2	2-	200-250	5.588-6.035	Poor
	2+	250-300	6.035-6.393	
3	3-	300-350	6.393-6.706	Marginal
	3+	350-400	6.706-7.018	
4	4-	400-450	7.018-7.287	Good
	4+	450-500	7.287-7.510	

5	5-	500-550	7.510-7.778	Very Good
	5+	550-600	7.778-8.002	
6	6-	600-700	8.002-8.404	Excellent
	6+	700-800	8.404-8.807	

Chapter Three

AERODYNAMICS OF WIND TURBINES

3.1. Introduction

Wind turbines are a device that focuses on wind power and transforms it into mechanic power. In this line, power generation in wind turbines depends on the co-operation between the rotor and the wind. Then, large parts of the performance of wind turbines, such as power output and loads, are dictated by wind forces produced by the wind. This must be understood with a deep appreciation of the optimal design of the permanent work of the State. In a similar fashion, this part mainly focuses on optimal design for a consistent case.

3.2. Aerodynamics of Horizontal-Axis Wind Turbines

Most of the part points of interest the traditional diagnostic approach for the HAWT examination and their forecast execution.

A direct model, known as actuator circle show, can be used to figure the power output of an impeccable turbine rotor and the breeze push on the rotor. Likewise, additionally created systems including theory of blade element and momentum and finally theory of BEM is displayed.

Blade Element and Momentum Theory is one of the most popular tools in HAWT engineering, due to its low computational costs and fast results. This theory is used to determine the optimum blade shape and also to predict the performance parameters of the rotor for ideal, steady operating conditions. Blade element momentum theory combines two methods to analyze the aerodynamic performance of a wind turbine. These are momentum theory and blade-element theory which are used to outline the governing equations for the aerodynamic design and power prediction of a HAWT rotor. The method combines the conservation of Momentum across the rotor (which is considered as an actuator disk) and the integration of aerodynamic forces over all blade elements. To achieve closure, the thrust calculated from the Momentum

Equation is equated with that calculated with the blade element equations; in this way, the induced velocities across the rotor can be assessed. BEM theory relies upon begin that the powers following up on the wind turbine blades are solely responsible for the change in axial momentum of the air experiencing the cleared locale of the blades. Blade Element theory relies upon the supposition that blades can be part up into small elements that show professionally of including elements and work proficiently as two-dimensional airfoils whose streamlined powers can be figured in perspective of the adjacent stream conditions. The total powers and moments applied on the turbine would then have the capacity to be figured by summing up these elemental powers along the cross of the blade. On the other hand of the BEM theory, the momentum theory expects that the loss of momentum in the rotor plane is caused by the work done by the wind current experiencing the rotor plane on the blade elements. With this theory, the started rates can be figured from the momentum lost in the stream in the axial and digressive orientation. Since these started speeds impact the inflow in the rotor plane, in result, they moreover impact the powers registered by the blade element theory.

As said heretofore, the BEM theory is executed by breaking the blades of a wind turbine into various elements along the cross of the blade. Fig. 3.1 shows the annular region that took after out by the elements as they as they rotate in the rotor plane. It is over this annular area in which the momentum modify happens Momentum theory suggests the control volume examination of the powers at blade in perspective of the safeguarding of straight and exact momentum. Blade Element theory suggests the examination of powers at a territory of the blade, as an element of blade geometry, in which the blade is part into zones along the length of the blade and each portion is analyzed autonomously.

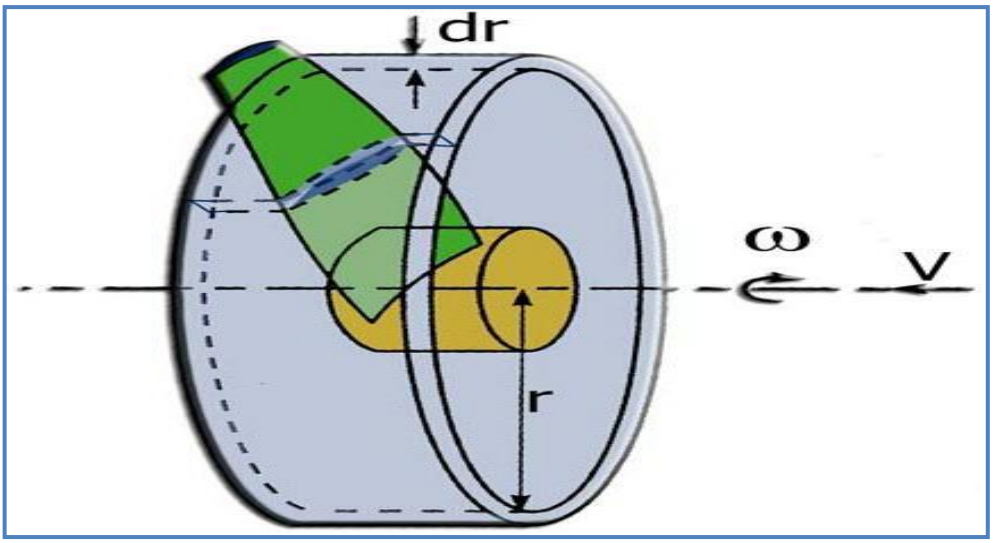

Fig. 3.1 Annular control Volume for BEM Analysis [24]

With BEM show, it is conceivable to figure the enduring burdens and accordingly likewise the power and thrust of various rotational speed, pitch angle and wind speed settings.

3.3. Principle of Actuator Disc

The analysis of the aerodynamic behavior of wind turbines can be started without any specific turbine design just by considering the energy extraction process. The easiest model of a wind turbine is the alleged actuator circle display where the turbine is supplanted by a round plate through which the airstream streams with a speed U_{∞} and crosswise over which there is a weight drop from p_u to p_d as exhibited in Fig. 3.2. At the start, stretch that the actuator circle theory is significant in discussing general efficiencies of turbines yet it can't be utilized to turbine blades outline fulfill a desired execution. Actuator circle demonstrate relies upon the suppositions like no frictional drag, homogenous, incompressible, continuing state fluid stream, steady weight expansion or push per unit zone over the plate, congruity of speed through the plate and an immense blades number [25].

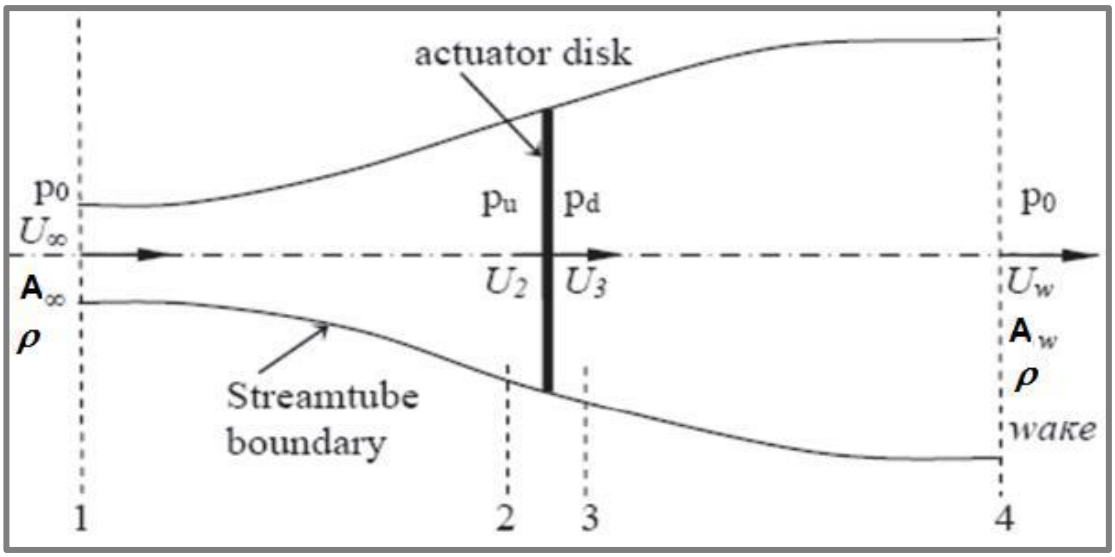

Fig. 3.2 Actuator Disk Model [26]

The examination of the actuator circle theory acknowledges a control volume in which the cutoff points are the surface dividers of a stream tube and two cross-zones. In order to research this control volume, four stations (1- far wake region, 2- just after the blades, 3- just before the blades, 4- free-stream region) ought to be seen as (Fig. 3.2). The mass stream rate proceeds as before all through the stream. So the movement Eq. along the stream tube can be made as:

$$\rho A_{\infty} U_{\infty} = \rho A_d U_d = \rho A_w U_w \tag{3.1}$$

Assuming the continuity of velocity through the disk gives Eq.:

$$U_2 = U_3 = U_R \tag{3.2}$$

For steady state flow the mass flow rate can be obtained using Eq. (3.3);

$$\dot{m} = \rho A U_R \tag{3.3}$$

Applying the conservation of linear momentum Eq. on both sides of the actuator disk gives Eq. (3.4).

$$T = \dot{m}\,(U_{\infty} - U_w) \tag{3.4}$$

Meanwhile the frictionless flow or vitality exchange is not done, Bernoulli Eq. could be used on the two sides of the rotor yield.

$$p_d + \frac{1}{2}\rho U_R{}^2 = p_0 + \frac{1}{2}\rho U_w{}^2 \tag{3.5}$$

$$p_0 + \frac{1}{2}\rho U_\infty{}^2 = p_u + \frac{1}{2}\rho U_R{}^2 \tag{3.6}$$

Δp is the pressure drop if joining Eq (3.5) and (3.6)

$$\Delta p = \frac{1}{2}\rho(U_\infty{}^2 - U_w{}^2) \tag{3.7}$$

Similarly, actuator disk rotor thrust could state by way of next:

$$T = \Delta p\, A \tag{3.8}$$

Where

$$\Delta p = (p_u - p_d) \tag{3.9}$$

Substituting Eq. (3.7) into Eq. (3.8) it will give the disk thrust

$$T = \frac{1}{2}\rho A(U_\infty{}^2 - U_w{}^2) \tag{3.10}$$

Combining Eq. (3.3), (3.4) with (3.10) the disk velocity could found as:

$$U_R = \frac{U_\infty + U_w}{2} \tag{3.11}$$

The factor of axial induction a can be defined as:

$$a = \frac{U_\infty - U_R}{U_\infty} \tag{3.12}$$

Gives Equations (3.13) and (3.14);

$$U_R = U_\infty(1-a) \tag{3.13}$$

$$U_w = U_\infty(1-2a) \tag{3.14}$$

The P as output power, is equivalent to velocity thrust times at the plane rotor.

$$P = TU_R \tag{3.15}$$

By substituting Eq. (3.10) into (3.15) gives the power output in light of the momentum adjust on the two sides of the actuator plate rotor in more express frame.

$$P = \frac{1}{2}\rho A(U_\infty{}^2 - U_w{}^2)U_R \tag{3.16}$$

Also substituting Equations (3.13) and (3.14) into Eq. (3.15) offers:

$$P = 2\rho A a U_\infty{}^3(1-a)^2 \tag{3.17}$$

Finally HAWT rotor performance parameters (thrust coefficient C_T, the tip-speed ratio λ, and power coefficient C_p) could expressed in form dimensionless:

$$C_p = \frac{2P}{\rho\pi U_\infty{}^3 R^2} \tag{3.18}$$

$$C_T = \frac{2T}{\rho\pi U_\infty{}^2 R^2} \tag{3.19}$$

$$\lambda = \frac{R\Omega}{U_\infty} \tag{3.20}$$

Substituting Eq. (3.17) into Eq. (3.18), the rotor power coefficient could have modified:

$$C_P = 4a(1-a)^2 \tag{3.21}$$

Also substituting Eq. (3.14) into Eq. (3.10) gives:

$$T = 2Aa\rho(1-a)U_\infty{}^2 \tag{3.22}$$

Finally substituting Eq. (3.22) into Eq. (3.19) offers the rotor coefficient thrust.

$$C_T = 4a(1-a) \tag{3.23}$$

The maximum C_T is equal one when a=1/2 and the velocity downstream equal 0. When the power output is maximum a=1/3, C_T value will be 8/9. A thrust coefficients and power chart for a Betz turbine is shown in Fig. 4.3.

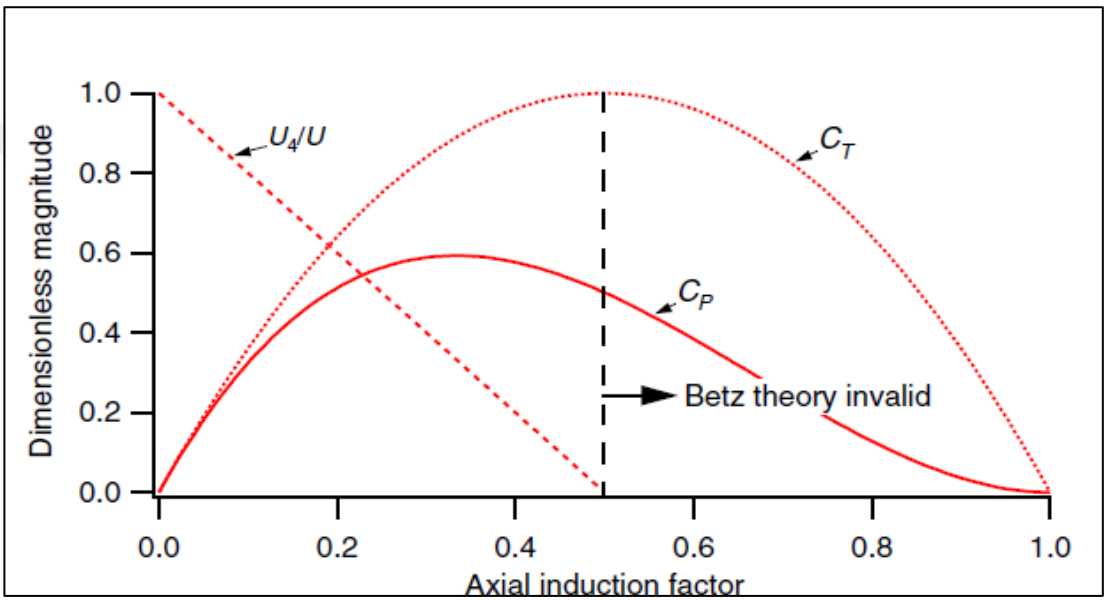

Fig. 3.3 Betz turbine Operating parameters. [26]

3.4. Rotating Annular Stream Tube Analysis

Up to this point the technique is created on the supposition that there was no rotational movement. To expand the technique built up, the impacts of this rotational movement should be incorporated so it is important to change the characteristics of the actuator plate by expecting that it can likewise grant a rotational segment to the liquid speed while the hub and spiral parts stay unaltered. Using a turning annular stream tube examination, conditions can be created that express the association between the wake speeds (both rotational and axial) and the looking at wind speeds at the rotor plate, and note that the precise speed increments from , while the axial speed stays unaltered [26].

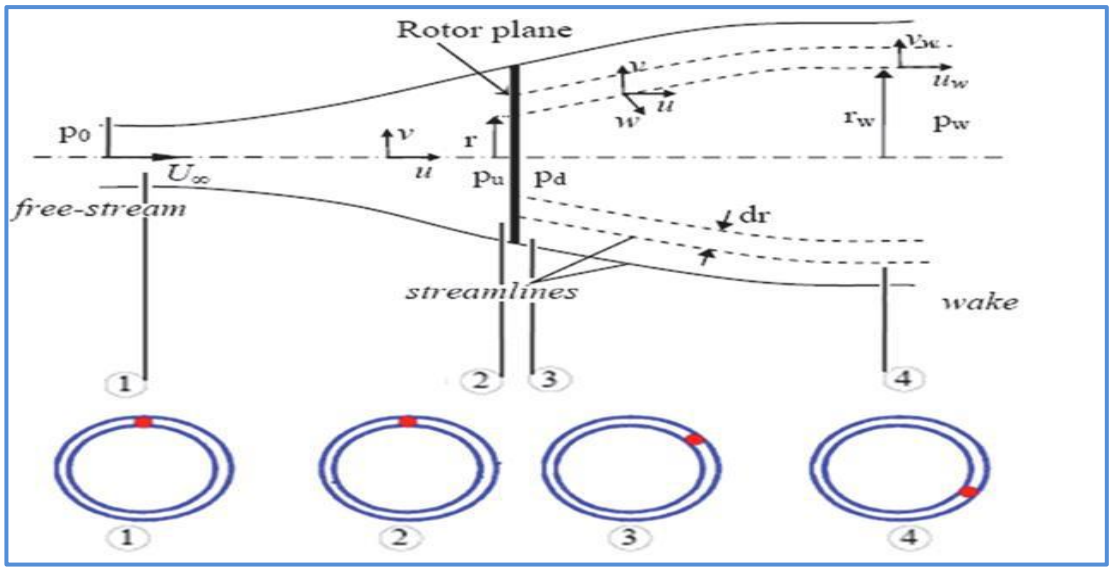

Fig. 3.4 Title Rotating Annular Stream Tube Analysis. [26]

This examination considers the protection of precise momentum in the annular stream tube Fig.3.4. On the off chance that the state of congruity of stream is connected for the annular element gone up against the rotor plane Eq. (4.24) can be composed. [26];

$$u_w r_w dr_w = urdr \tag{3.24}$$

Applying the protection of the angular momentum on upstream and the wake region of the stream range gives:

$$w_w r_w^2 = wr^2 \tag{3.25}$$

Additionally, the torque caused by the precise momentum adjust on the differential annular element can be gotten utilizing Eq. (3.26);

$$dQ = \rho u w r^2 dA \tag{3.26}$$

Where $dA = 2r\pi dr$. When Bernoulli Eq. applied between one and two station and next between three and four provides constants of Bernoulli as:

$$H_0 = P_0 + \frac{1}{2}\rho U_\infty{}^2 = P_u + \frac{1}{2}\rho(u^2 + v^2) \tag{3.27}$$

$$H_1 = P_d + \frac{1}{2}\rho(u^2 + v^2 + w^2 r^2) = P_w + \frac{1}{2}\rho(u_w^2 + r_w^2 + w_w^2) \qquad (3.28)$$

And taking the distinction between these constants gives:

$$H_0 - H_1 = \Delta p - \frac{1}{2}\rho(w^2 r^2) \qquad (3.29)$$

Which implies the active energy of the rotational movement given to the liquid by the torque of the blade is equivalent to $(-\frac{1}{2})\rho(w^2 r^2)$. So the aggregate weight head between the two sides of the rotor progresses toward becoming:

$$P_0 - P_w = \frac{1}{2}\rho(u_w^2 - U_\infty^2) + \frac{1}{2}w_w^2 \rho r_w^2 + (H_0 - H_1) \qquad (3.30)$$

$$= \frac{1}{2}\rho(u_w^2 - U_\infty^2) + \frac{1}{2}\rho(w_w^2\ r_w^2 - w^2 r^2) + \Delta p \qquad (3.31)$$

When Bernoulli Eq. applied between two and three station provides the weight drop:

$$\Delta p = \frac{1}{2}\rho\left[-\Omega^2 + (\Omega + w)^2\right] r^2 = \rho(\Omega + \frac{w}{2})\mathrm{wr}^2 \qquad (3.32)$$

Where Ω the blade angular speed and w is the wind rakish speed. Subsequently the pivotal thrust power dT can be analyze as next:

$$dT = \rho\left(\Omega + \frac{w}{2}\right)\mathrm{wr}^2\mathrm{dr} \qquad (3.33)$$

Also the thrust on the differential element is equal to:

$$dT = 2\rho u(u - U_\infty)dA = 4\pi\rho U_\infty^2\ a(1-a)r\,dr \qquad (3.34)$$

Using Eq. (3.34) Eq. (3.35) can be rewritten as:

$$dT = \Delta p dA = 2\pi\rho\left(\Omega + \frac{w}{2}\right)wr^2 dr \qquad (3.35)$$

If the defined factor of angular induction is $a = \frac{w}{2\Omega}$, so Eq. (3.36) will be:

$$dT = 4\pi\rho\,\Omega^2 a'(1+a')r^3 dr \tag{3.36}$$

And to gain a link between the factor of angular induction and axial induction, Eq. (3.34) and (3.36) have to equate:

$$\frac{a(1-a)}{a'(1+a')} = \frac{\Omega^2 r^2}{U_\infty^2} = \lambda r^2 \tag{3.37}$$

Using Eq. (3.26) the differential element torque could calculate as:

$$dQ = 4\pi\rho U_\infty \Omega a'(1-a)r^3 dr \tag{3.38}$$

At every radial element, power will generate as $dP = \Omega dQ$ and $\lambda_r = \frac{\Omega r}{U_\infty}$

Substituting Eq. (3.38) into this Eq. gives:

$$dP = \frac{1}{2}\rho A U_\infty^3 \left[\frac{8}{\lambda^2} a'(1-a)\lambda_r^3\, d\lambda_r\right] \tag{3.39}$$

And the coefficient of power for every differential annular ring could be:

$$dC_P = \frac{2dP}{\rho U_\infty^3 A} \tag{3.40}$$

Substituting Eq. (3.39) into the Eq. (3.40) and adding to the ratio of tip speed from ratio of hub tip speed gives coefficient of power for the whole rotor. [19]

$$C_P = \frac{8}{\lambda^2}\int_{\lambda_h}^{\lambda} a'(1-a)\lambda_r^3\, d\lambda_r \tag{3.41}$$

By solving Equation. (3.40) for a' yields.

$$a' = -\frac{1}{2} + \frac{1}{2}\sqrt{1+\frac{4}{\lambda_r^2}a(1-a)} \tag{3.42}$$

Solving the Equations (3.41) and (3.42) composed for extreme probable power production:

$$\lambda_r^2 = \frac{(1-a)(4a-1)^2}{(1-3a)} \tag{3.43}$$

Also substituting Eq. (3.43) into Eq. (3.37) gives the angular induction factor in each annular ring for maximum power.

$$a = \frac{(1-3a)}{(4a-1)} \tag{3.44}$$

Differentiating Eq. (3.43) with respect to axial induction factor at rotor plane, a relationship between $d\lambda_r$ and da can be obtained.

$$2\lambda_r d\lambda_r = \left[6(4a-1)(1-2a)^2 / (1-3a)^2 \right] da \tag{3.45}$$

Finally, substituting the Equations (3.43) (3.44), (3.45) into Eq. (3.41) provides the extreme coefficient of power of the rotor:

$$C_{P,\max} = \frac{24}{\lambda^2} \int_{a_1}^{a_2} \left[\frac{(1-a)(1-2a)(1-4a)}{(1-3a)} \right]^2 da \tag{3.46}$$

The corresponding factor of axial induction a_1 for $\lambda_r = \lambda_h$ and a_2 is the corresponding axial induction factor for $\lambda_r = \lambda_h$.

3.5. Theory of Blade Element

Until this point the momentum theory is attempted to be elucidated by temperance of HAWT rotor design anyway it doesn't consider the effects of rotor geometry qualities like agreement and twist scatterings of the blade airfoil. Consequently, blade element theory ought to be added to the design procedure. In order to apply blade element examination, it is acknowledged that the blade is isolated into N portions. This examination relies upon a couple of suppositions including no aerodynamic

participation between different blade elements and the powers on the blade elements are only managed by the lift and drag coefficients [26].

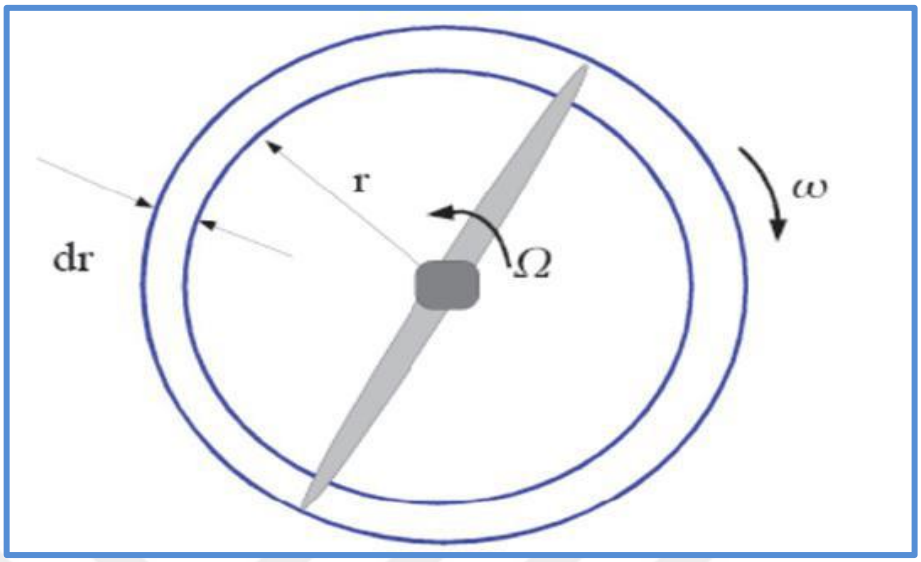

Fig. 3.5 Rotating Annular Stream Tube [26]

Every blade element has an alternate geometric attributes and rotational speed which would encounter the marginally extraordinary stream. The theory of blade element includes separating blades to eight elements and computing the stream at every one (Fig. 3.5 and Fig. 3.6). General execution attributes of the blade are then dictated by numerical combination along the blade traverse [26].

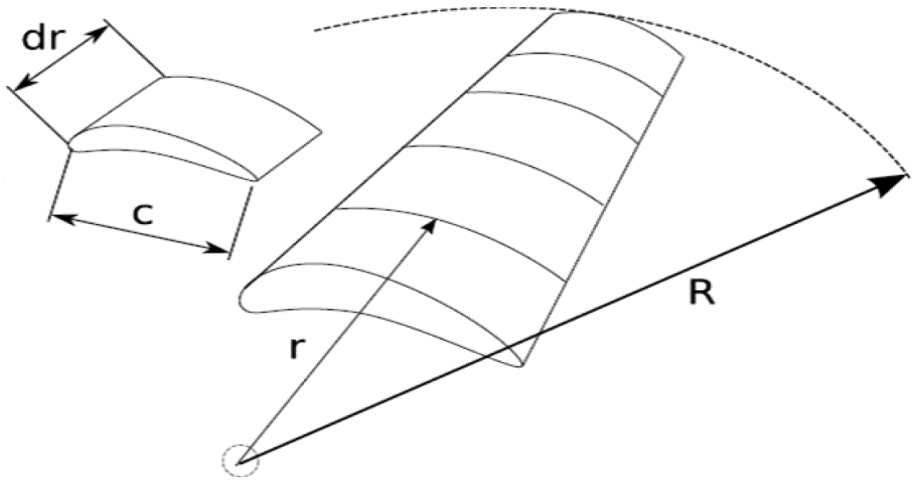

Fig. 3.6 The Model of Blade Element [17]

Lift and drag coefficient data are open for a combination of airfoils from wind tunnel data. Since most wind tunnel testing is done with the airfoil stationary, the relative velocity over the airfoil is used as a piece of demand to relate the stream over the moving airfoil with the stationary test (Fig. 3.7).

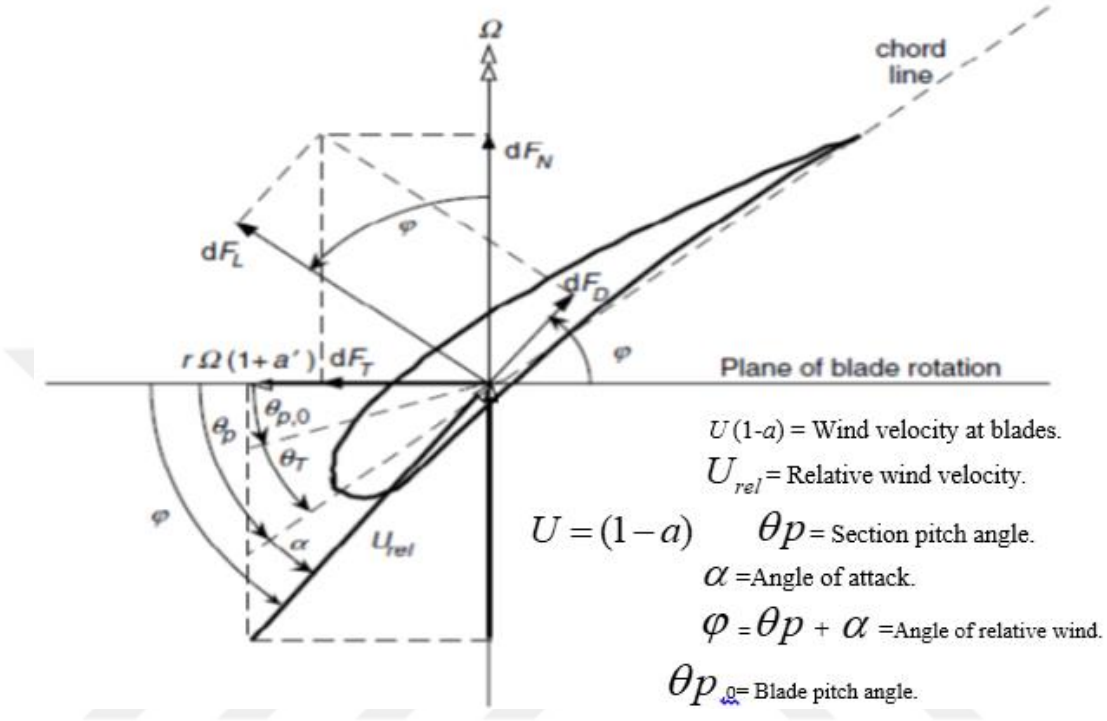

Fig. 3.7 HAWT Rotor analysis Blade Geometry [27]

- θp : Section pitch angle, which describes the angle between the chord line and the rotor plane of rotation.
- θp ,0: Blade pitch angle at the tip of the blade.
- θT : Blade twist angle.
- α : Angle of attack I.E. the angle between the chord line and the incoming relative wind.
- φ : Angle of the incoming relative wind.
- dF_L : Incremental lift force.
- dF_D : Incremental drag force.
- dF_N : Incremental force normal to the plane of rotation, a major contributor to the thrust force.
- dF_T : Incremental force tangential to the circle swept by the rotor.
- U_{rel} : Magnitude of the relative wind velocity.

From Fig. 3.7.the following relationships may be determined:

$$u_{rel} = \sqrt{[(1-a)u_\infty]^2 + [(1+a')\omega r]^2} \tag{3.47}$$

$$\tan(\varphi) = \frac{U_\infty(1-a)}{\Omega r(1+a')} = \frac{(1-a)}{(1+a')\lambda_r} \tag{3.48}$$

$$dF_L = C_L \frac{1}{2}\rho U_{rel}^2 \; cdr \tag{3.49}$$

$$dF_D = C_D \frac{1}{2}\rho U_{rel}^2 \; cdr \tag{3.50}$$

$$dF_T = dF_L \; \sin\varphi - dF_D \; \cos\varphi \tag{3.51}$$

$$dF_N = dF_L \; \cos\varphi - dF_D \; \sin\varphi \tag{3.52}$$

In order to account for the fact that blade element theory describes the effect of the forces on individual rotor blade sections and not an actuator disk comprised of an infinite number of rotor blades, as was used in the momentum theory, the actual number of rotor blades must be incorporated into the derivation of the aerodynamic forces. Therefore, if "B" refers to the number of rotor blades the normal force and torque occurring at a distance, r, from the axis of rotation may defined, respectively, by combining the previous Equations

$$dF_T = B\frac{1}{2}\rho U_{rel}^2 (C_L \; \sin\varphi - C_D \cos\varphi) cdr \tag{3.53}$$

$$dF_N = B\frac{1}{2}\rho U_{rel}^2 (C_L \; \cos\varphi - C_D \sin\varphi) cdr \tag{3.54}$$

The elemental torque can be written as $dQ = rdF_T$ which gives:

$$d_Q = B\frac{1}{2}\rho U_{rel}^2 (C_L \; \sin\varphi - C_D \cos\varphi) crdr \tag{3.55}$$

The solidity ratio can be defined as [7]:

$$\sigma = \frac{Bc}{2\pi r} \tag{3.56}$$

Lastly, the elemental thrust and torque Eq form generally will be

Eq. (3.57) and Eq. (3.58) define the tangential force (torque), the normal force (thrust) on annular rotor sector.

$$dF_N = \sigma\pi\rho \frac{U_\infty^2 (1-a)^2}{\sin^2 \varphi}(C_L \cos \varphi - C_D \sin\varphi) r dr \tag{3.57}$$

$$dQ = \sigma\pi\rho \frac{U_\infty^2 (1-a)^2}{\sin^2 \varphi}(C_L \sin\varphi - C_D \cos\varphi) r^2 dr \tag{3.58}$$

With the necessary blade section geometry and force characteristics now able to be calculated the optimum blade shape may be designed. The required airfoil data, including the lift and drag coefficients, will have a significant impact on the aerodynamic forces and the rotor performance.

Therefore, much care must be taken in determining those values in order to generate a rotor for optimum performance. [17].

3.6. Blade Element Momentum (BEM) theory

Generally, momentum theory thought was composed to the development of the fluid and the acting following up on the blades were settled. The disfigurement of the general momentum theory was that it gave no indication of the condition of blade required to make the reactions considered. The rule of the blade element theory was to consider the powers experienced by the blades of the rotor in their development through the air and this theory was thusly, by and by stressed over the geometrical condition of the blade. Remembering the true objective to overcome any block between these two theories, the blade element momentum theory (BEM) otherwise called strip theory has been delivered. BEM theory relates rotor execution to rotor geometry and particularly basic estimate of this theory is the effect of constrained blade number. The suppositions for BEM theory are obviously the mix of those which were made for general momentum and blade element theory [26].

- Individual stream tubes (the intersection of a stream tube and the surface swept by the blades) can be analyzed independently of the rest of the flow as assumed before for the blade element theory.

- Related with the headway of BEM theory is that navigate sharp stream is unimportant, and thusly airfoil data taken from two-dimensional section tests are agreeable as acknowledged before in again blade element theory.
- Stream conditions don't move the circumferential way, i.e. rotate symmetric stream. With this supposition the stream tube to be examined is a uniform annular ring focused on the axis of turmoil of course before all things considered momentum theory.

As it is communicated before BEM theory suggests the affirmation of a wind turbine blade execution by uniting the conditions of general momentum theory and blade element theory, so Eq. (3.34) and (3.36) can be contrasted with procure the going with verbalization [26].

$$\frac{a}{(1-a)} = (\sigma C_L)\frac{\cos\varphi}{\sin^2\varphi}\left[1+(C_D/C_L)\tan\varphi\right] \tag{3.59}$$

Also equating Equations (3.38) and (3.58) in the same manner gives:

$$\frac{a'}{(1-a')} = \frac{(\sigma C_L)}{4\lambda_r \sin\varphi}\left[1-(C_D/C_L)\cot\varphi\right] \tag{3.60}$$

By rearranging Eq. (3.60) and combining it with Eq. (3.48)

$$\frac{a'}{(1+a')} = \frac{(\sigma C_L)}{4\cos\varphi}\left[1-(C_D/C_L)\cot\varphi\right] \tag{3.61}$$

Can be written. In order to calculate the induction factors a and a' , C_D can be set to zero. Thus the induction factors can be determined independently from airfoil characteristics. [2][3]

Subsequently, Equations (3.59), (3.60) and (3.61) can be rewritten as Equations (3.62), (3.63), and (3.64) respectively.

$$\frac{a}{(1-a)} = (\sigma C_L)\frac{\cos\varphi}{4\sin^2\varphi} \tag{3.62}$$

$$\frac{a'}{(1-a)} = \frac{(\sigma C_L)}{4\lambda_r \sin\varphi} \tag{3.63}$$

$$\frac{a'}{(1+a')} = \frac{(\sigma C_L)}{4\cos\varphi} \tag{3.64}$$

Finally, by rearranging Eq. (3.62), (3.63) and (3.64) and solving it for a and a', the following useful analytical relationships can be obtained.

$$a = \frac{1}{\left[1+[4\sin^2\varphi/(\sigma C_L)\cos\varphi]\right]} \tag{3.65}$$

$$a' = \frac{1}{\left[[4\cos\varphi/(\sigma C_L)]-1\right]} \tag{3.66}$$

$$a/a' = \lambda_r/\tan\varphi \tag{3.67}$$

$$C_L = \frac{4\sin\varphi(\cos\varphi - \lambda_r \sin\varphi)}{\sigma\ (\sin\varphi + \lambda_r\cos\varphi)} \tag{3.68}$$

The total power of the rotor can be calculated by integrating the power of each differential annular element from the radius of the hub to the radius of the rotor.

$$P = \int_{r_h}^{R} dP = \int_{r_h}^{R} \Omega dQ \tag{3.69}$$

Where;

$$C_P = \frac{2P}{\rho U_\infty^3 \pi R^2} \tag{3.70}$$

And rewriting the power coefficient given in Eq. (3.69) using Eq. (3.70) gives:

$$C_P = \frac{P}{\frac{1}{2}\rho U_\infty^3 A} = \frac{\int_{r_h}^{R} \Omega dQ}{\frac{1}{2}\rho U_\infty^3 \pi R^2} \tag{3.71}$$

Using Eq. (3.62) (3.63) and (3.67) the power coefficient relation can be rearranged as: [28]

$$C_P = \frac{8}{\lambda^2}\int_{\lambda_h}^{\lambda} \lambda_r^3 a' (1-a)[1-(C_D / C_L)\cot\varphi] d\lambda_r \tag{3.72}$$

Finally, by rearranging Eq. (3.65), (3.68) in to (3.72) can be obtained:

$$C_P = \frac{8}{\lambda^2}\int_{\lambda_h}^{\lambda} \sin^2\varphi(\cos\varphi - \lambda_r \sin\varphi)(\sin\varphi + \lambda_r \cos\varphi)[1-(C_D/C_L)\cot\varphi]\lambda_r^2 d\lambda_r \tag{3.73}$$

3.7. Optimum Wind Rotor

Shape of blade Design from an identified airfoil type for a perfect rotor which no impacts to wake pivot could resolved utilizing examination produced to a rotor generally, this streamlining no wake turn $(a' = 0)$, disregard drag power $(C_D = 0)$ and tip misfortunes $(F = 1)$, Betz ideal rotor. In this manner a general relationship can be found between perfect relative wind angle and local tip-speed ratio which will be proper for any airfoil sort by taking the incomplete subsidiary of that piece of the indispensable for C_p (Eq. 3.72) which is an element of the angle of the relative wind, and setting it equivalent to zero, i.e. [26].

$$\frac{\partial}{\partial\varphi} = \left\{\sin^2\varphi(\cos\varphi - \lambda_r \sin\varphi)(\sin\varphi + \lambda_r \cos\varphi)\right\} = 0 \tag{3.74}$$

This yields the relation for flow angle:

$$\lambda_r = \frac{\sin\varphi(2\cos\varphi - 1)}{[(1-\cos\varphi)(2\cos\varphi + 1)]} \tag{3.75}$$

Some more algebra reveals that [3];

$$\varphi_{opt} = \left(\frac{2}{3}\right)\tan^{-1}(1/\lambda_r) \tag{3.76}$$

From blade-element theory, can be calculated twist angle:

$$\theta_T = \theta_p - \theta_{p,o} \tag{3.77}$$

Of course the twist angle is blade geometry purpose, while θ_p, variations if the position of the blade $\theta_{p,o}$ is changed. Moreover, from Fig. 3.7.

$$\varphi = \theta_p + \alpha \tag{3.78}$$

And the chord-length can be calculated by:

$$c = \frac{8\pi r}{BC_L}(1-\cos\varphi) \tag{3.79}$$

We can also calculate the angle of attack by:

$$\alpha = \phi - \beta \tag{3.80}$$

Also, Reynolds number for each of the element can be calculated by:

$$\mathrm{Re} = \frac{\rho c u_{rel}}{\mu} \tag{3.81}$$

Where ρ and μ are density and dynamic viscosity of the flowing fluid respectively, c denotes the chord length of the airfoil and is the relative wind speed.

3.8. Correction of Tip Losses

At turbine blade tip losses are displayed. The ratio of the typical estimation of tip losses factor to that at a blade position is given in Fig. 3.8. As it is shown in the Figure simply near the tip the ratio begins to tumble to zero so it is called 'the tip-loss factor. With uniform dispersal the azimuthal typical estimation of is in like manner

radially uniform yet that construes an inconsistency of axial velocity at as far as possible with a relating irregularity in pressure. While such discontinuities are satisfactory in the celebrated actuator circle condition they won't occur basically with a constrained blades number.

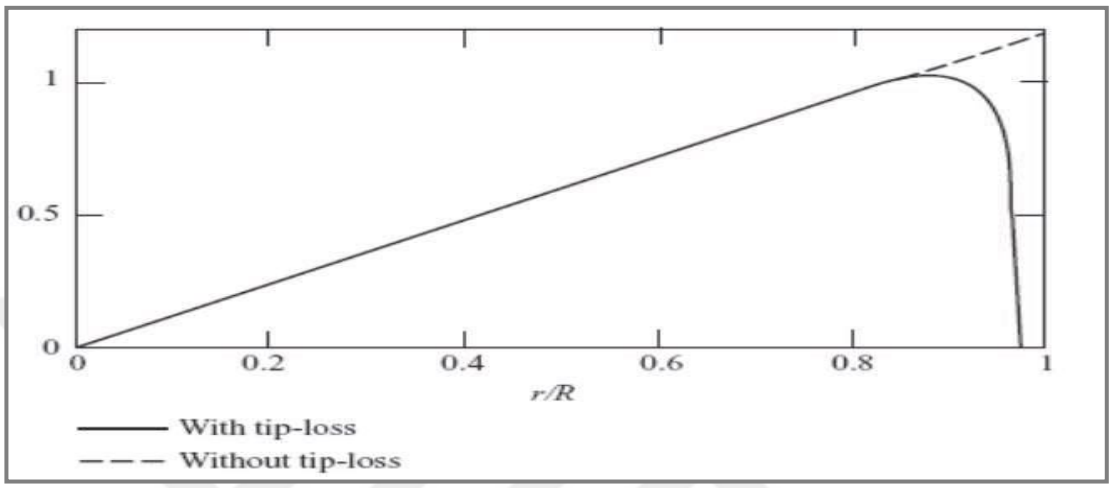

Fig. 3.8 Span-wise Variation of Power Extraction.

The tip-loss at the blade tips can be spoken to in BEM theory by techniques for correction factor, F which shifts from 0 to 1 and depicts the reducing in powers along the blade. A surmised strategy for evaluating the impact of tip-loss has been given by L. Prandtl and the articulation got by Prandtl for tip-loss factor is given by Eq. (3.82).

$$F = \frac{2}{\pi}\cos^{-1}\left\{\exp\left[\frac{-(B/2)[1-(\frac{r}{R})]}{(\frac{r}{R})\sin\varphi}\right]\right\} \tag{3.82}$$

The use of this Eq. for the losses at the blade tips is to give an estimated rectification to the arrangement of equations for foreseeing rotor execution and blade design.

Bringing the tip-loss factor through the estimations, the progressions will be as following:

$$\frac{a}{(1-a)} = (\sigma C_L)\frac{\cos\varphi}{4F\sin^2\varphi} \tag{3.83}$$

$$\frac{a'}{(1-a)} = \frac{\sigma C_L}{4F\cos\varphi} \tag{3.84}$$

$$\frac{a'}{(1+a')} = \frac{\sigma C_L}{4F\cos\varphi} \tag{3.85}$$

$$C_L = \frac{4F\sin\varphi}{\sigma}\frac{(\cos\varphi - \lambda_r \sin\varphi)}{(\sin\varphi + \lambda_r \cos\varphi)} \tag{3.86}$$

$$a = \frac{1}{1+\left[\dfrac{4F\sin^2\varphi}{(\sigma C_L)\cos\varphi}\right]} \tag{3.87}$$

$$a' = \frac{1}{\left[\dfrac{4F\cos\varphi}{(\sigma C_L)} - 1\right]} \tag{3.88}$$

$$C_P = \frac{8}{\lambda^2}\int_{\lambda_h}^{\lambda} F\sin^2\varphi(\cos\varphi - \lambda_r\sin\varphi)(\sin\varphi + \lambda_r\cos\varphi)\left[1 - \frac{C_D}{C_L}\cot\varphi\right]\lambda_r^2 d\lambda_r \tag{3.89}$$

3.9. Horizontal-axis Wind Turbines Flow States

Measured wind turbine execution eagerly approximates the consequences of BEM Theory at low estimations of the axial induction factors however broad momentum theory isn't any more real at vital selection factors more unmistakable than 0.5, because according to the Eq. (3.14), the wind speed in the far wake would be negative. Eventually, as the essential enrollment factor augments more than 0.5, the stream designs through the wind turbine end up being extensively more personality boggling than those expected by the general momentum theory. [3].

The thrust coefficient addressed by the Eq. (3.23) can be used to portray the unmistakable stream states of a rotor. Fig. 3.8 shows stream states and thrust drive vectors T related with a broad assortment of significant selection factors. As showed by this Fig., for negative selection factors $(a < 0)$ it is anything but difficult to continue with the examination to exhibit that the device will go about as a force

making an upwind power (i.e. $C_T < 0$) that adds vitality to the wake. This is regular of the propeller state. The working states imperative to HAWT are designated by the windmill state and the turbulent wake state. The windmill state is the customary working state. The windmill state is depicted by the stream conditions portrayed by general momentum theory for critical enlistment factors not precisely about $a = 0.4$ as outlined by the data in Fig. 3.8 got on wind turbines, above $a = 0.5$ rotor thrust increments up to 2 with expanding acknowledgment factor in the turbulent wake state, rather than diminishing as expected by the Eq. (3.23) while general momentum theory never again portrays the turbine direct, Glauert's empirical condition for center point enlistment factor from 0.4 to 1.0 are as often as possible used as a piece of HAWT rotor design for envisioning wind turbine stream states [3].

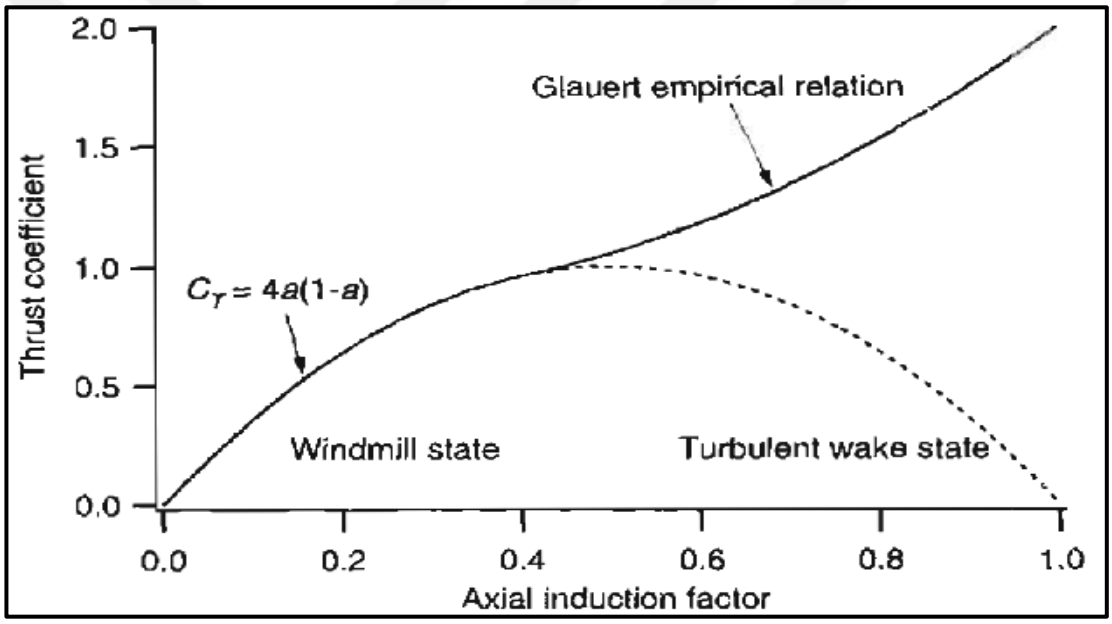

Fig. 3.9 Relationship between the thrust, flow state and axial induction factor of a rotor [29]

3.10. Glauert and Buhl Empirical Corrections

In the turbulent wake state, as expressed before an answer can be found by using the Glauert empirical correction between the axial induction factor a, and the thrust coefficient C_T in conjunction with the blade element theory. The empirical relationship made by Glauert, including tip losses is [25];

$$a = \frac{18F - 20 - 3\sqrt{C_T(50 - 36F) + 12F(3F - 4)}}{30F - 50} \tag{3.90}$$

This Eq. is substantial for $a > 0.4$ or similarly for $C_{Tr} > 0.96$ The Glauert empirical relationship was resolved for the general thrust coefficient for a rotor. It is standard, nonetheless, to acknowledge that it applies similarly to equivalently close-by thrust coefficients for each blade zone [7]. The local thrust coefficient C_{Tr} can be described for each annular rotor zone as;

$$C_{Tr} = \frac{dF_N}{\frac{1}{2}\rho U_\infty^2 2\pi r dr} \tag{3.91}$$

From the Eq. (3.60). From theory of blade element of the elemental thrust compel, the nearby thrust coefficient progresses toward becoming:

$$C_{Tr} = \frac{\sigma(1-a)^2(C_L \cos\varphi + C_D \sin\varphi)}{\sin^2\varphi} \tag{3.92}$$

With a specific end goal to incorporate the blade design and power execution of profoundly stacked HAWTs that are working at ratios of high tip-speed, the Glauert empirical equation is utilized as a part of the creating of the PC program. It initially ascertains the nearby thrust coefficient for every blade segment as indicated by the Eq. (3.60) and if $C_{Tr} < 0.96$ then uses the already determined Eq. for the blade design. If $C_{Tr} > 0.96$ then it gauges hub acceptance factor utilizing Eq. (3.90) and this new estimation of pivotal acceptance factor is utilized as a part of the equations for the design [26].

Chapter Four

MODIFIED OF (BEM) ANALYSIS TOOL

4.1. Introduction

In the previous section it was stated that the most common method for prediction of rotor performance in the aerodynamic design of rotors was the Blade Element Momentum (BEM) method and that it required low computational means. In the sections that follow, the various elements required for the aerodynamic design of rotors using BEM are described. Because the aerodynamic rotor design should be considered as integrated in the design of the entire wind turbine, aspects such as constraints relating to the aerodynamic rotor design process, are described [30]. This chapter, shows the results of (BEM) theory of the wind turbine which are using NACA 63 (4)-221 airfoil type, validation with Risoe wind turbine test case and compared with NREL phase II and IV wind tunnel tested data. This is important to know how (BEM) Analysis Tool predicted the best performance of wind turbine which is closest solution to the experimental data.

4.2. Airfoil Families and Experimental Wind Turbine Database

4.2.1. Airfoil families' database

Most acclaimed airfoil families are conveyed by NACA. The instances of NACA airfoil families which are used furthermore in wind turbine applications are NACA 63, NACA 64 and NACA 65 airfoil families. Also there are several airfoil families developed by European and US research institutes for wind turbine applications. For instance, Risoe-A1, A2 or Risoe-B1 airfoil families which are planned by Risoe National Laboratory in Denmark. Diverse commended airfoil families are produced by Delft University in Netherlands which are called as DU airfoil families. NREL (National Renewable Energy Laboratory) in US also made airfoil families which are called as NREL S-game plan airfoils. There are a couple of various airfoils made and

used as a piece of wind turbine applications. In most of the airfoil families conveyed for wind turbines, fundamental concerns are incorporated into airfoil plan [31]. In this dissertation, NACA 6 series airfoils are used as airfoils of a wind turbine (NACA 63 (4)-221 airfoil), Fig. 4.1, 4.2, 4.3 and 4.4 will show airfoil Geometry, Lift, drag coefficient versus angle of attack, and lift over drag coefficient versus angle of attack which are analyzed by using XFLR5 software with different range of Reynolds numbers [32]. Database of coordinates of airfoil were obtained from the UIUC airfoil database [33] which described the airfoil by 50 points, presented in Appendix [B].

NACA 63 (4)-221 airfoil which has max thickness of 21% at 34.9% chord and max camber 1.1% at 50% chord.

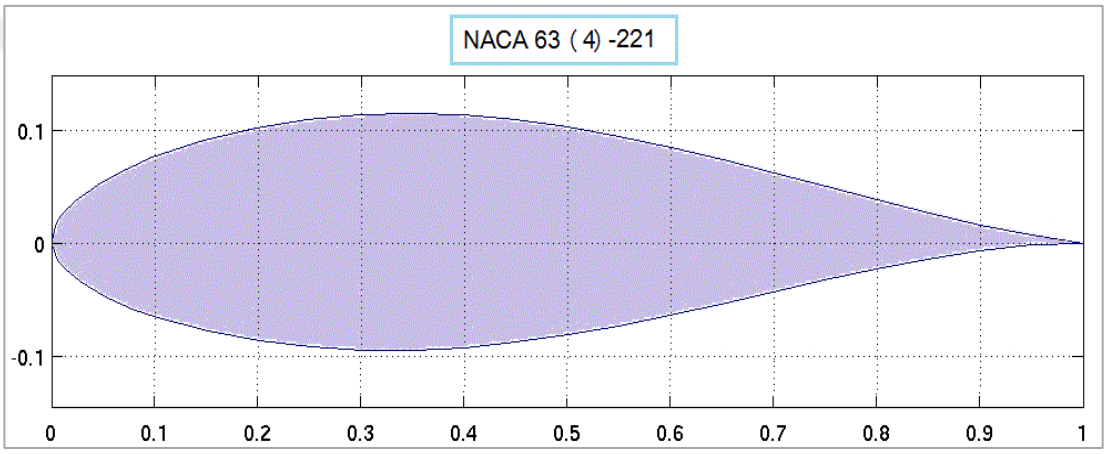

Fig. 4.1 NACA 63 (4)-221 airfoil Geometry

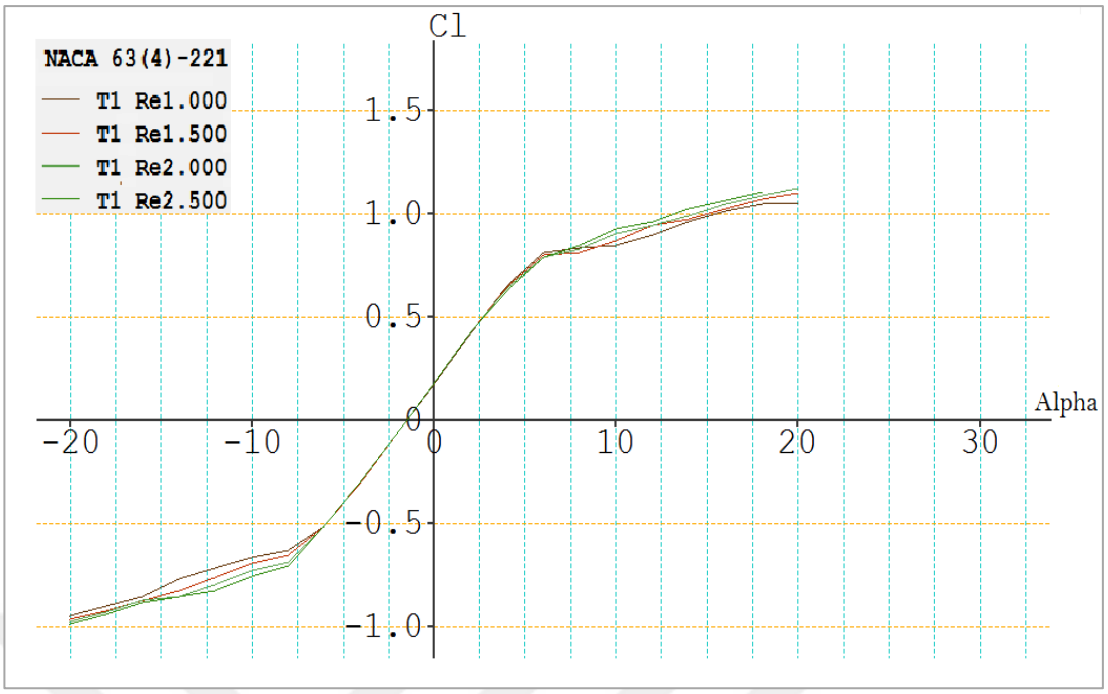

Fig. 4.2 Lift coefficient Cl versus different angle of attack range

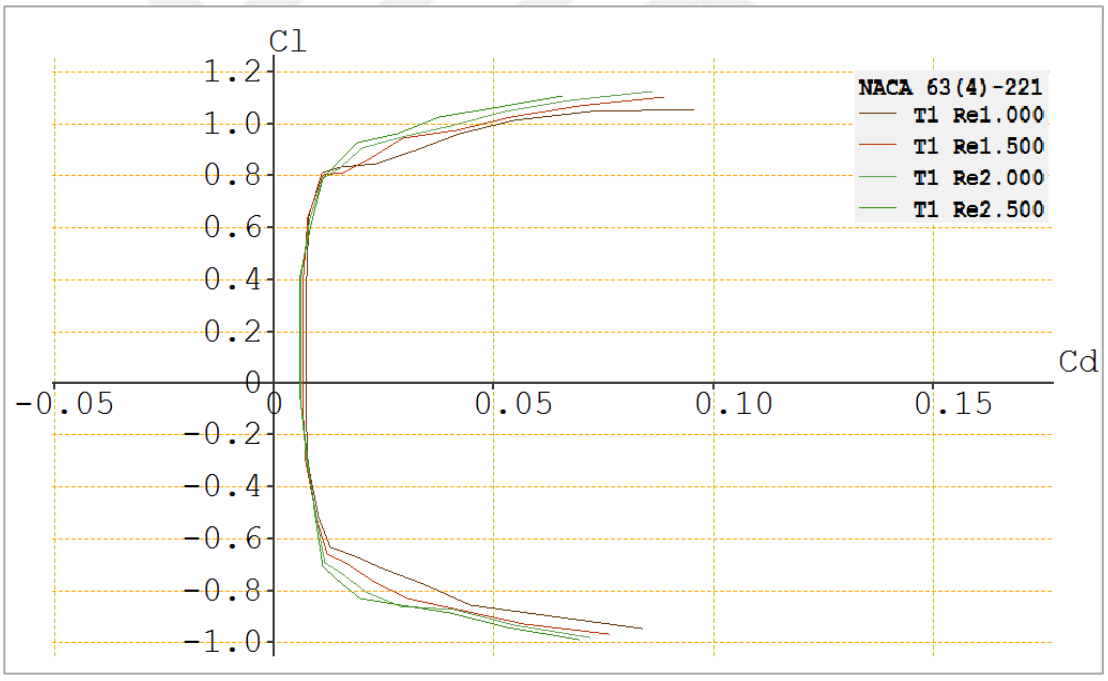

Fig. 4.3 Drag coefficient Cd versus different angle of attack range

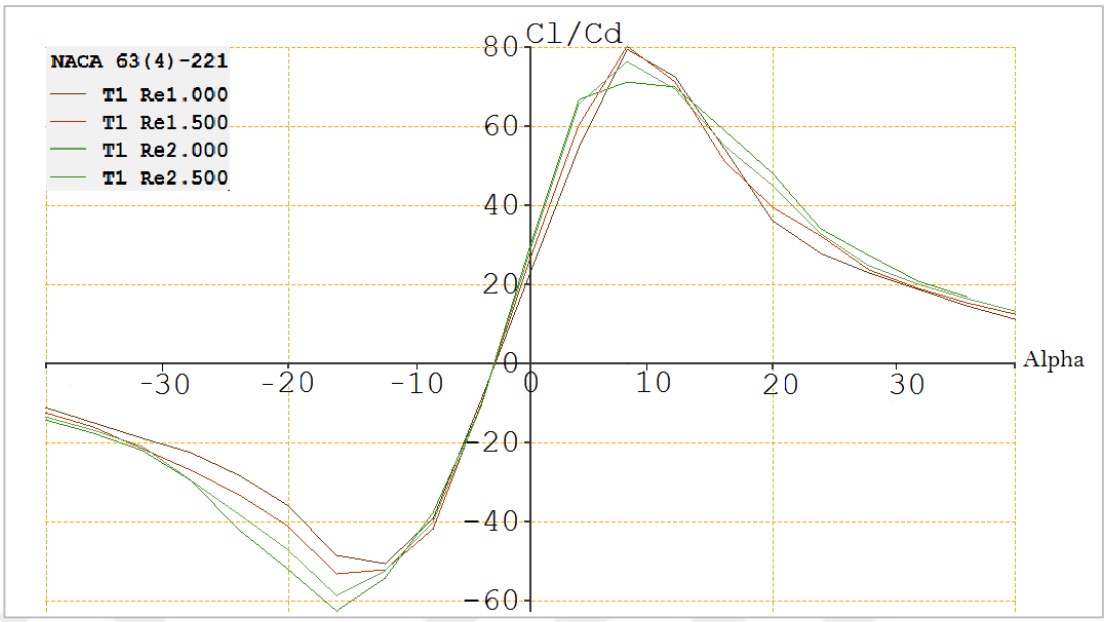

Fig. 4.4 Cl/Cd versus different angle of attack range

The streamlined execution of a wind turbine is essentially affected by Reynolds number of the airfoil used for the turbine sharp edges. The Reynolds number of a wind turbine is with respect to the concordance length and the wind speed. Impact of Reynolds number on the streamlined parameters (lift and drag coefficients) are vital, the lift is constantly ordinary to the approaching stream while the drag is dependably toward the stream. From previous figures which analyzed by using (XFLR5 software), we can conclude that, for low range of angle of attack, lift and drag coefficient (α , C_l and C_d) there are adult different between the results for all value of Reynolds number . While, for higher α and C_l approaching maximum, lift and drag coefficient (C_l and C_d) is increasing, which reflects the start of separation typically from the trailing edge. Increasing α will increase the amount of separation, which at the end will cause the airfoil to stall from the leading edge with massively separated Flow. Since lift coefficient C_l can be deciphered as a creation term C_d as a loss term, a measure for the airfoil effectiveness is the lift– drag ratio, (C_l / C_d). The power coefficient adding to the power is reliant on the lift coefficient C_l , the inverse lift–drag ratio, (C_l / C_d) and the inflow angle φ . Commonly, the point at which we find maximum (C_l / C_d) is called the design point, with the

corresponding design lift ($C_{l,design}$), and design angle of attack, α_{design} which was 10° .Thus, an airfoil for use on a wind turbine should operate at a point with high (C_l / C_d). Through the past Figures we can take note of that the most extreme lift coefficient diminishes with diminish in Reynolds number while the drag coefficient increments when Reynolds number is reduced. And from Fig. (4.4) we can observe that the lift to drag proportion decreases commandingly with diminish in Reynolds number, which brings about extraordinary execution of the medium and substantial scale wind turbines. There are pile sorts of airfoil open that have been made for different purposes. Each of these airfoils has specific extent of stream Reynolds number where it performs productively. The determination of a fitting airfoil, which is sensible for the working extent of given Reynolds number, is the in particular wander for accomplishing commendable execution of a small scale wind turbine. The power output is with respect to the square of the breadth of wind turbine and 3D state of the wind speed. As the measure of the wind turbine and the wind speed diminish, the power diminishes definitely and underneath certain most remote point its size is too low to legitimize the advancement and operational cost. Along these lines, accomplishing most extreme conceivable effectiveness ought to be the critical goal in the advancement of wind turbines. Another essential metric while taking a shot at the small scale is the cut-in speed. This addresses the undisturbed upstream speed of the wind at which the turbine begins delivering power. It depends upon the total inactivity and the interior grinding of the system including the rotor, metal balls, outfit plan, and generator.

4.2.2. experimental wind Turbine database

Three trial test cases are utilized for approval of blade element momentum theory (BEM) investigation of wind turbine blade. Two experiments are acquired from the National Renewable Energy Laboratory (NREL), which are NREL Phase II and NREL Phase VI even hub wind turbine (HAWT) rotors. The third case are Risoe wind turbine which are gotten from (National Laboratory for Sustainable Energy).

4.2.2.1. NREL un-tapered and un-twisted Wind Turbine

Wind turbine is called Phase II tests and the turbine is called Phase II turbine the test information for NREL Phase II is gotten from the IEA Annex XIV database [34]. This database was filled in as a dedication of various European research labs and the NREL to store and report the exploratory information for various attempted wind turbines and make it accessible to scientists. NREL Phase II with a steady harmony of 0.4572 m, is a small three-bladed HAWT framework with a width of 10.06 m and the appraised power output of 15.0 kW. The rotational speed is 71.63 RPM in each wind speed and the blade pitch is 12° settled along the blade [34]. The geometrical properties of the NREL Phase ii wind turbine are exhibited in Fig. (4.5) and the points of interest of the applicable parameters are clarified in the Table (4.1).

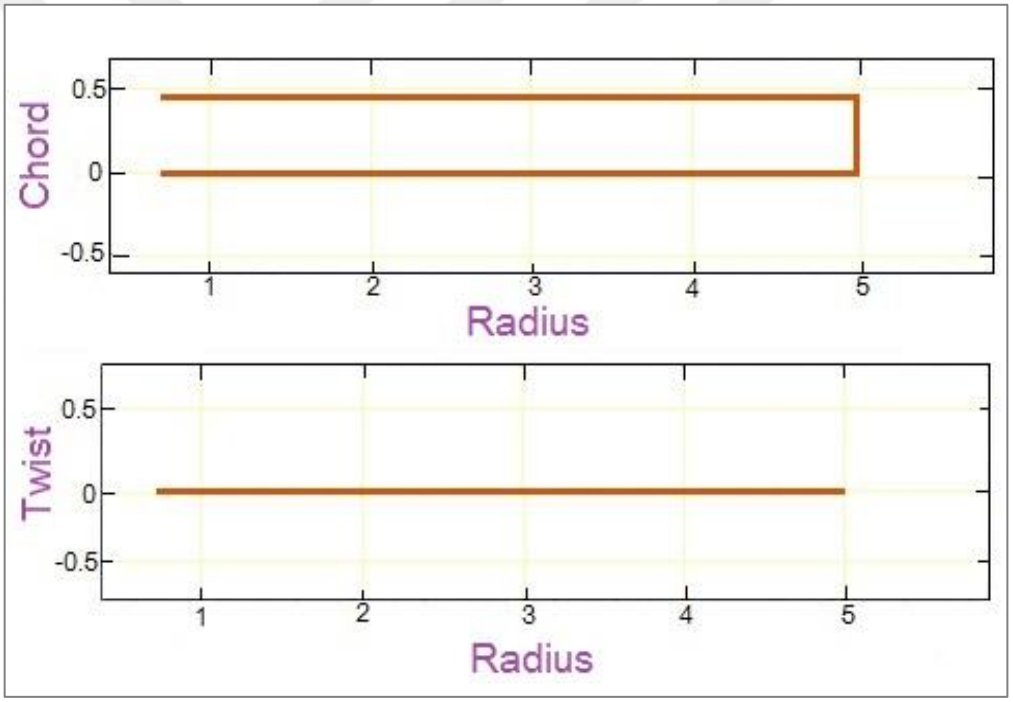

Fig. 4.5 NREL Geometry information Phase II wind turbine [31]

Table 4.1 NREL Phase II wind turbine general characteristics. [34]

Number of blades	3
Turbine diameter	10.06 m
Rotational Speed	71.3 rpm
Cone angle	3 degrees 25’
Power regulation	Stall regulated
Cut-in wind speed	6 m/s
Root extension	0.723 m
Pitch angle	12 degrees
Twist angle	0 degrees along the span
Blade chord length	0.4572 m, constant along the span
Blade profile	S809
Blade thickness	At 14.4% span, t/c = 43% At 30% span, t/c = 21% Outward 30%span, t/c = 21%

NREL Phase II wind turbine is HAWT with three blades and they are un-twisted and un-tapered. The S809 airfoil is utilized all through the blades traverse. The S809 airfoil has 21% max thickness at 39.5% harmony and max camber at 1% at 82.3% harmony. This airfoil designed for HAWT purposes. The airfoil pitching and geometry in Fig. (4.6) [34].

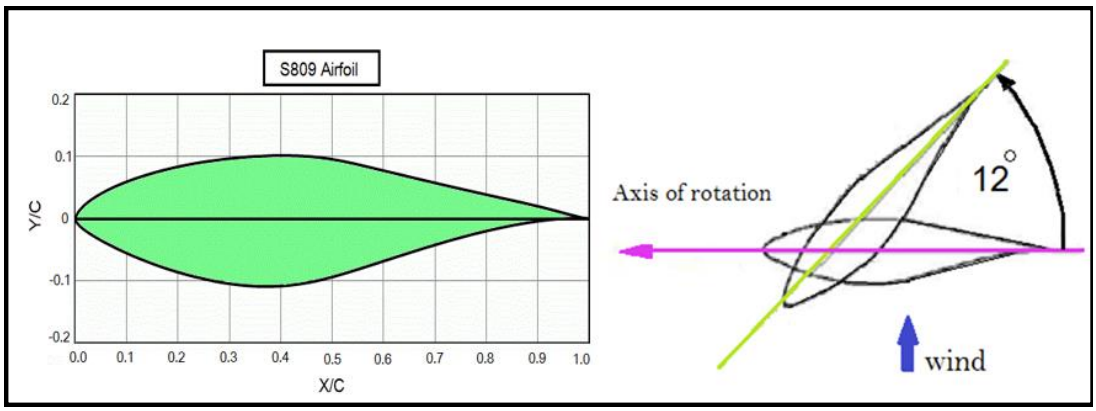

Fig. 4.6 The Geometry and pitch angle of s809 airfoil. [34]

Cl and *Cd* coefficients of this airfoil are analyzed by using XFLR5 software [34] for different angle of attack and different Reynolds number values. The Coordinates of S809 Airfoil presented in Appendix [B].

4.2.2.2. NREL Twisted and tapered Wind Turbine

NREL explore different avenues regarding turned and un-decreased wind turbine is called Phase VI tests and the wind turbine is called Phase VI wind turbine. This wind turbine is intended for testing purposes as Phase II wind turbine. NREL Phase VI wind turbine has two-bladed HAWT the cutting edges are diminished and twisted, with S809 airfoil segment from root to tip Similar to NREL Phase II. NREL Phase VI has a harmony of 0.358 m – 0.728 m (straightly decreased), breadth of 10.06 m, rotational speed is 71.63 RPM in each wind speed and the blade pitch is 3° settled along the blade. Points of interest of the significant parameters are clarified in the Table (4.2), and the turn appropriation along the blade is introduced in Fig. (4.7)

Table 4.2 NREL Phase VI wind turbine general characteristics. [34]

Number of blades	2
Turbine diameter	10.06 m
Rotational Speed	71.63 rpm
Cone angle	0 degrees
Power regulation	Stall regulated
Cut-in wind speed	6 m/s
Pitch angle	3 degrees
Twist angle	Non-linear twist along the span
Blade chord length	0.358 m – 0.728 m (linearly tapered)
Blade profile	S809
Blade thickness	t/c = 21% throughout the span

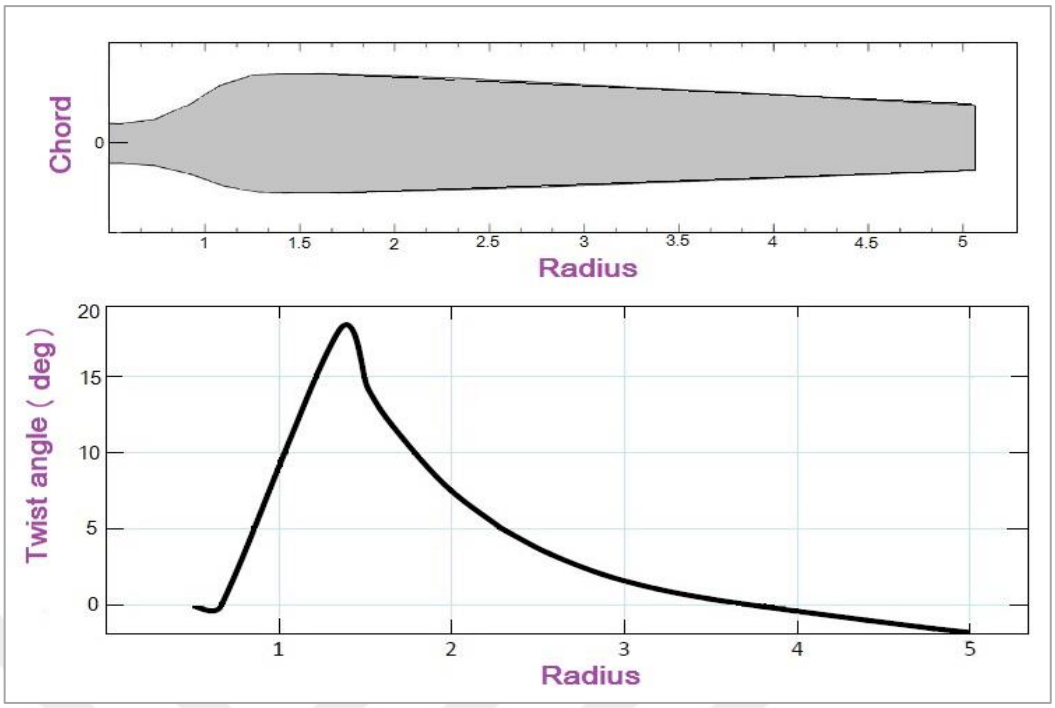

Fig. 4.7 NREL VI blade twist distribution. [34]

4.2.2.3. Risoe Wind Turbine

Risoe wind turbine is the last application. This one come with three bladed HAWT, turned and decreased blades. In Risoe wind turbine, NACA 63-2xx arrangement airfoils are utilized. Risoe wind turbine has root harmony of 1.09 m and tip harmony of 0.45m, distance across of 10.06 m, rotational speed is 35.6 - 47.5 RPM for every wind speed, the blade pitch angle is 1.8° settled along the blade and appraised power 100 kW [31]. Risoe wind turbine General attributes shown in Table 4.3 and qualities geometrically in Fig. 4.8.

Table 4.3 General characteristics of Risoe wind turbine. [31]

Number of Blades	3
Turbine diameter	19.0 m
Rotational Speed	35.6 and 47.5 rpm
Cut-in wind speed	4 m/s
Control	Stall Control
Rated power	100 kW
Root extension	2.3 m
Blade set angle	1.8 degrees
Twist	15 degrees (max.)
Root Chord	1.09 m
Tip Chord	0.45 m
Airfoil	NACA 63-2xx Series

In Risoe wind turbine, *Cl* and *Cd* airfoils coefficients for other attack angle and different Reynolds number values are presented in Appendix [C].

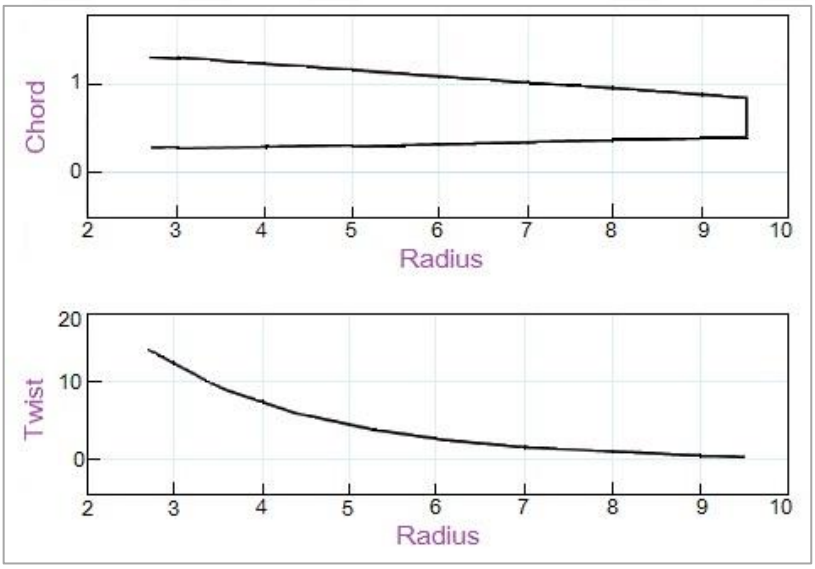

Fig. 4.8 Geometry information of Risoe wind turbine. [31]

4.3. Wind Turbine Performance Analysis Using BEM Theory

In all circumstances, Blade Element Momentum examination instruments are utilized for 2 destinations. The aim is demonstrating the typical Blade Element Momentum investigation that the computation system incorporates some essential parameters as hub and extraneous stream enlistment variables, thrust and torque for every blade element, power coefficient, turbine productivity, *Cl* and *Cd* coefficients. And so forth. Other reason for existing is to demonstrate the impact in power creation, when the estimation of (BEM) Applied without its adjustment factor as tip loss factor.

4.3.1. Iteration method

Wind turbine execution examination with BEM theory is the expectation of hub and unrelated stream enlistment factors (a and a'), point of assaults, thrust for every blade element independently and the other imperative parameters. To do this, enlistment factors are should have been computed earliest that are an iterative process. Comparable techniques are in [35] is utilized because of this reason. The principle ventures of the iterative technique utilized as a part of this investigation are below [14]:

a. Divide the blades into 15-20 numbers of span-wise elements.
b. Start with some guess values of a and a' (e.g. a =0 and a' =0).
c. Calculate relative wind speed (u_{rel}) and relative inflow angle (ϕ) using Equations (3.47) and (3.48) for all the elements.
d. Determine the value of angle of attack α using Eq. (3.80) for the given local twist angle β of each element.
e. Calculate Reynolds number for each of the element using Eq. (3.81)
f. Look up the values of lift and drag coefficients (C_L and C_D) for the given airfoil at the calculated values of angle of attack and Reynolds number.
g. Calculate the blade loss factor F and thrust coefficient by using Equations (3.82) and (3.92).

h. Once the thrust coefficient and tip loss factor is calculated, the axial induction is calculated. If $C_T > 0.96F$, then the blade is highly loaded and modified Glauert correction is applied by using Equation (3.90).

i. Calculate the value of (a') by using Eq. (3.88).

j. Calculate the differences between updated $(a \text{ and } a')$ and previous guesses, If differences > 0.01 Continue iteration by replacing initial values with updated ones, If differences <0.01 Take updated $(a \text{ and } a')$ as actual values for considered blade element.

k. Finally calculate the power coefficient using Eq. (3.89).

Something else, the blade is gently stacked and standard BEM theory is utilized Eq. (3.87). Extraneous enlistment factor is computed specifically from BEM theory Eq. (3.88). This figuring technique is an iterative procedure which is portrayed in Fig. (4.9) beneath. Circle closes when the coveted exactness is accomplished in enlistment factors and the strategy is associated for each blade element. Once the acknowledgment factors are torque, ascertained and thrust of each blade element are found from the Eq. (3.53) and (3.55). [29]

Amid the cycle procedure, lift and drag coefficients are given as commitment to the program. For each blade element, airfoil information is required with congruity and curve regards. Lift and drag coefficients must be given concurring diverse to approach rate. The emphasis and power computation strategy clarified here is coded by utilizing MATLAB programming. BEM examination instrument predicts the wind turbines execution as indicated by the given variables geometrically as in Fig. (4.9) as information sources box. BEM examination instrument is approved with the exploratory information got from writing which is clarified in the following segment.

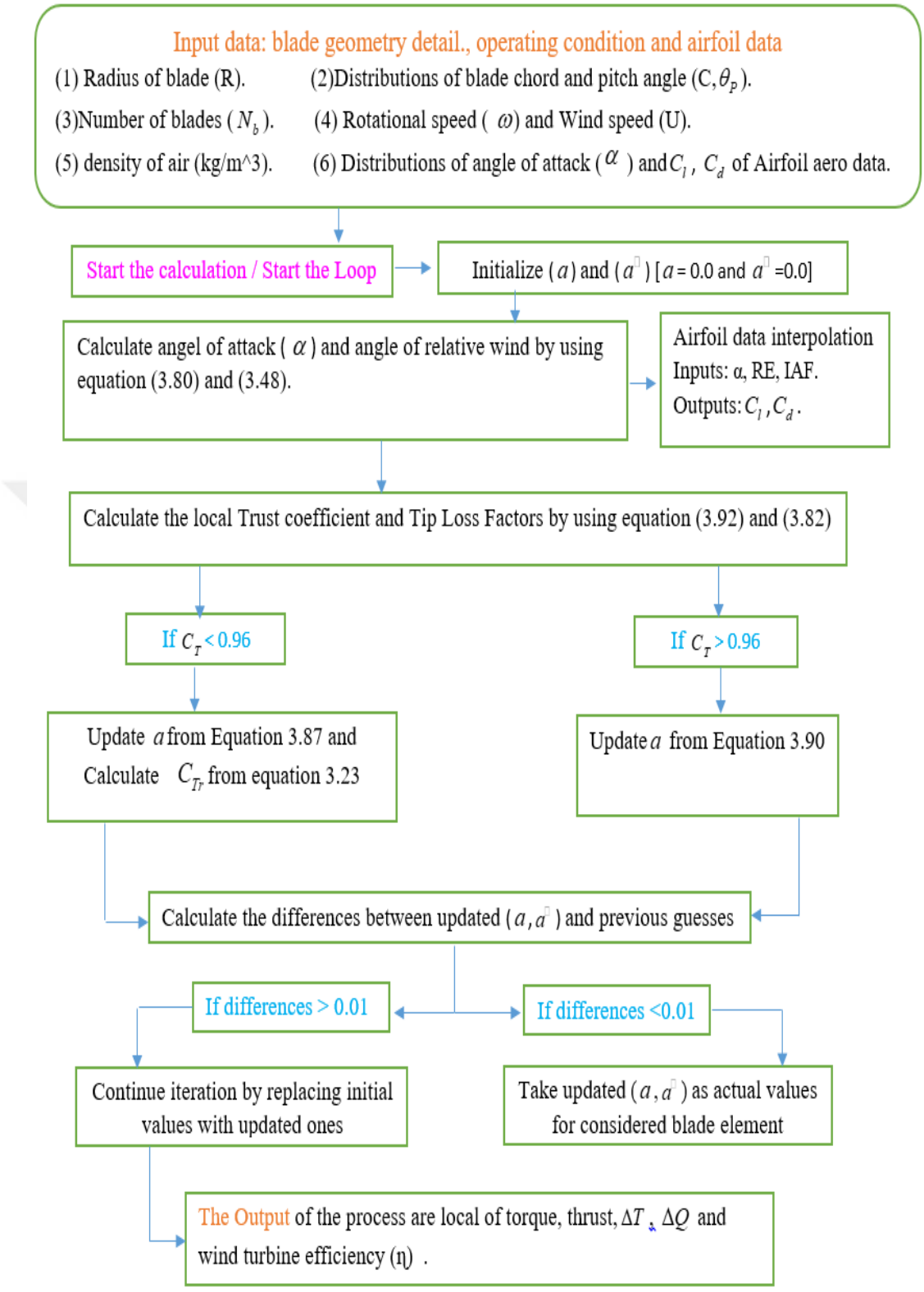

Fig. 4.9 The flow chart of iterative procedure based on BEM theory

4.4. Modified Blade Element Momentum Theory (BEM) Comparison

4.4.1. BEM analysis of wind turbine which has NACA 63 (4)-221 Airfoil type, are compare with NERL phase II and VI and Risoe wind Turbine experimental test.

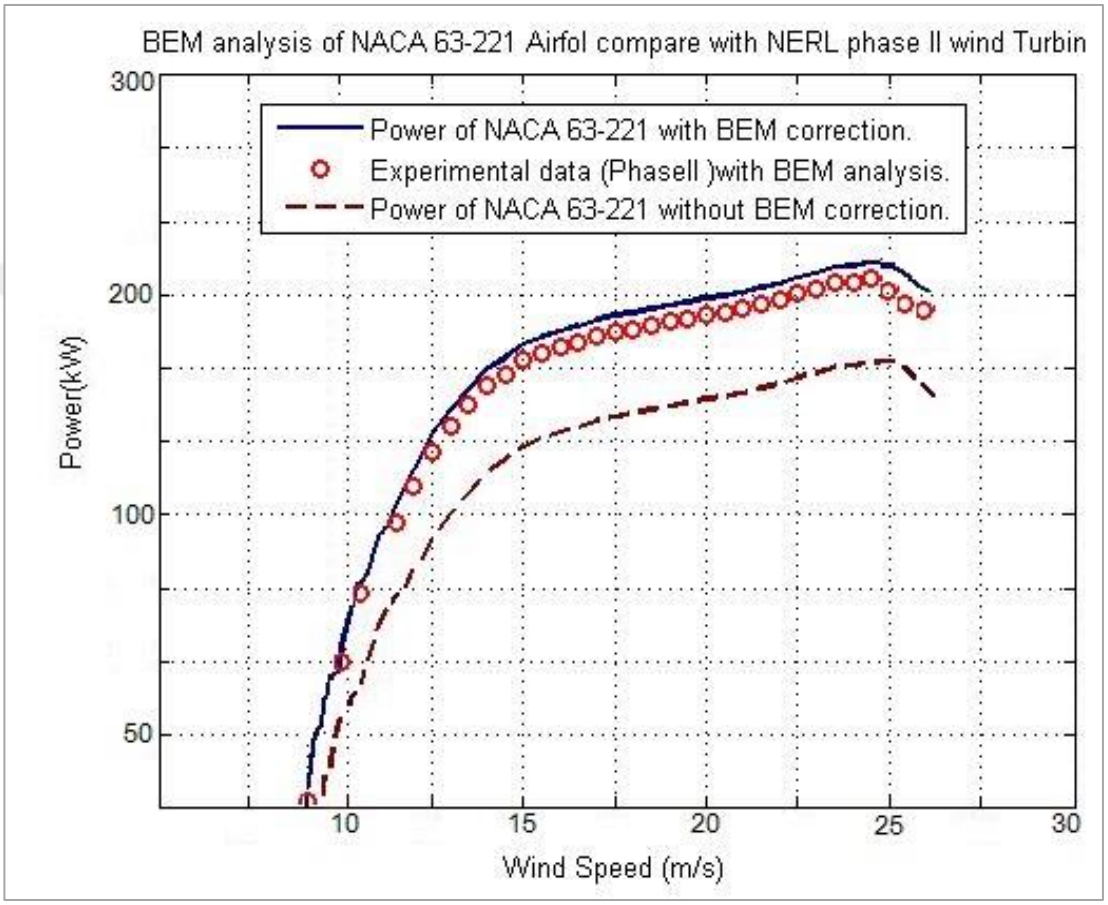

Fig. 4.10 compare the results of BEM analysis with (NREL) Phase II

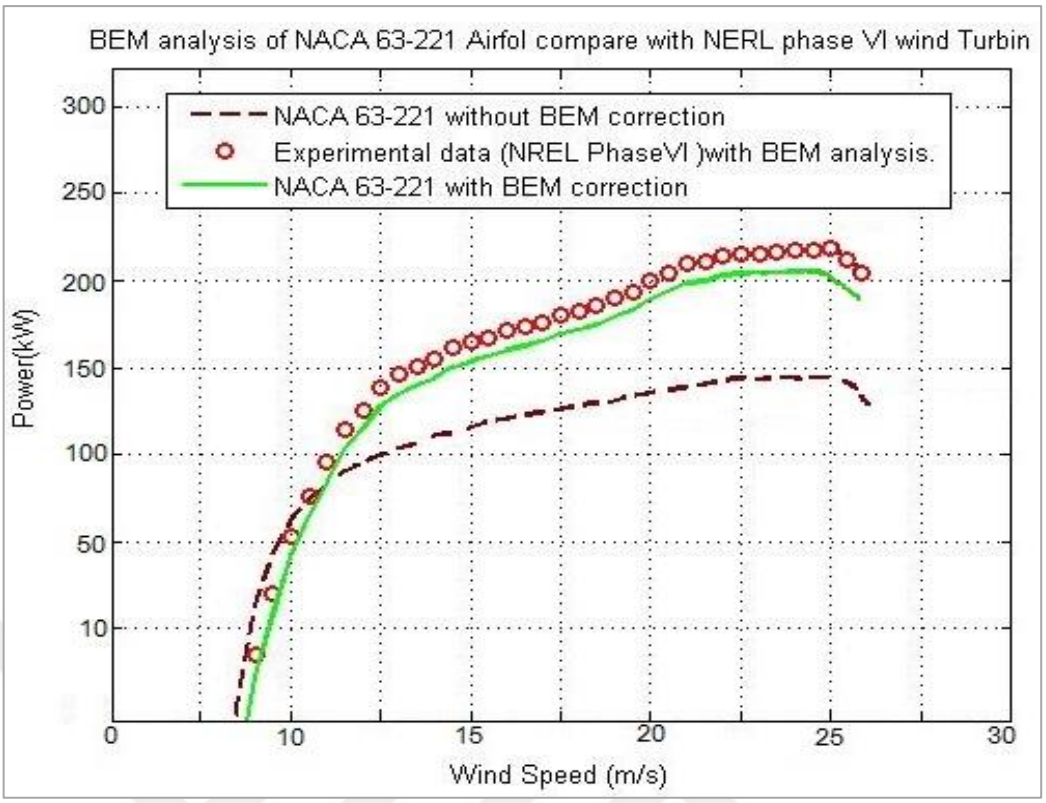

Fig. 4.11 compare the results of BEM analysis with (NREL) Phase VI

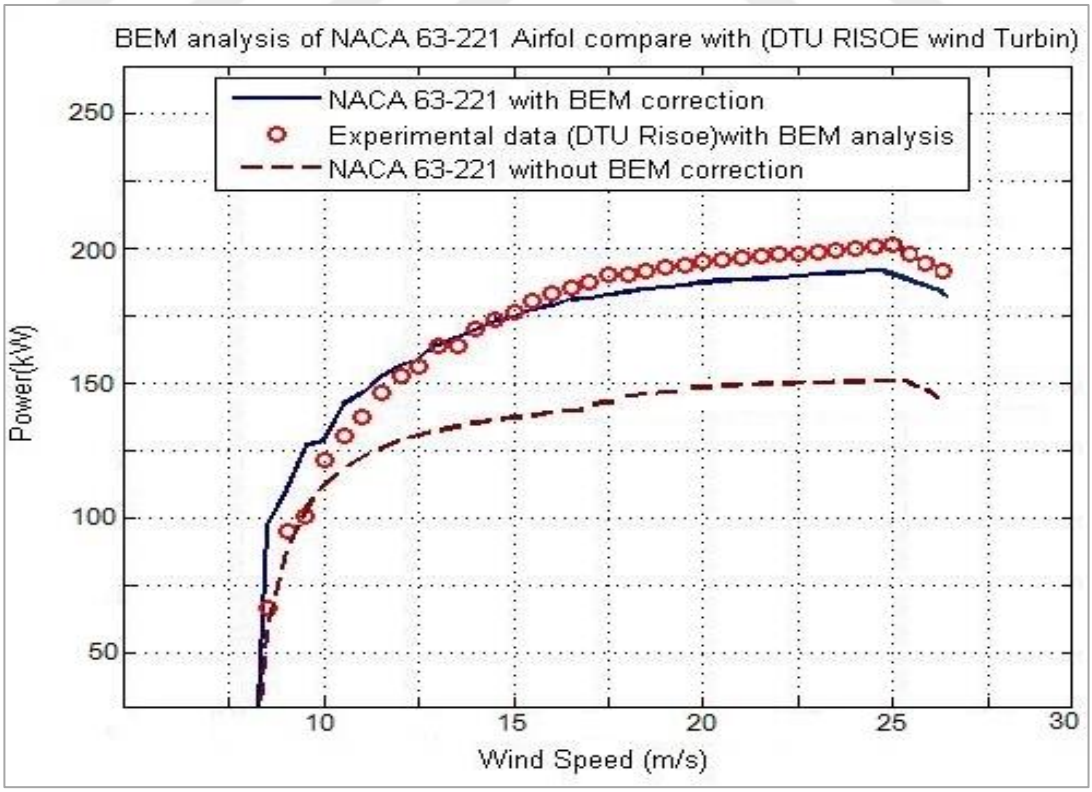

Fig. 4.12 validation the results of BEM analysis with (NLSE) Risoe wind turbine

In all the cases, wind turbine using NACA 63(4)-221 airfoil are analyzed with BEM analysis tool, for different wind speeds power production of the wind turbine is calculated. This analysis was with and without correction factors. Two different analysis results are compared with two experimental test cases which are (NERL phase II, VI). Moreover, validation the results of BEM analysis was only with (NLSE) Risoe wind turbine because, they have the same airfoil type. Modified BEM prediction was successful with using both of Glauert empirical and Prandtl tip loss correction factors, because there is only a delta difference between analysis and test results for all wind speeds. Whereas, in the analysis without the correction factors was poor prediction of the power performance

Consequently, the cut-in speed and the capability of the wind turbine may moreover be upgraded by diminishing the frictional misfortunes from the course and the rigging get ready. The rigging gets ready and bearing can be avoided if the generator is particularly connected with the wind turbine. In any case, this presents challenge similarly as accomplishing needed cycles each minute (rpm) of the rotor shaft. In this way, picking a small size generator with the low beginning torque and high voltage-to-rpm proportion is a key progress. Deciding the rigging proportion is another basic propel which ought to be done when the power transmitting gearbox is unavoidable. Apparatus proportion depends upon the extent of speed and torque required by the generator to perform for the most part capably. Once in a while, size of the nacelle also confines the measure of the apparatus enclose and this way the rigging proportion. Cost, clatter and unwavering quality in operation are the three crucial parts which should in like manner be considered while settling the sort and setup of gearing system.

Chapter Five

ROTOR DESIGN AND PERFORMANCE ANALYSIS

5.1. Introduction

In this section, BEM theory will be connected to design the rotor blade and to anticipate its streamlined execution. The prologue to rotor design focusses on the Blade Element Momentum (BEM) technique, and this is trailed by a clarification of how choices are come to concerning rotational speed, rotor estimate, rotor power and number of blades, what the design imperatives are, and how the rotor design is assessed. Some important geometrical constraints for wind turbine blades that should have been modified. The most vital among them are the bend point, blade edge, decreasing edge, harmony length, robustness, and number of blades.

5.2. Airfoil Terminology and Airfoil Classification

Airfoil design has come a long way since the early days of their inception and therefore many different airfoil types have been designed to suit a multitude of unique wind turbine blade, propeller, and aircraft wing designs. The general approach to selecting airfoils for a wind turbine rotor is to utilize at least two different airfoil types to provide for two key goals, structural and aerodynamic performance. The first goal is to have a structurally sound blade, which necessitates the use of a thicker airfoil to withstand the large bending moment caused by the aerodynamic and intrinsic gravity loads exerted on the blade during the wind turbine's operation at the root of the blade. The second goal is to be as aerodynamically efficient as possible at the outer blade sections in order to generate the required lift force with as little wind speed, and therefore available power, as possible so as to allow for power generation to occur at low wind speeds. [31]

Various terms are utilized to portray an airfoil, as introduced in Fig. 5.1 the mean camber line is the locus of focuses somewhere between the upper and lower surfaces of the airfoil. The most forward and rearward purposes of the mean camber line are

on the main and trailing edges, individually. The straight line associating the main and trailing edges is the harmony line of the airfoil, and the separation from the main to the trailing edge measured along the harmony line is designated as the chord C of the airfoil. The camber is the separation between the mean camber line and the harmony line, measured opposite to the harmony line. The thickness is the separation between the upper and lower surfaces, additionally measured opposite to the harmony line. At last, the approach α, is characterized as the angle between the relative wind and the harmony line. Not displayed in the Figure is the traverse of the airfoil, which is the length of the airfoil opposite to its cross-area. The geometric parameters that affect the airfoil streamlined execution includes: mean camber line, main angle span, most extreme thickness and profile appropriation and trailing edge. [31]

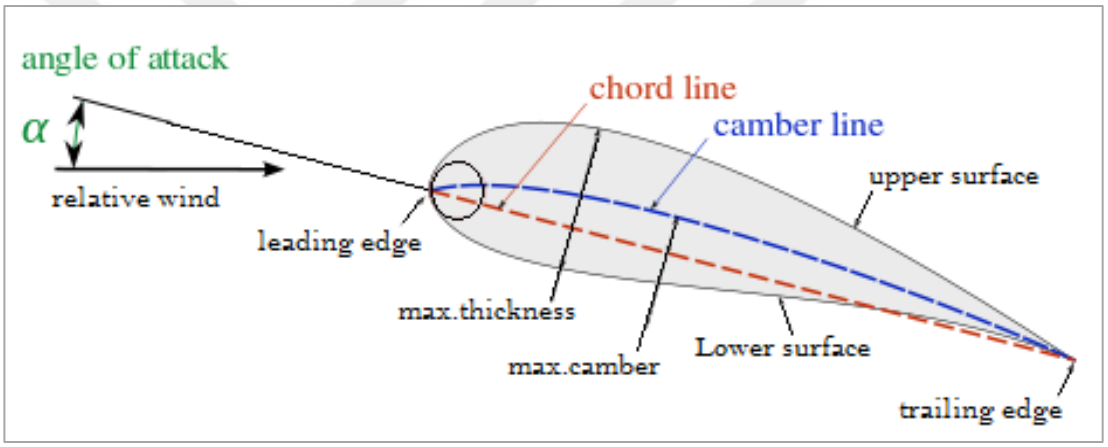

Fig. 5.1 Critical airfoil design parameters. [36]

More often than not, measurements connected by airfoils are agreed by way of referenced of chord length. Thickness of airfoil is normally spoken to by greatest thickness level for airfoil identified with chord. Camber of the airfoil additionally has comparative description, likewise it spoken to through most extreme camber rate identified with chord.

5.3. The basics Aerodynamics of Airfoils

Stream over of airfoil makes conveyed constrain on airfoil. At a point when stream ignores the higher or raised cross of an airfoil, stream speed builds which have

diminishes of weight following up at first glance. Then again, stream speed diminishes when it is passing on the lower (for the most part curved) surface of airfoil and accordingly, weight on this surface increments.

In addition, grating amongst air and airfoil surface exists and wind current speed diminishes after it compasses for surface of airfoil. The weight contrasts also, erosion make a net power and moment on airfoil. The net power following up on an airfoil is partitioned into two segments as drag compel and lift power. Lift force is segment of net power on airfoil opposite to stream course. The force of drag constrain is the segment for the net power on the airfoil parallel the stream heading. The moment of following up on chord of quarter is termed equally pitching moment. [31]

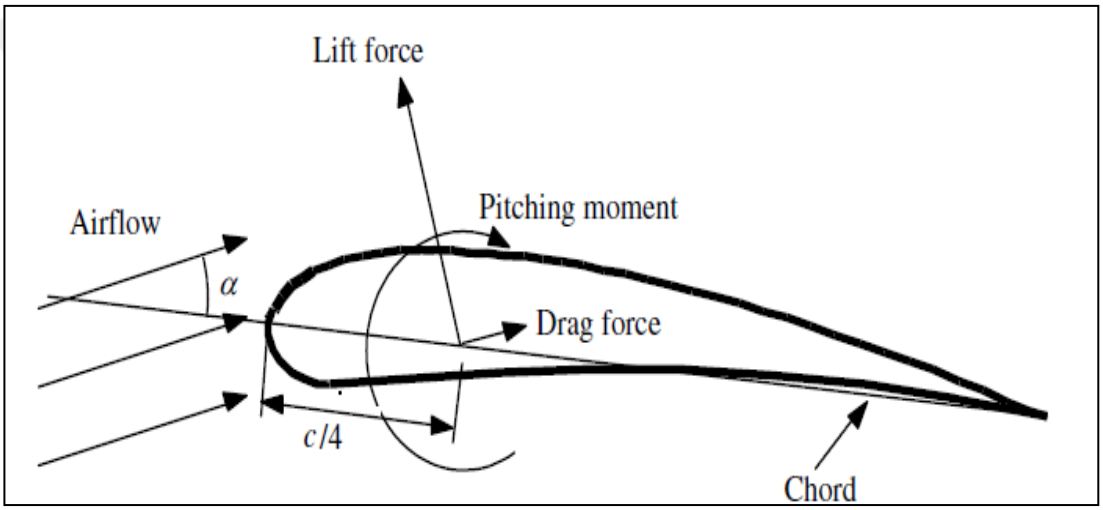

Fig. 5.2 Drag and lift forces on stationary airfoil α angle of attack C chord. [26]

These forces and pitching moment calculations are illustrated in Eq. (5.1), (5.2) and (5.3).

$$Lift = l = C_l \frac{1}{2} \rho U^2 c \tag{5.1}$$

$$Drag = d = C_d \frac{1}{2} \rho U^2 c \tag{5.2}$$

$$Moment = m = C_m \frac{1}{2} \rho U^2 c \tag{5.3}$$

In this Eq. *Cd* is drag coefficient, *Cl* is airfoil lift coefficient *Cm* is the moment coefficient, C is the chord size.

Stream transitory on surface of the airfoil isn't generally the similar. Identified with impacts, for example, speed, temperature, air surrounding weight, thickness, and the length of airfoil and so on. Stream has diverse attributes. Subsequently, powers and moments on an airfoil are extraordinary. A large portion of these impacts are spoken to by a no dimensional number which named as soon as Reynolds Number Which are ratio of latency powers done gooey powers. Reynolds number is ascertained with Eq. 5.4. [36]

$$\mathrm{Re} = \frac{UL}{v} = \frac{\rho UL}{\mu} = \frac{Inertia\ forces}{Viscous\ forces} \tag{5.4}$$

In this definition, *L* and *U* are reference length and velocity, μ is dynamic consistency, ρ is liquid thickness and v is kinematic thickness. Reynolds number essentially speaks to appeal of stream and affects the power coefficients. For airplane requests, Reynolds numbers are normally high, considerably more than that a couple of lots. Be that as it may, in wind turbine applications Reynolds numbers are typically low (with the exception of gigantic wind turbines), not as much as a million or just a couple of millions, then the wind speeds are low. This implies airfoils are design for high Reynolds numbers may be not reasonable for low Reynolds number applications. To design the wind turbine, genuine attributes of airfoil must be recognized and choice ought to be finished by allowing for these impacts. [31]

5.4. Rotor Sizing

Before beginning, design wind turbine, some snippets of data are required for appraise a span of imminent of wind turbine. To start with, the required power coefficient output and, the normal speed of the wind the area where it may be introduced. The width (D) of the turbine can be computed utilizing the accompanying articulation:

$$D = \sqrt{\frac{8P}{\eta\rho\pi u_{\infty}^{3}}} \tag{5.5}$$

Begin by deciding what required power output (design power) P_d is needed at a particular rated wind speed U_d first step in wind rotor design process is concerned with the determination of the rotor diameter. However, to do even this, one still required to know other design parameter, namely design power coefficient C_{Pd}, generator and gear-train efficiencies η_g and η_t, respectively.

The available wind power in flow stream of cross section area A_s is given in Eq. (2.8), but not all of this power may be extracted. The actual electrical power is affected by the rotor coefficient and by efficiency of the mechanical transmission system η_t and the generator itself η_g thus the actual electrical power P can be expressed in the form:

$$P_w = \frac{1}{2} \rho \, U_\infty^3 \, A_s \, C_p \, \eta_t \, \eta_g \qquad (5.6)$$

Now, in almost any design procedure, a design operating point is normally selected. As far as wind rotor design concerned, this point is usually the design operating condition. Hence Eq. (5.6) rewritten as:

$$P = \frac{1}{8} \rho \pi \, D^2 \, U_d^3 \, C_{Pd} \, \eta_g \, \eta_t \qquad (5.7)$$

Where the subscript "d" refers to the design condition. Therefore, the rotor diameter D can be easily determined once P_d, U_d , η_t and η_g are specified. As to C_{Pd} a value is selected based on experience.

5.5. Blade Design Procedure

Methodology starts by decision for different parameters of rotor as show in area (5.4) and the decision of an airfoil. An underlying blade shape (chord dissemination and contort circulation along the blade length) is then decided utilizing the optimum blade shape. The last blade shape and execution are resolved iteratively.

5.5.1. Input design data

In order to start the design process, a number of input data have to specified, namely:

- Design output power P_d : The design output power (power requirement) for the proposed rotor has been selected to be 50kw.
- Design wind speed U_d : By considering mean wind speed for Elspiaa 7.48 m/s for data of year 2013 at height of 40m, and 7.98 m/s for data of year 2014 at height of 40m, then the wind speed suitable design is 11.97 m/s. Knowing the design wind speed is usually 1.5 times the average wind speed $U_d \approx 1.5\ U_a$ [37].
- Blade cross-section: The airfoils NACA 63(4)-221, has been selected. The drag coefficient and also lift coefficient versus angle of attack (from -0° to 180°) for different values of Reynolds number are presented in the last chapter. It is presented that the maximum lift coefficient at stall increases as Reynolds number increases. The lift coefficient and drag coefficient are nearly independent of the Reynolds number at high incidence.
- Design tip speed ratio λ_d : According to the application of wind turbine, the value of the design tip speed ratio should be in the range of $4 < \lambda_d < 10$ [26]. In this study λ_d was taken as ($\lambda_d = 7$).
- Design power coefficient C_{Pd} : Based on the practical experience, the value of power coefficient C_{Pd} , varies in the range 0.4 to 0.45 [38]. In the present wind rotor, the design power coefficient has been selected to be 0.45 ($C_{Pd} = 0.45$).
- The mechanical transmission (gear-train) efficiency η_t and the generator characteristics in items of the generator efficiency η_g would be taken into account. For the present wind rotor, it was assumed that: $\eta_t = \eta_g = 0.95$
- Number of wind rotor blades: According to table 5.1 the number of blades was chosen as three ($B = 3$).

Table 5.1 Suggested blade number B for different tip speed ratio λ .

λ	B
1	8-24
2	6-12
3	3-6
4	3-4
>4	1-3

5.5.2. Rotor size and blade geometry

The rotor diameter is determined by using Eq. (5.7) and based on the design input data, hence:

- The rotor diameter is D = 11.708 m.
- Rotor hub ratio was assumed to be R_h / R = 0.15.
- The rotor hub radius (R_h) will to be $R_h = 0.15 * R$ = 0.878m, then the blade length is L_b = 4.98.814 m.

Since the blade section and the rotor diameter has been determined, the blade chord and twist distribution $c(r)$ and $\theta_T(r)$ are determined using equations 3.77 and 3.79 respectively, as following:

The blade length has been divided into 8 elements, and the theory of optimum rotor used the shape to estimate the eighth blade elements at radial stations. The local speed ratio λ_r is determined for each blade element, and based on the selected design (tip-speed ratio).

- The local optimum angle relative wind at radial station is determined from Eq. 3.76.
- Based on the chosen design aerodynamic conditions, $C_{L\ design}$ and $C_{D\ design}$ such that $C_{D\ design}$ / $C_{L\ design}$ is at a minimum and α_{opt} = 10, the local chord $c(r)$ is computed by using Eq. 3.79.

- The local twist angle $\theta_T(r)$ is determined by subtracting $\theta_p(r)$ from θ_p, o by using Equations 3.77 and 3.78.
- The local solidity can be calculated from Eq. 3.56.
- The above procedure is then repeated for the rest of the blade elements from blade root (root hub) to blade tip. Then the maximum power coefficient as a function of blade geometry that can be extracted from the wind, can be calculated for optimum rotor by using Eq. 3.89.

5.6. Wind Rotor Performance

After we obtained the rotor geometry, the performance characteristics in term of power, torque and thrust coefficients $C_p, C_q,\ C_T$ respectively at different tip-speed ratio λ may then be computed. One of many methods might be chosen to predict the blade performance is iterative solution. The procedures of this method at a given radial station r/R and at a midpoint radius of r_i for each section are as following:

- Assume initial value of the axial induction factor $a(r)$.
- Based on the selected tip-speed ratio λ and for a given blade element lying at a given radial station, the local ratio λ_r is determined. Then the local angular induction factor $a'(r)$ is computed from Eq. 3.42.
- The relative wind local angle $\varphi(r)$ is calculated by Eq. 3.48, and the local tip-loss factor $F(r)$ is computed by using Eq. 3.82.
- The local angle of attack α is determined by subtracting $\varphi(r)$ from $\theta_p(r)$ moreover, knowing α leads to determined local lift and drag coefficients C_L and C_D from the airfoil lift and drag data.
- The local thrust coefficient is calculated from Eq. 3.92 and corresponding to its value a new value of $a(r)$ is determined: if C_{Tr} <0.96 update a from Eq. 3.87, and if C_{Tr} > 0.96 update a from Eq. 3.90.
- If the new local axial induction factor is within acceptable limits for the previous estimate, other performance parameters can be calculated. If not,

then the process is repeated until the newly calculated inductance induction factor is within acceptable tolerance of its predecessor.

Repetition of the above procedures for different radial stations r/R , and by using Equations 3.89 and 3.92 the values of the C_P and C_T can be computed respectively, and the torque coefficient is then computed as : $C_Q(\lambda) = C_P(\lambda) / \lambda$

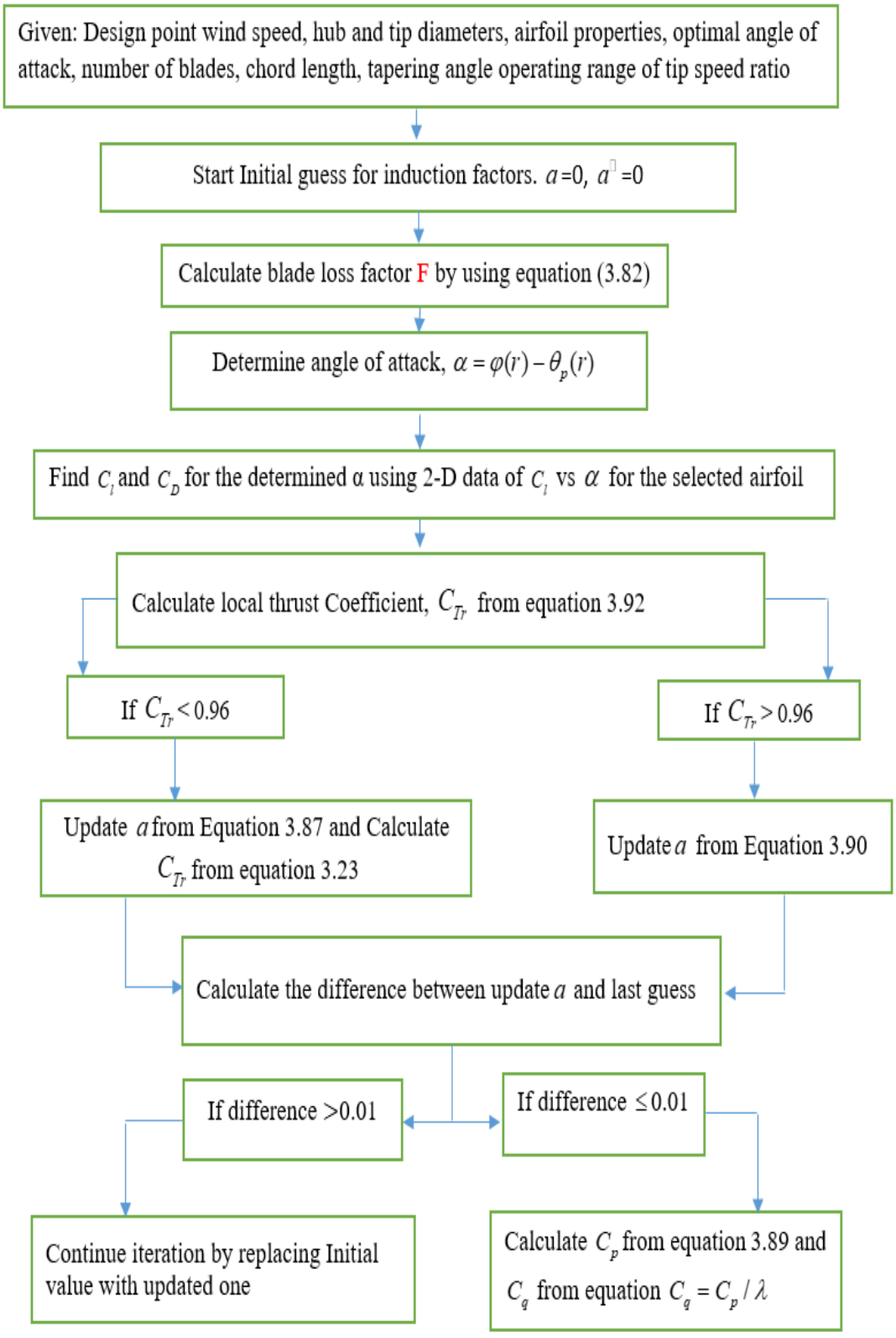

Fig. 5.3 Flow chart of iteration procedure for determining C_p, C_q, C_t coefficient.

Chapter Six

RESULTS AND DISCUSSIONS

6.1. Introduction

In this section, BEM theory will be connected to design the rotor blade and to foresee its streamlined execution.

A PC program (FORTRAN 90) has been incorporated bringing with consider the accessible info information and the required goal of the wind turbine.

The part is finished with the outcomes and logical Figures demonstrating the impact of a few parameters identifying with the blade design.

It ought to be noted here that different strategies [39] [40] [41] for blade design of HAWT with rotor foreseeing execution has been examined with critical ideas [17] [42] for design strategy have been utilized while building up the PC program to blade design.

6.2. Results of Blade Performance

After the rotor geometry has been obtained, and implementation of the iterative solution method, we can see the prediction of blade performance.

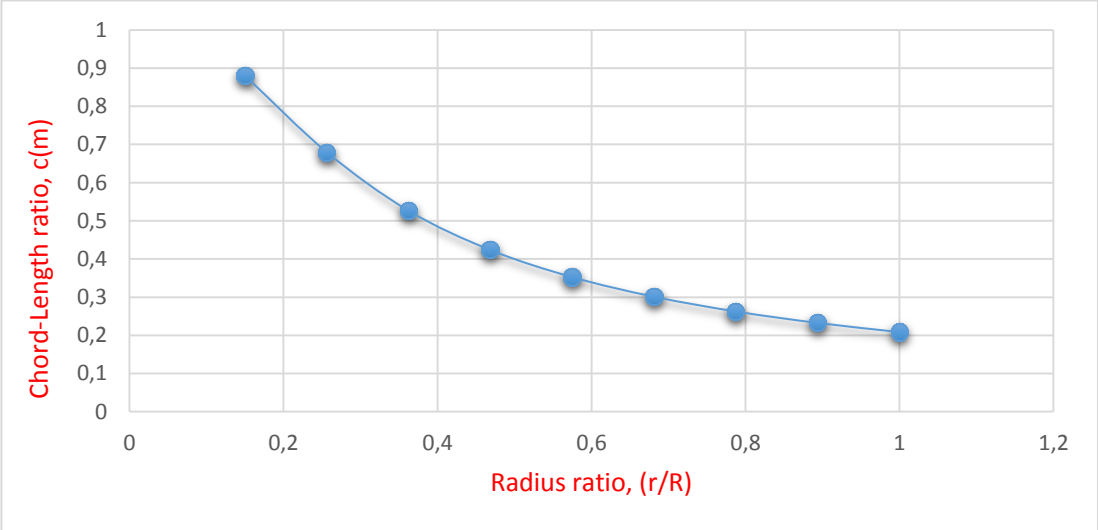

Fig. 6.1 The designed blade Chord-length distribution

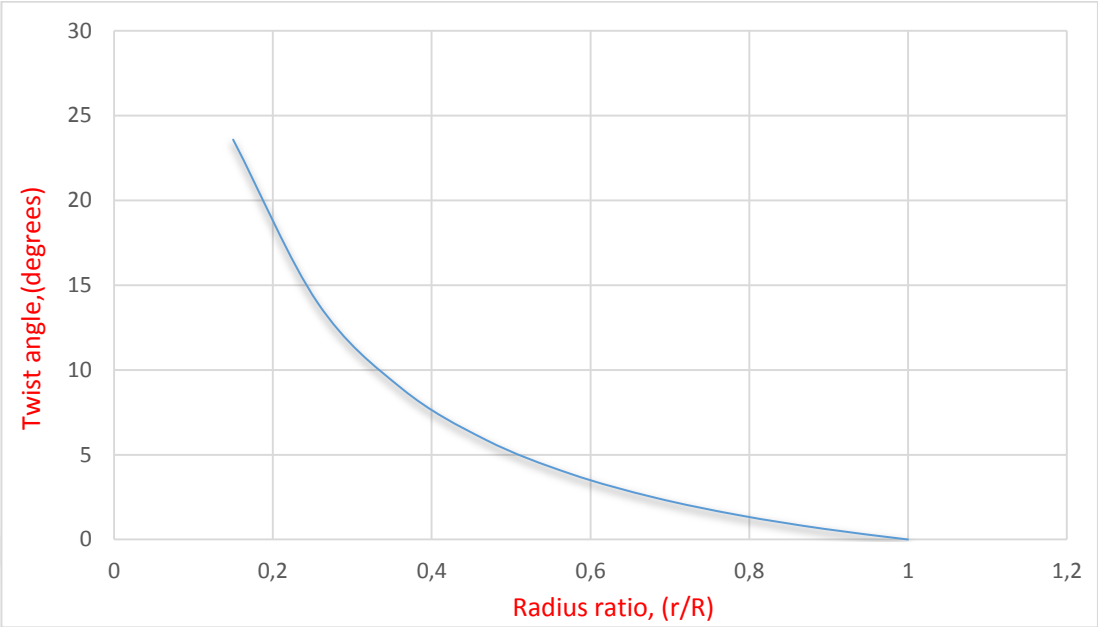

Fig. 6.2 Twist distribution for the designed blade

Fig. 6.1 and 6.2 present the resulting chord and twist distributions. Moreover it may be shown as the twist angle diminishes progressively from blade root to tip in a non-linear form with $\theta_T(r)$ taking its maximum ($\theta_{T,\max}$ = 23.591°) and minimum ($\theta_{T,\min}$ = 0°) value at blade tip with maximum chord ($C_{\max}$ =0.880) and minimum chord ($C_{\min}$ =0.208) occurring at blade root and tip, respectively. Moreover, Fig. 6.3, 6.4 and 6.5 present rotor performance in terms of power, torque and thrust coefficients, and as a function of tip-speed ratio respectively. These results were obtained by a computer program written on the basis of the performance analysis presented above.

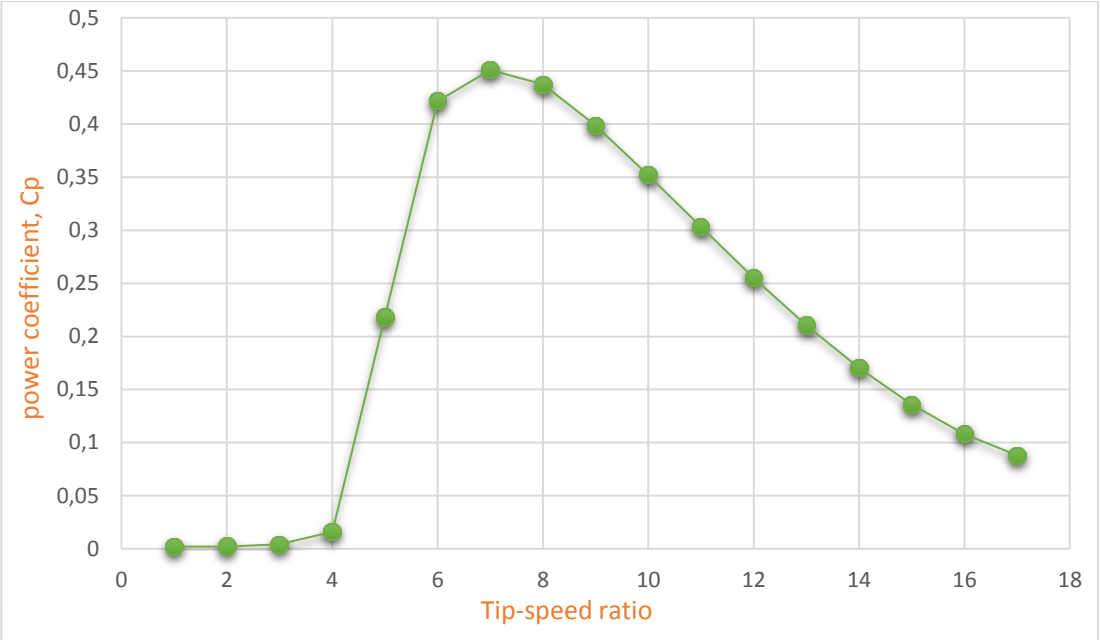

Fig. 6.3 Variation of power coefficient with Tip-speed ratio for optimum blade

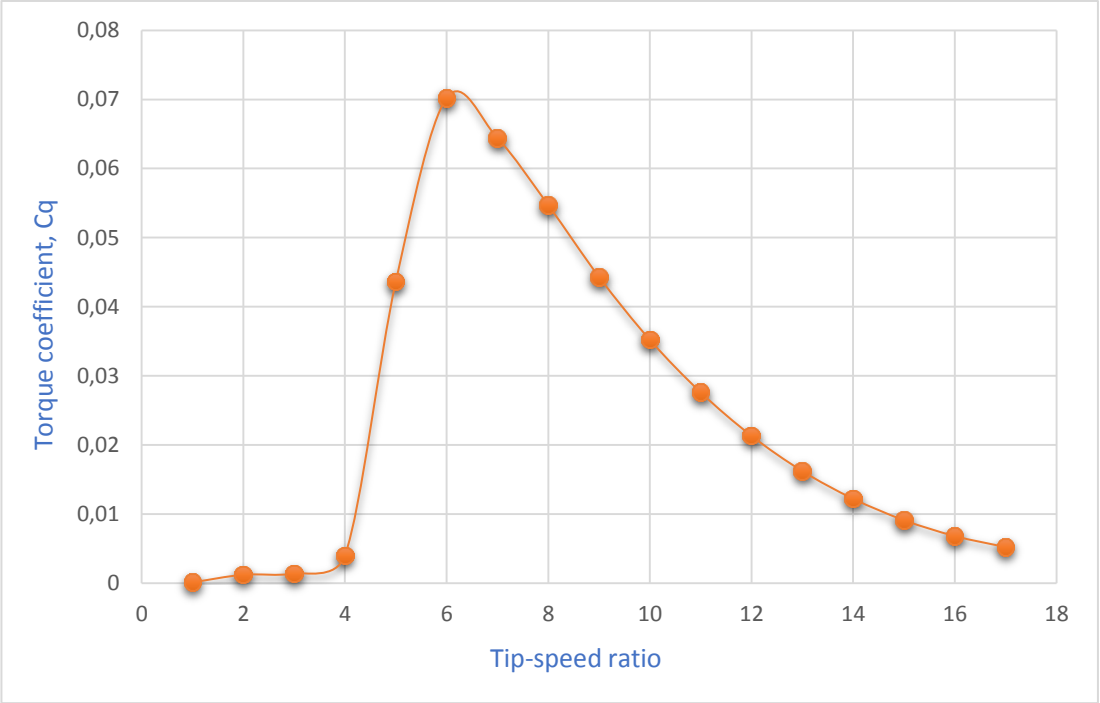

Fig. 6.4 Variation of torque coefficient with Tip-speed ratio for optimum blade

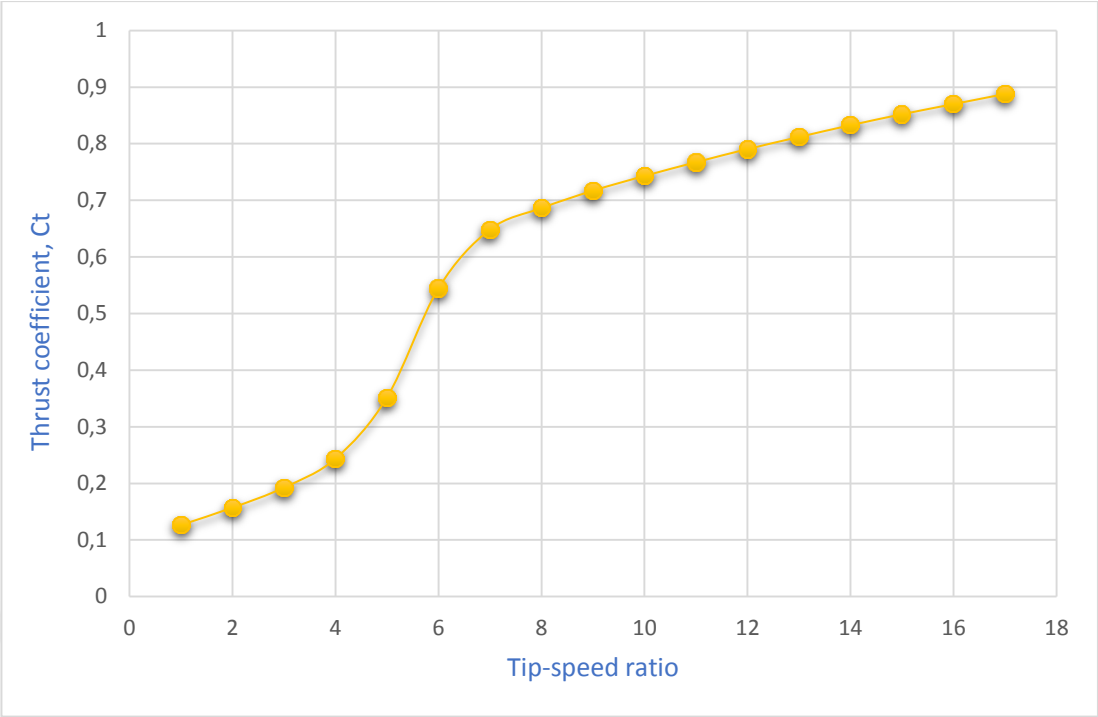

Fig. 6.5 Variation of thrust coefficient with Tip-speed ratio for optimum blade

Fig. 6.3, 6.4 and 6.5 present rotor performance in terms of power, torque and thrust coefficients C_P , C_Q and C_T as a function of tip-speed ratio λ respectively. These results were obtained by a computer program written on the basis of the performance analysis presented above.

The variation of power coefficient with tip-speed ratio is presented in Fig. 6.3. It is clear from this Fig., that at low values of tip-speed ratios the power coefficient C_P increases sharply as the tip-speed ratio increases, due to stall. The rate of increasing starts to diminish at $\lambda \approx 6$. Note that C_P reaching a maximum value at $\lambda \approx 7$ which is about the same value of the selected design tip-speed ratio λ_d, due to tip-losses effect. Further increasing of λ beyond 7, C_P decreases, due to drag losses. Moreover, an acceptable value of power coefficient is obtained in the range of $4 < \lambda < 10$.

Fig. 6.4 shows that $C_Q(\lambda)$ follows the same trends the case of $C_P(\lambda)$ with a maximum value of C_Q is shifted to the left occurring at $\lambda \approx 6$.

Fig. 6.5, indicates that the rotor thrust coefficient increases rapidly at lower tip-speed ratio until $\lambda \approx 7$, due to stall and tip-losses effects. Then it is increases steeply at λ more than 7 whereas the thrust maintain its highest value, due to drag losses.

6.3. Design Output Data

Table 6.1 Blade chord and twist distribution for an optimum Three-Bladed HAWT

Radius ratio	Radius	Local tip-speed ratio	Chord length	Chord length ratio	Twist angle	Solidity
r/R	r(m)	λ_r	c(m)	c/R	θ_T	σ
0.1500	0.9151	1.05000	0.87997	0.2077	23.591	0.45803
0.2562	1.5633	1.79375	0.67943	0.16039	13.972	0.20701
0.3625	2.2114	2.53750	0.52597	0.12417	8.897	0.11328
0.4687	2.8596	3.28125	0.42317	0.0999	5.865	0.07048
0.5750	3.5078	4.02500	0.35213	0.08313	3.872	0.04781
0.6812	4.1560	4.76875	0.30078	0.07101	2.469	0.03447
0.7875	4.8041	5.51250	0.26216	0.06189	1.431	0.02599
0.8937	5.4523	6.25625	0.23217	0.05481	0.633	0.02028
1.0000	6.1005	7.00000	0.20823	0.049157	0.000	0.01626

(Airfoil NACA 63-221 $C_{L,design}$ =1.1, α_{design} = 10, γ = 0.0166)

Table 6.2 Modified blade (optimum chord-linearized twist) for a Three-Bladed HAWT

Radius ratio	Radius	Local tip-speed ratio	Chord length	Chord length ratio	Twist angle	Solidity
r/R	r(m)	λ_r	c(m)	c/R	θ_T	σ
0.1500	0.9151	1.05000	0.87997	0.2077	16	0.39062
0.2562	1.5633	1.79375	0.67943	0.16039	14	0.20454
0.3625	2.2114	2.53750	0.52597	0.12417	12	0.12755
0.4687	2.8596	3.28125	0.42317	0.0999	10	0.08545
0.5750	3.5078	4.02500	0.35213	0.08313	8	0.05892
0.6812	4.1560	4.76875	0.30078	0.07101	6	0.04066
0.7875	4.8041	5.51250	0.26216	0.06189	4	0.02733
0.8937	5.4523	6.25625	0.23217	0.05481	2	0.01716
1.0000	6.1005	7.00000	0.20823	0.049157	0	0.00916

(Airfoil NACA 63-221 $C_{L,design} = 1.1$, $\alpha_{design} = 10$)

6.4. Effect of Some Parameters Relating to the Blade Design

6.4.1. Effect of solidity on wind rotor performance

Solidity is critical constraints that impacts the coefficient of wind turbine power. Increment by strength influences a wind turbine optimal design in two different ways. Higher robustness gives more noteworthy region of blade surface for wind with this manner they build streamlined torque. Be that as it may, drag incited losses additionally increment with increment in strength.

Fig. 6.6 demonstrates the impact of strength (number of blades) with variety of the blade chord agreeing the Eq. 5.74 on power coefficient. The outcomes demonstrate that the greatest power coefficient increments as the quantity of blades increments, in light of the fact that the drag losses diminish as the strength increments. Likewise, for number of blades between 3 and 5 creates a limited execution curve with a sharp pinnacle making the turbine extremely touchy to tip-speed ratio changes and, optimum strength gives off an impression of being accomplished with three blades.

While for the tip-speed ratio under 6 and more prominent than 12 the impact of strength is disregarded, because of different parameters are very consequences for power coefficient.

The impact of robustness on torque coefficient is appear in Fig. 6.7. The torque coefficient is gotten from the power coefficient. The pinnacle of the torque curve happens at a lower tip-speed ratio than the pinnacle of the power curve.

At long last, the impact of strength on thrust coefficient for the adjusted blade shape is introduced in Fig. 6.8. The thrust coefficient on the rotor diminishes with expands strength. While for the tip-speed ratio more prominent than 6 the impact of strength is disregarded, because of impacts of different parameters, for example, drag losses, tip losses and variety of pitch edge.

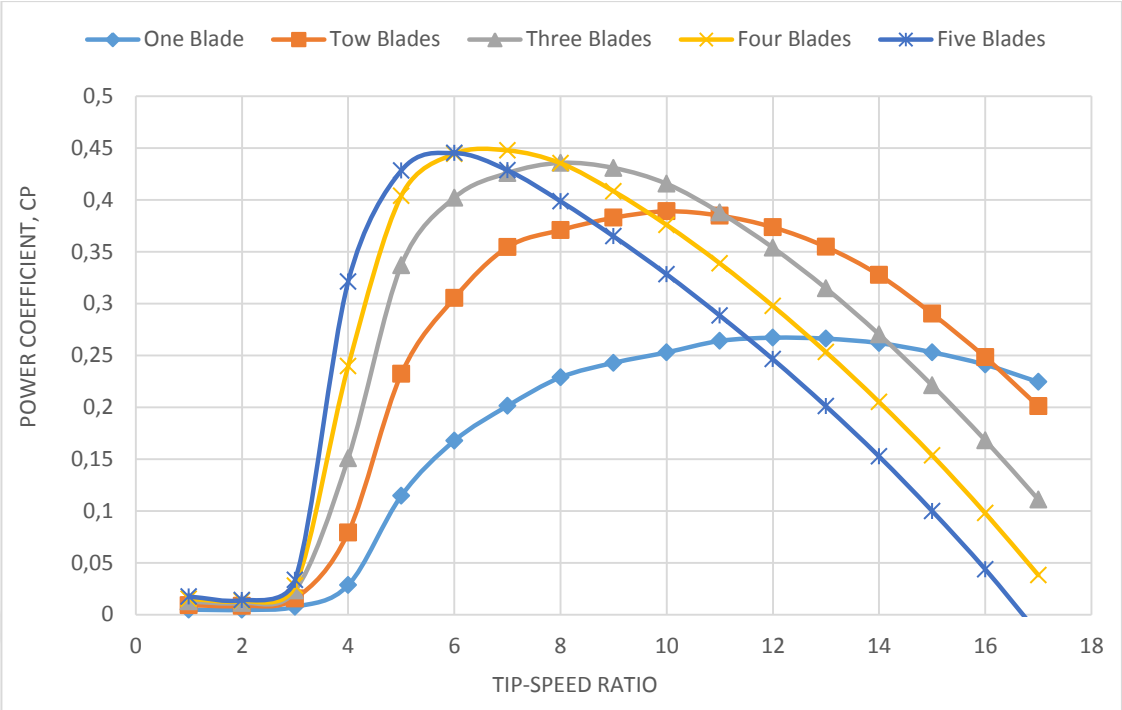

Fig. 6.6 Effect of solidity on power coefficient the case of optimum blade

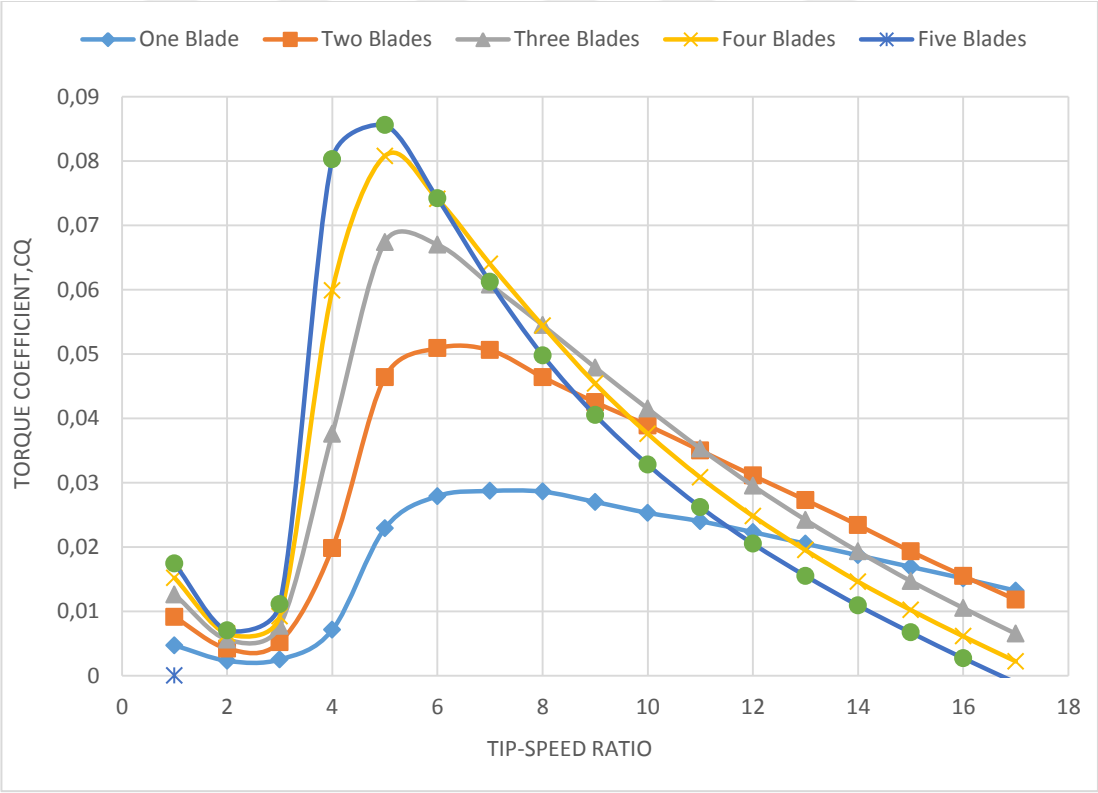

Fig. 6.7 Effect of solidity on torque coefficient the case of optimum blade

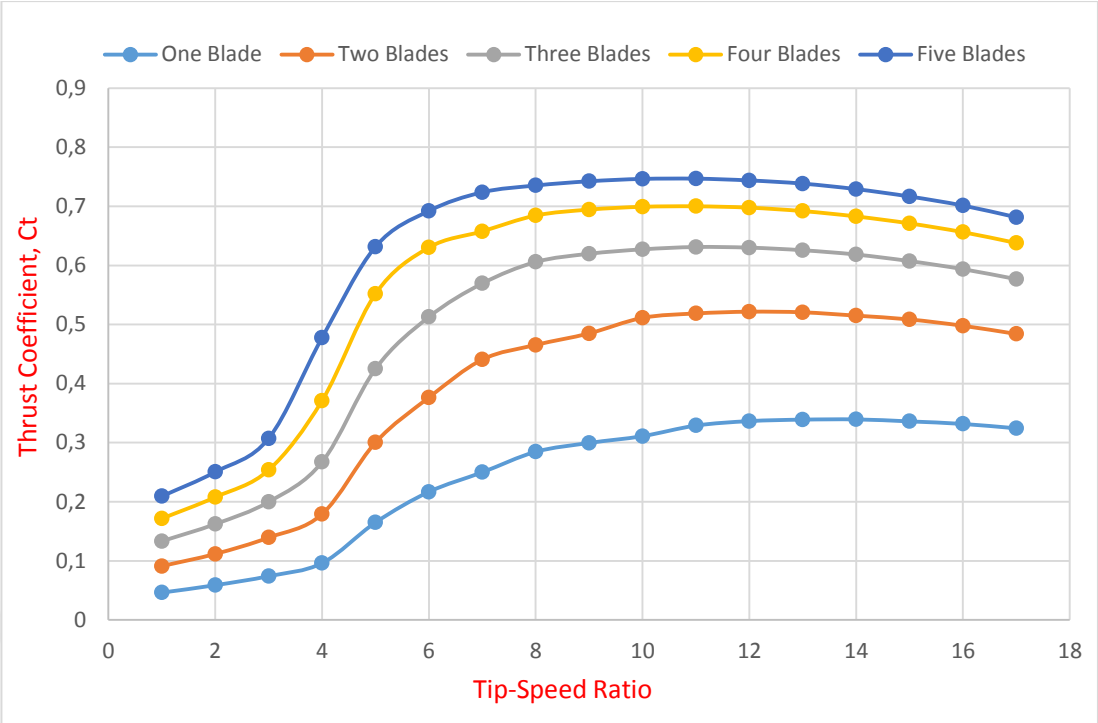

Fig. 6.8 Effect of solidity on thrust coefficient the case of optimum blade

6.4.2. Effect of Tip-Losses on wind rotor performance

Fig. 6.9 illustrates tip losses impact on greatest coefficient of power. Unmistakably the tip-losses diminish the most extreme power coefficient. While for the tip-speed ratio under 6 and more prominent than 9 the impact of Tip-Losses is disregarded, because of different parameters are consequences for power coefficient. Likewise, Fig. 6.10 demonstrates the impact of tip loss that happens just at the furthest parts of the blades on the grounds that the weight on blade suction side are low more than inside of pressure that reasons for pivotal stream acceptance factor a is larger at the external parts of the blade at that point, the inflow angle will be small and the lift power will be practically typical to the rotor plane. The segment of the lift constrain the extraneous way will be small and so will be its commitment to the torque.

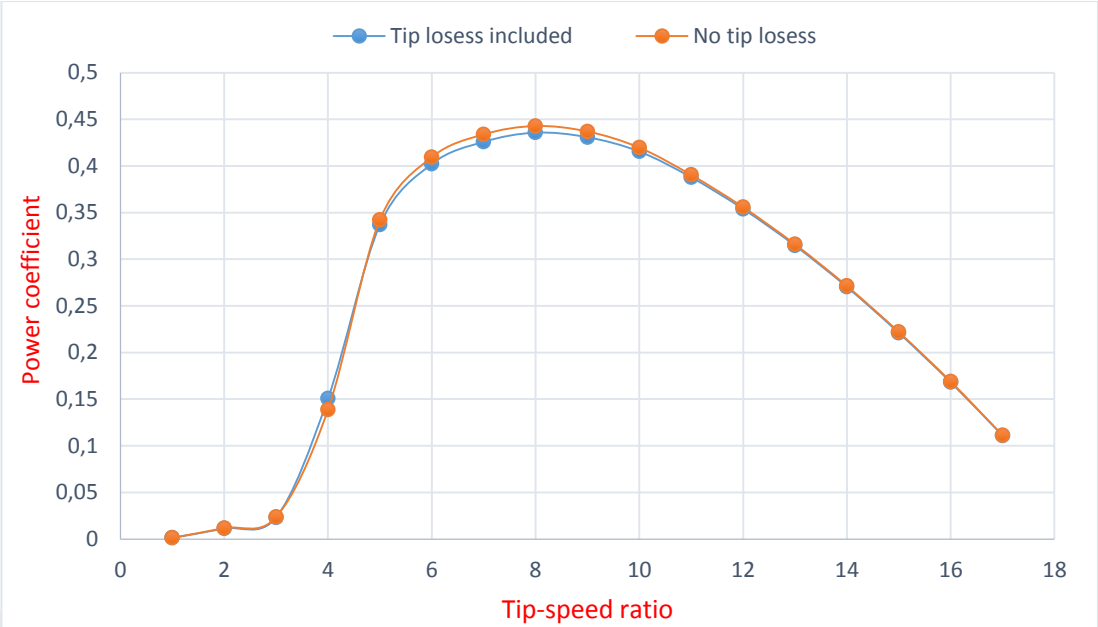

Fig. 6.9 Effect of tip losses on power coefficient (the case of optimum blade)

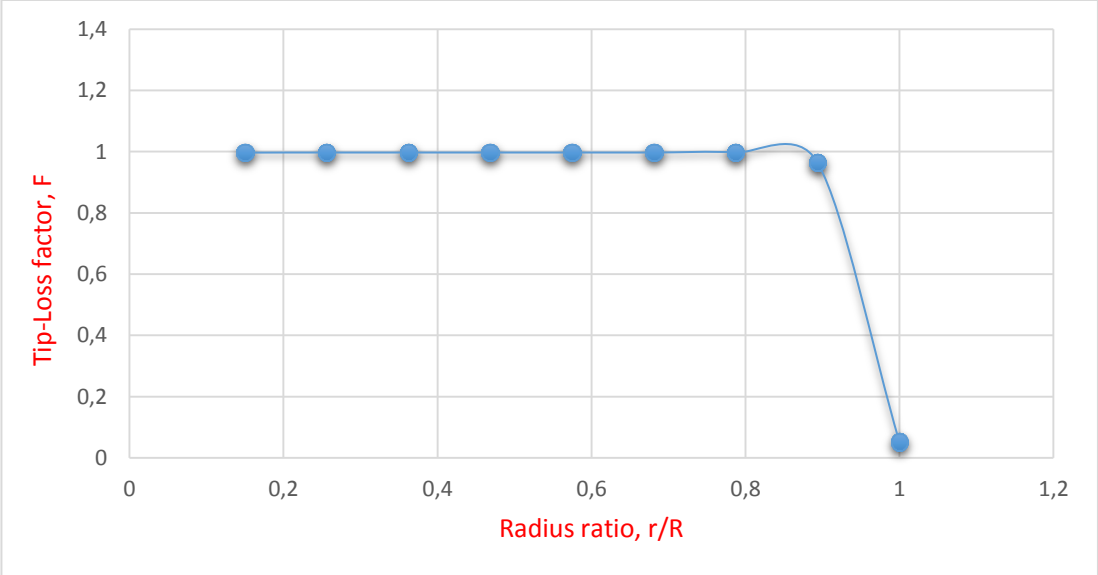

Fig. 6.10 Variation of the tip-loss factor along the non-dimensional blade radius

6.4.3. Effect of modified blade geometry on wind rotor performance

At the point when that blade which is designed keep running at an alternate tip-speed ratio different than the one for that is designed, it is never again optimum. In this manner, blade shape is for the most part redesigned with the end goal of diminishing

the thrust compel following up on a blade amid its process to endeavoring by keeping coefficient power design near the one that is gotten for designed blade.

By and large, an iterative approach is utilized. That is, a blade shape can be accepted and anticipated its execution and another blade shape is expected and the expectation of execution is rehashed until the point that an appropriate shape has been picked.

6.4.3.1. Modification of chord distribution

The chord variety of a designed blade shape isn't linear particularly close to the root as it is displayed in Fig. 6.1. Here such type of designed blade shape will be adjusted with the end goal that its shape winds up plainly straight decreased. The changed chord ought to be nearest to the designed blade shape. In this proposition, this change has been performed with the end goal that chord circulation of the designed blade has been linearized by utilizing the minimum square strategy [37], and from Eq.:$C_1 = a_1 r_1 + b_1$. Where a , b_1 are coefficients for the chosen chord. Optimum, linear and constant ($C = 0.42m$, which represents the chord length at mean of the blade chord the case of optimum blade) blade chord variation along the non-dimensional blade radius is presented in Fig. 6.11.

Fig. 6.12 shows the effect of chord distribution on power coefficient. This Fig. shows for ($\lambda < 5$) the performance of rotor in three cases are no difference. It can be seen that for ($\lambda > 5.5$) the power coefficient the cases of linear chord and optimum blade higher than constant chord, due to drag losses effect the case of constant chord higher than the cases of linear chord and optimum blade .

Fig. 6.13 shows that the effect on torque coefficient by chord distribution follows the same trend discussed in $C_P - \lambda$ curve. The variations of thrust coefficient with tip-speed ratio are presented in Fig. 6.14. This Fig. shows that for higher tip-speed ratio ($\lambda > 10$), rotor with constant chord blade have higher values of C_T, due to drag losses effect the case of constant chord higher than the cases of linear chord and optimum blade.

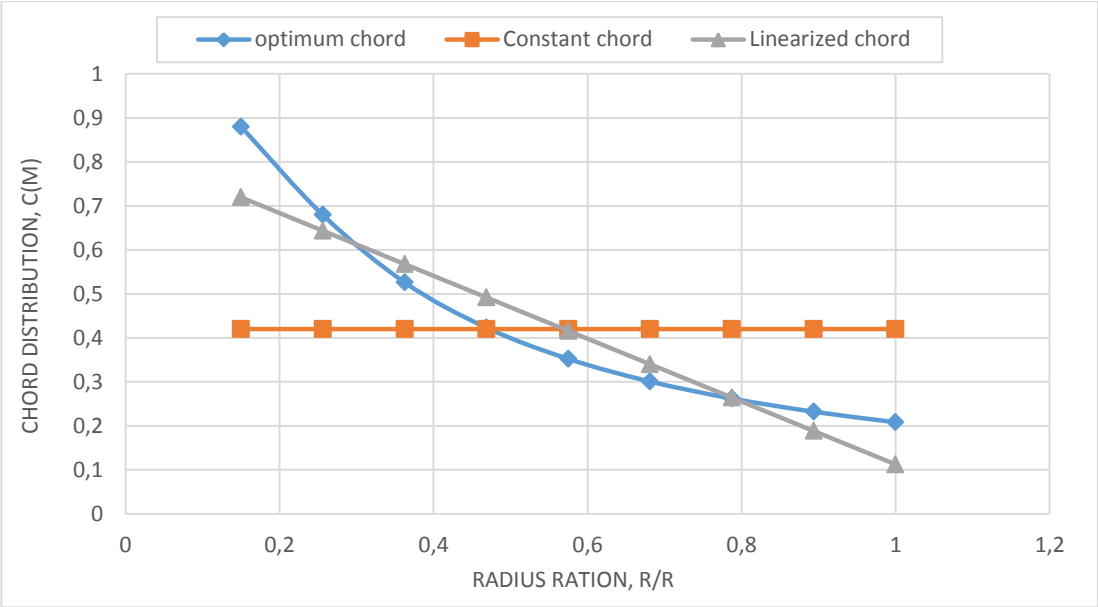

Fig. 6.11 Distribution of optimum, linearized and constant chord along the blade radius ratio

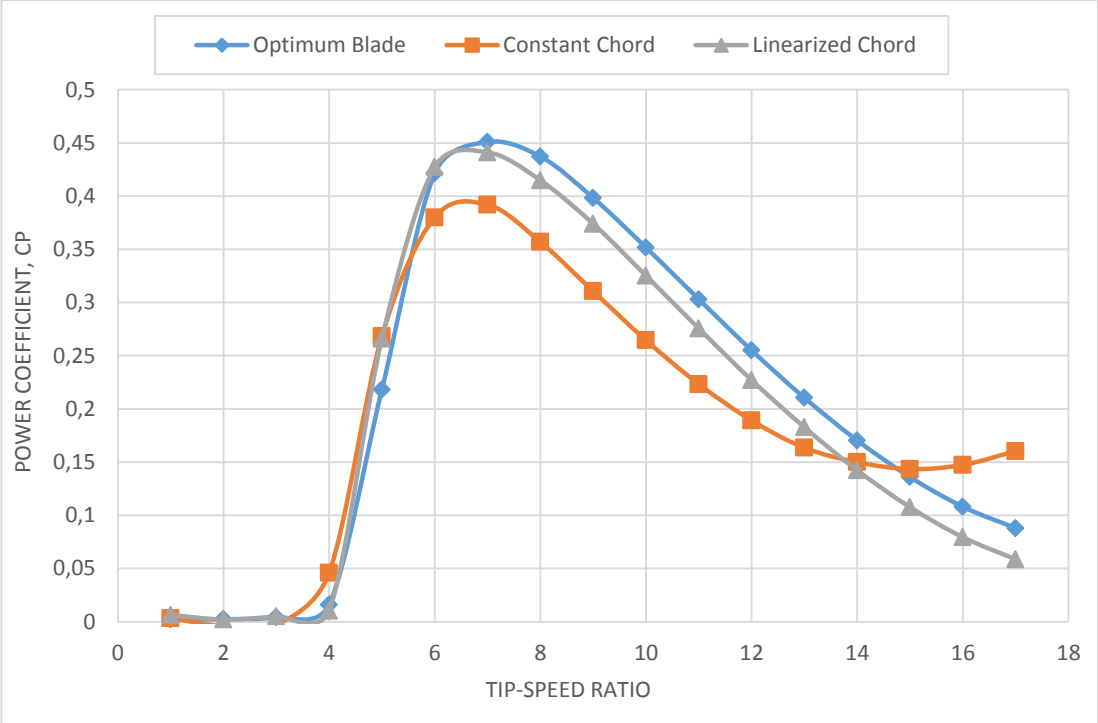

Fig. 6.12 Effect of linearized and constant chord distribution at optimum twist on power coefficient

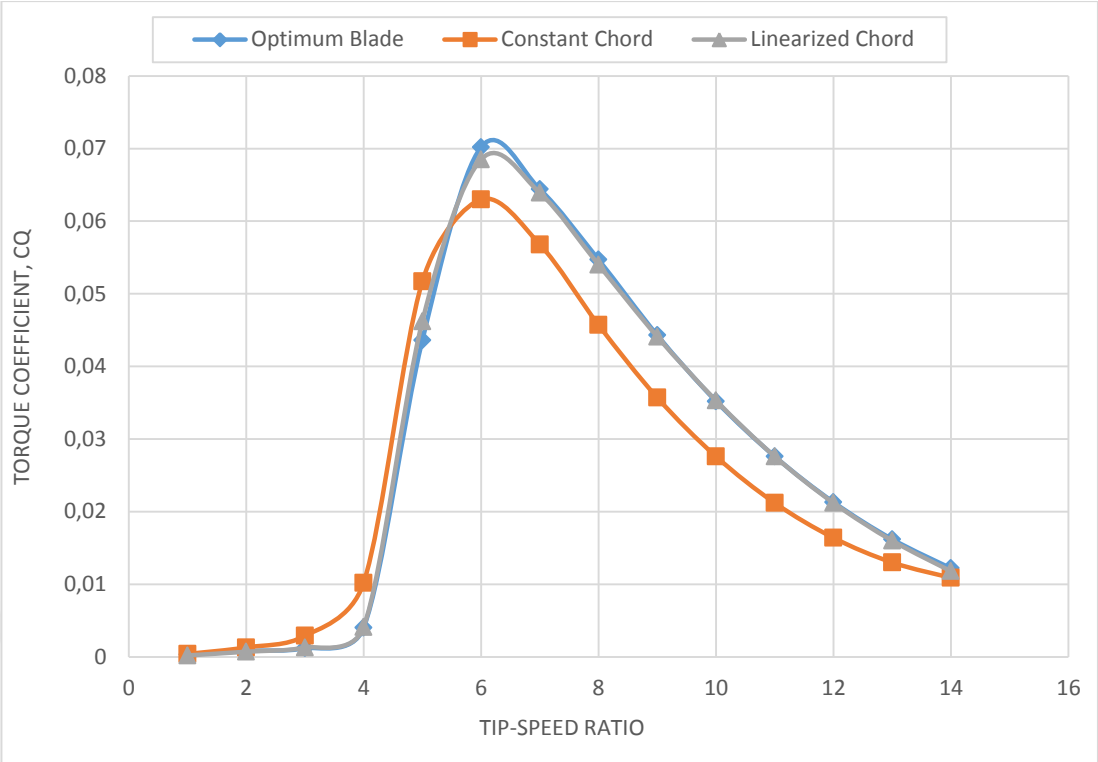

Fig. 6.13 Effect of Linearized and constant chord distribution at optimum twist on torque coefficient

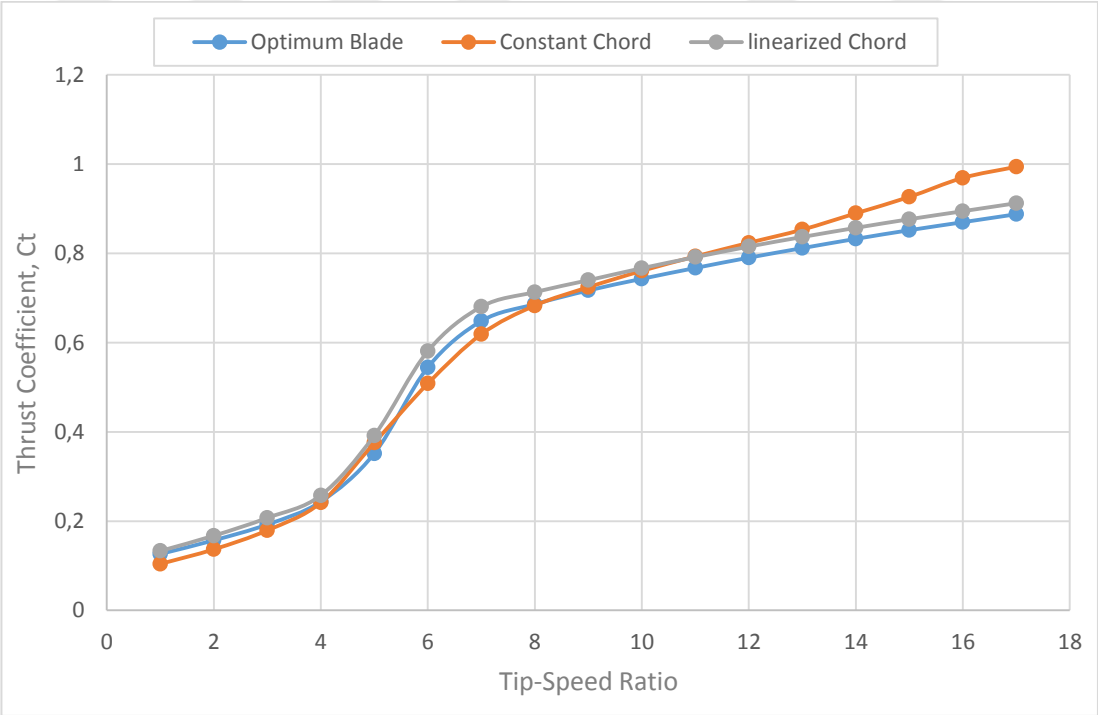

Fig. 6.14 Effect of Linearized and constant chord distribution at optimum twist on thrust coefficient

6.4.3.2. Modification of twist distribution

It can be seen that a designed blade that the twist distribution is not linearly, especially near the root again as it occurs in the chord variation of the same blade. For that reason, twist distribution can also be modified considering the ease of fabrication. Also by using the least-square method [42], and from Eq.: $\theta_{T,i} = a_2(R - r_i)$. Where

a_2 is coefficient for the chosen twist. Optimum twist of the designed blade has been linearized. Fig. 6.15 shows the linear twist distribution along the non-dimensional blade radius. The result of linearized twist and optimum chord distribution for modified blade is tabulated in table 6.2.

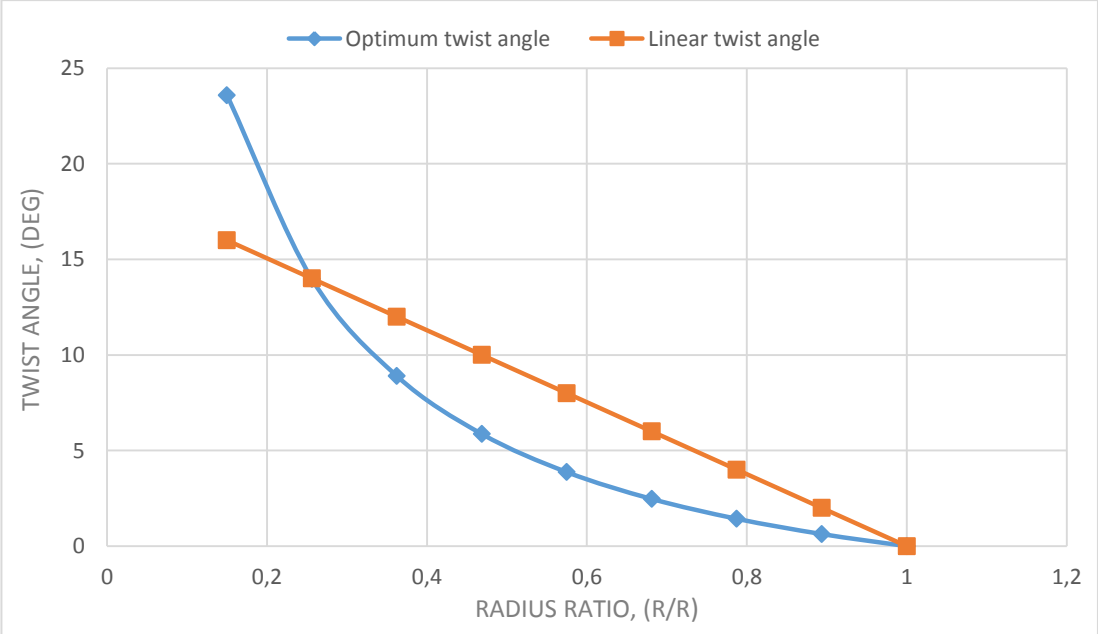

Fig. 6.15 Linearized and optimum blade twist distribution along blade radius ratio

Also, Fig. 6.16 shows the effect of linearized twist on power coefficient. The case which is studied in this Fig., linear twist-optimum chord and compared with optimum twist- optimum chord which is (optimum blade). At tip-speed ratio between $5.5 < \lambda < 8$ the cases of optimum blade have the maximum value of C_P compared with linear twist -optimum chord at this range, because the tip losses effect the case of linear twist-optimum chord higher than the case of optimum blade.

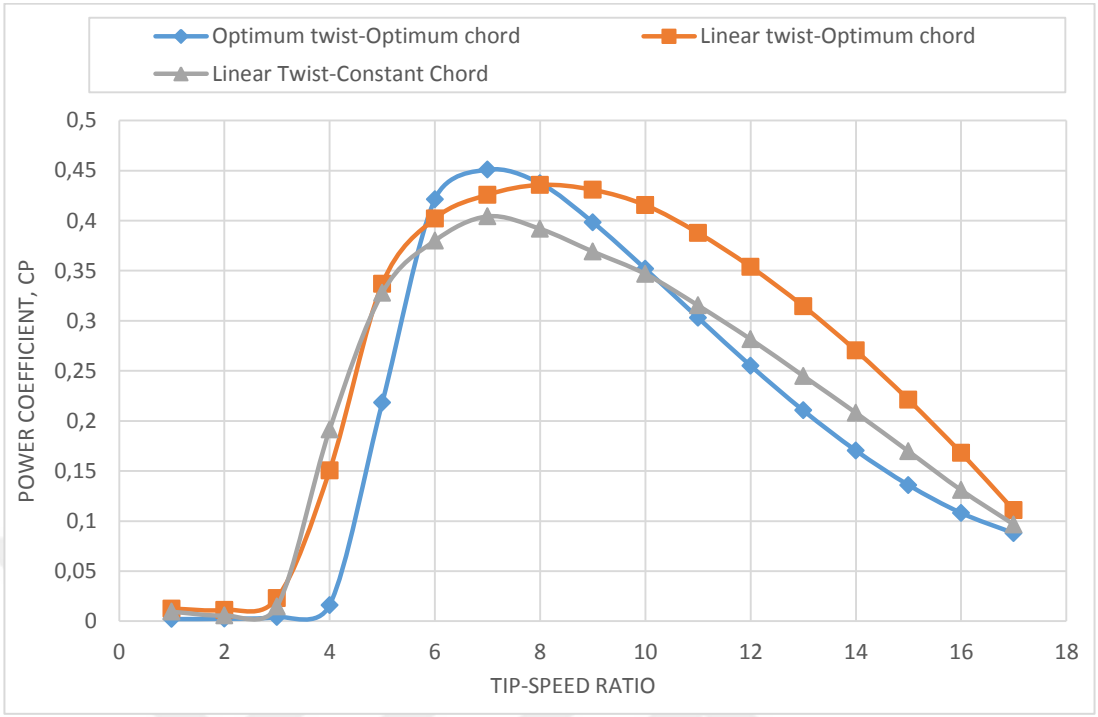

Fig. 6.16 Effect of modification twist distribution on power coefficient for three cases

Also, Fig. 6.17 shows the effect of linearized twist distribution on torque coefficient C_Q . It's clear that the relation follows the same trends as discussed for C_P.

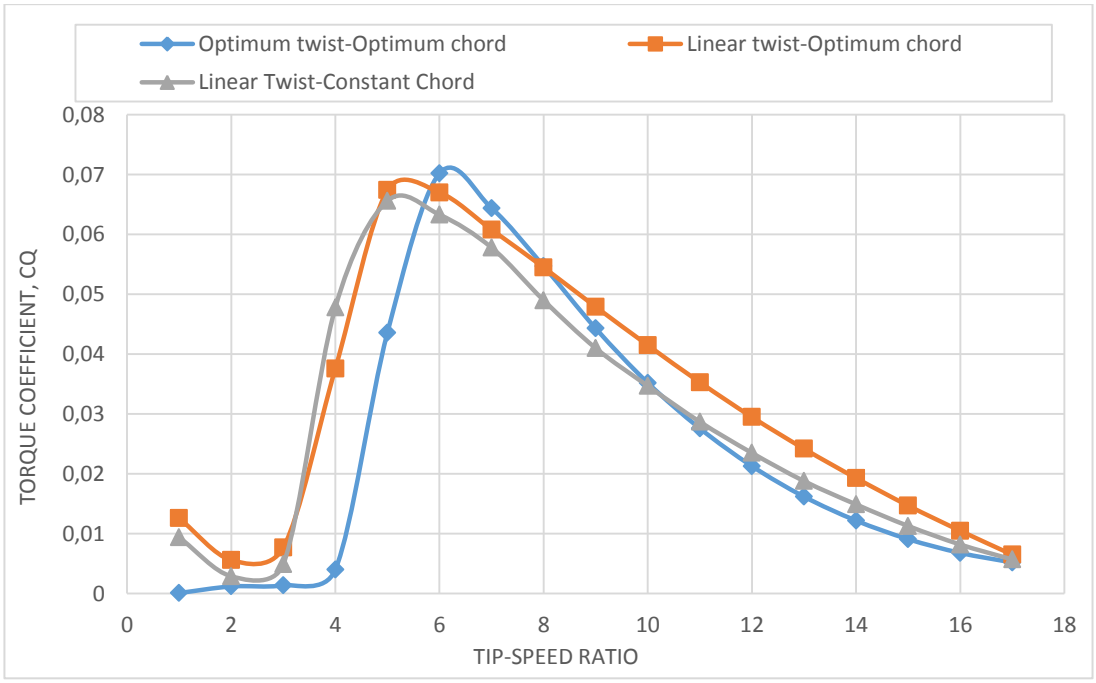

Fig. 6.15 Effect of modification twist distribution on torque coefficient for three cases

The variations of thrust coefficient with different tip-speed ratio are presented in Fig. 6.18. This Fig. shows that over a wide range (λ>5) of tip-speed ratio rotor with optimum twist- optimum chord have leas values of C_T which was expected. Also, due to drag losses, the case of linear twist-constant chord higher than the author cases.

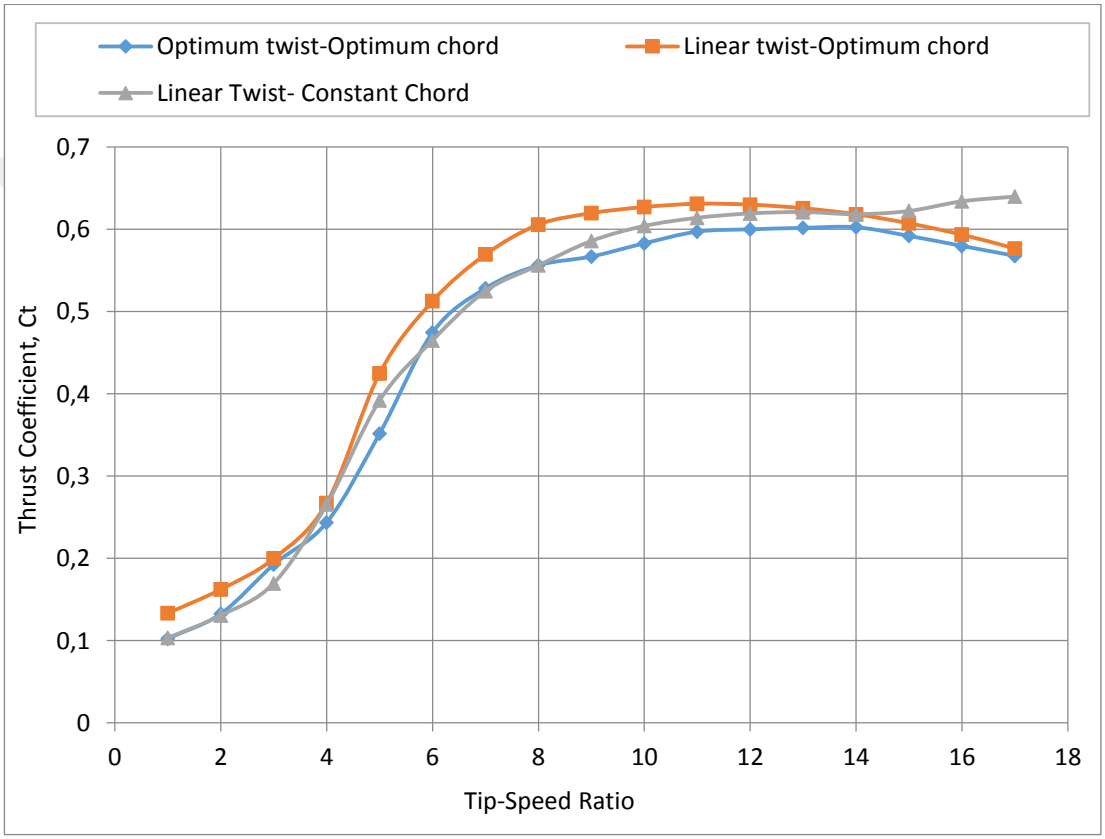

Fig. 6.16 Effect of modification twist distribution on thrust coefficient for three cases

6.4.3.3. Effect of pitch angle and chord length on wind rotor performance

The investigation of stacking and quality of a blade is imperative amid typical operation, as the blade's outside shape and structure is fundamental for the wind turbine to have adequate quality, solidness and dependability. To understand the blade quality, streamlined stacking must be done. BEM theory is the normal rule to break down the streamlined stacking. The outcomes will indicate how the torque, thrust and productivity change with change of pitch angle and chord length of the

wind turbine rotor. There are various parameters that will be chosen for the wind turbine which has NACA 63(4)221 airfoil. These parameters incorporate chord length of the blade, blade Numbers, pitch angle variety and generator speed (RPM). Table 6.3 demonstrates the distinctive parameter rate that will be utilized to acquire diverse outcomes with the MATLAB Code. The chord length and the pitch angle variety are the parameters that will be changed the most, while there will be just two unique rate for generator speed (RPM). The contribute angle Table 6.3 is shown by two numbers, the principal relates to the pitch angle of the blade at 20% of the sweep from the hub. The second number compares to the pitch angle at the tip of the blade.

Table 6.3 Variable parameters for BEM Theory model

Blade Numbers	3		
Generator speed [RPM]	1800-2100		
Pitch angle [degrees]	50-20	70-40	80-60

These parameters will be utilized as a part of request to acquire the torque and thrust created by the wind turbine blades

The model was running with all the diverse contribute angle varieties as introduced Table 6.3 keeping in mind the end goal to have an exhaustive and far reaching set of results. All through this segment, three settings of pitch angle varieties will be displayed to exhibit the distinction comes about. The first will be the 50° at 20% span from the hub and 20° at tip of the blade. The second pitch angle setting is 70° at 20% span and 40° at tip of the blade and the third pitch angle setting is 80°at 20% sweep and 60° at tip of the blade.

As a thrust to limit the measure of Fig. in this area, Fig. 6.19, 6.20 and 6.21 show how the torque of the wind turbine changes with seven diverse chord length rate, and distinctive pitch angle and 2 generator speed (RPM) settings inside a turbine 3 blades.

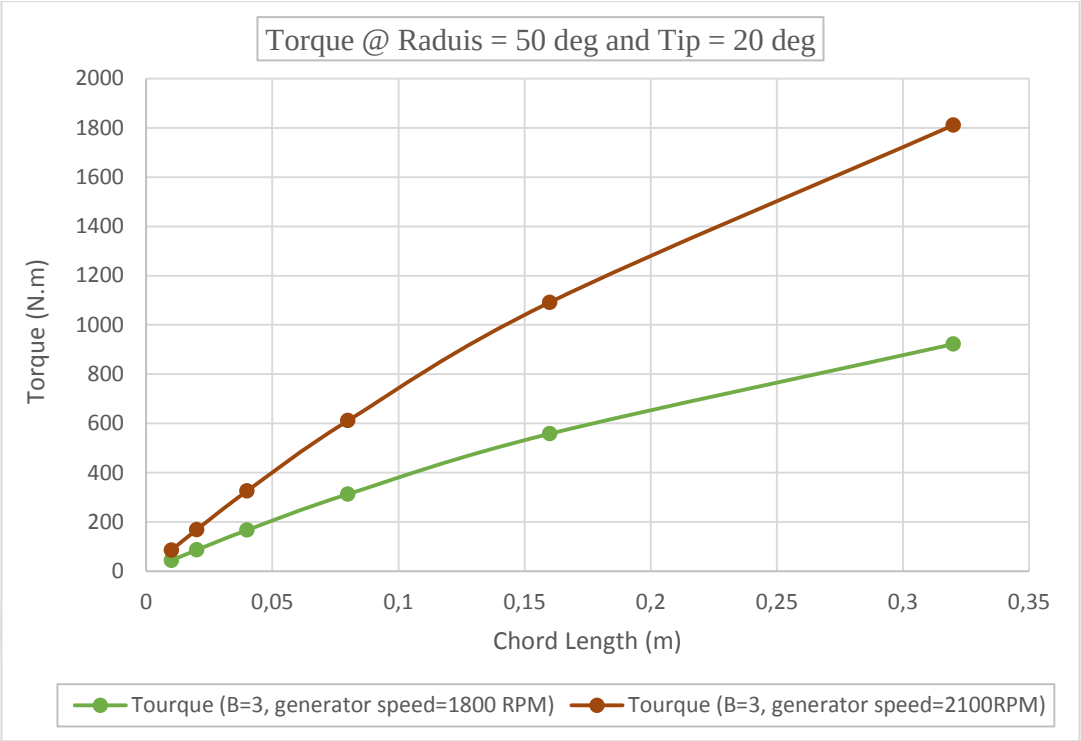

Fig. 6.17 Effect of chord length and pitch angle on torque coefficient

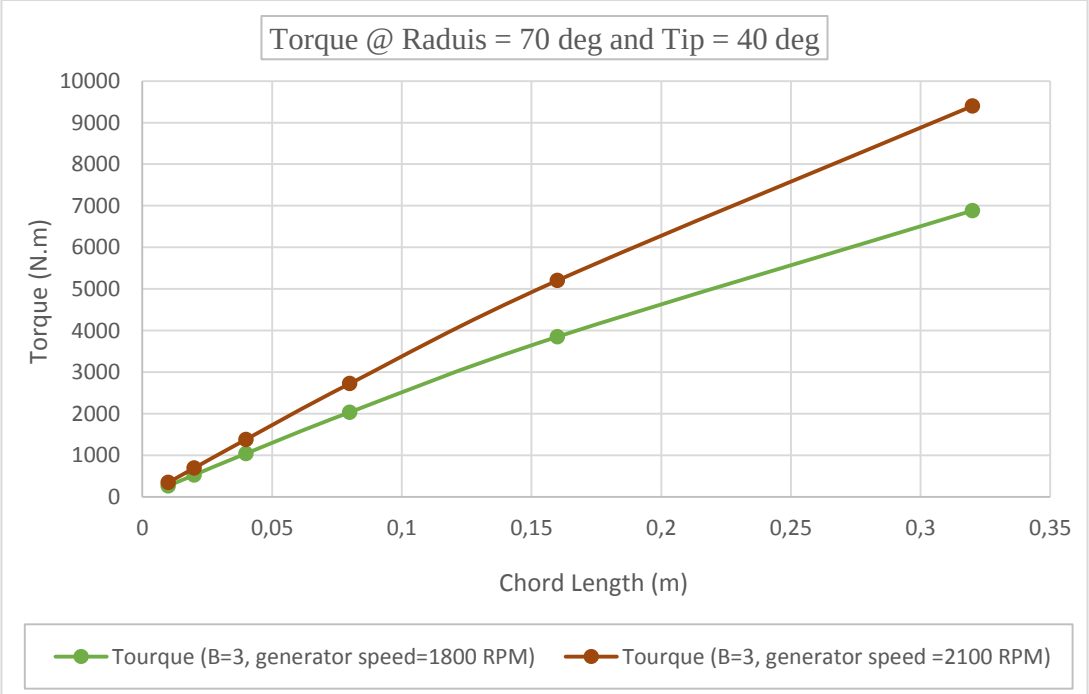

Fig. 6.18 Effect of chord length and pitch angle on torque coefficient

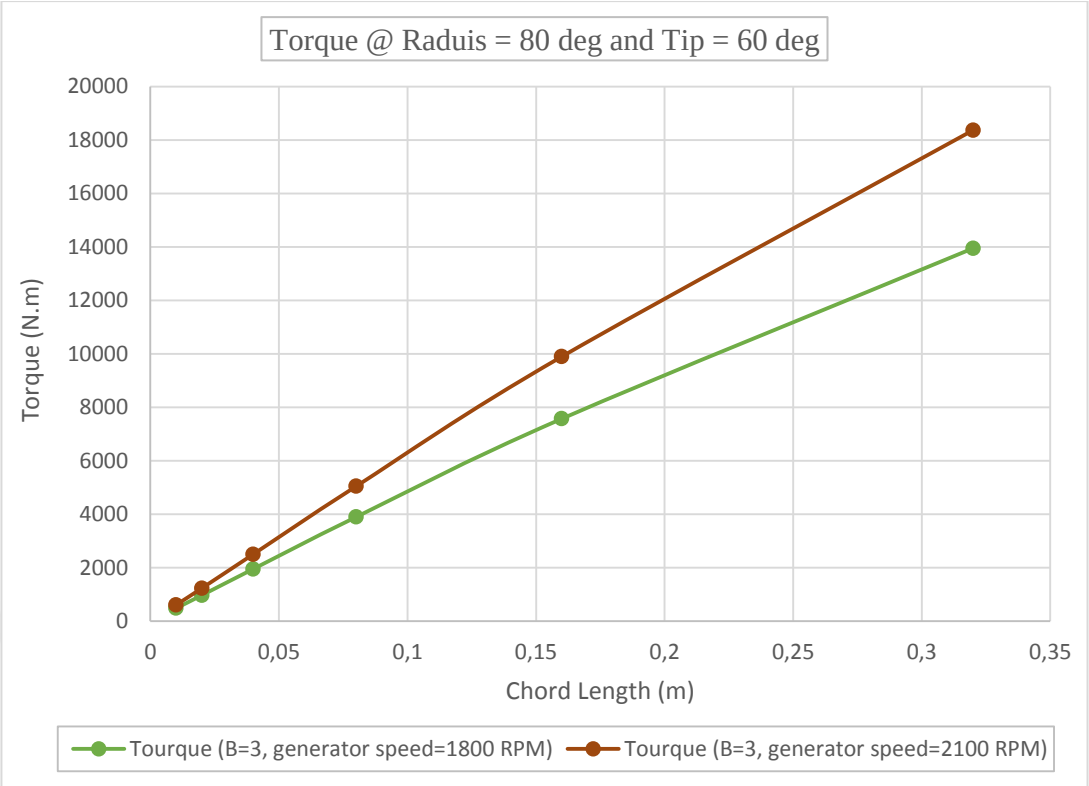

Fig. 6.19 Effect of chord length and pitch angle on torque coefficient

In the same manner, Fig. 6.22, 6.23 and 6.24 reflect the Thrust generated by the wind turbine at the same chord length settings, generator speed (RPM) values and number of blade as previously presented in the thrust results.

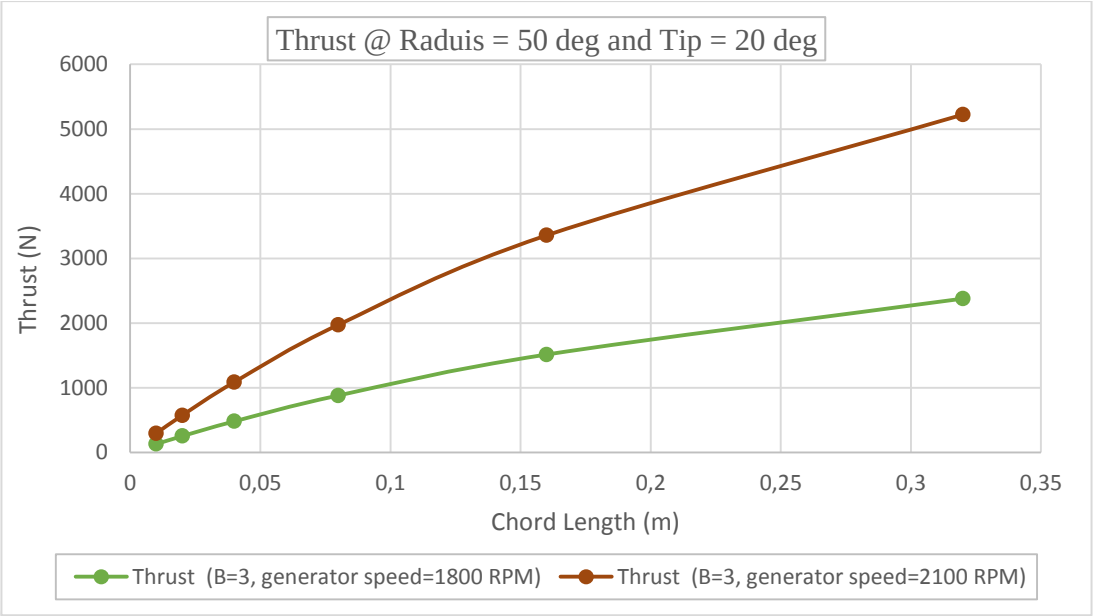

Fig. 6.20 Effect of chord length and pitch angle on thrust coefficient

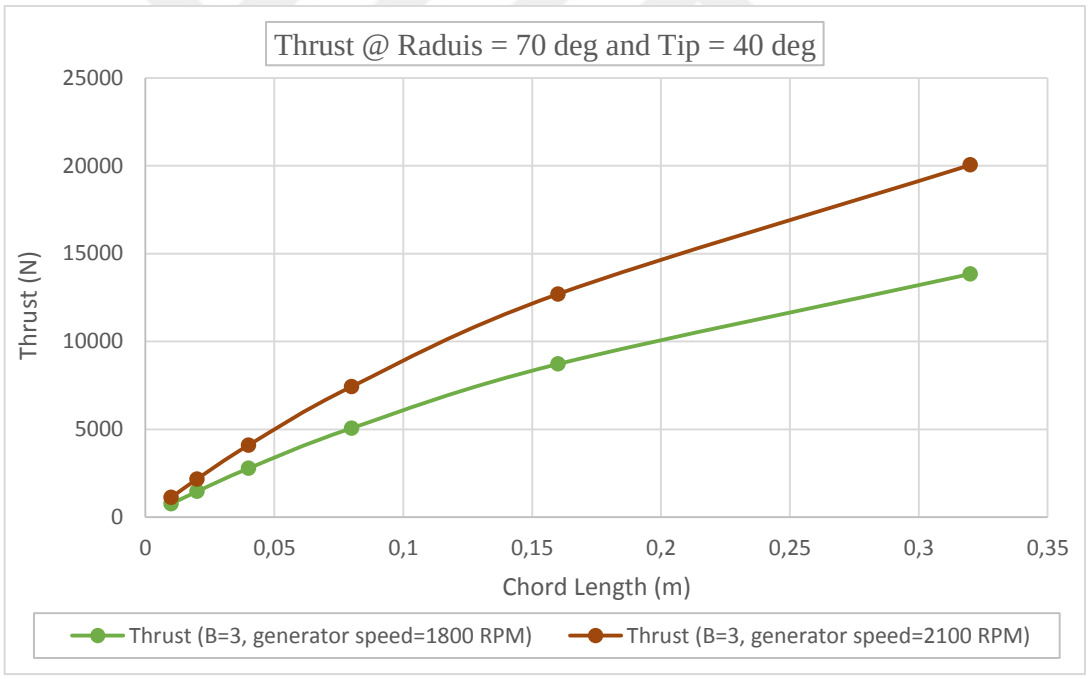

Fig. 6.21 Effect of chord length and pitch angle on thrust coefficient

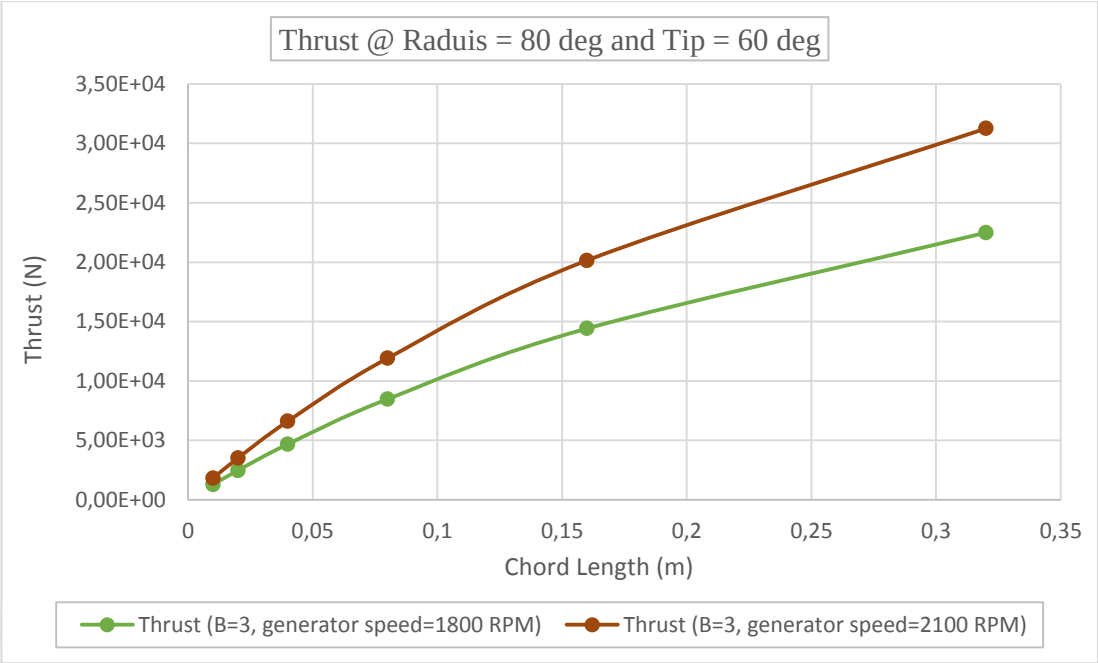

Fig. 6.22 Effect of chord length and pitch angle on thrust coefficient

Similarly, as done in Fig. 6.19 through Fig. 6.25, Fig. 6.26 and Fig. 6.27 demonstrate how the wind turbine efficiency behaves at the different parameter settings.

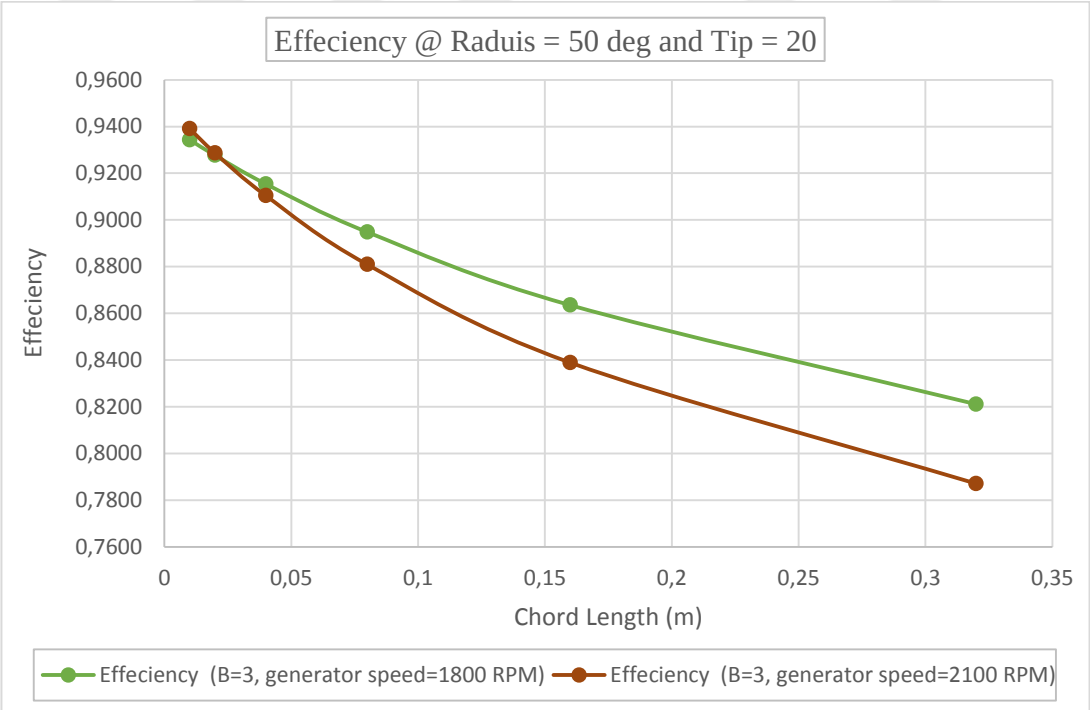

Fig. 6.23 Wind Turbine Efficiency at 50-20 pitch angle degree

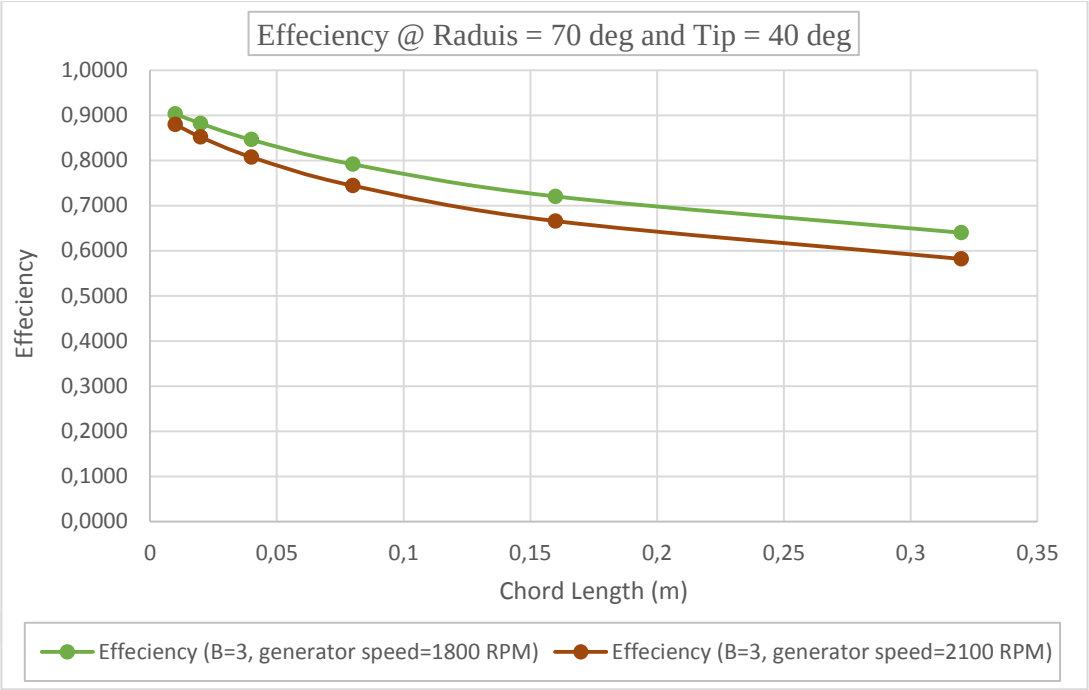

Fig. 6.24 Wind Turbine Efficiency at 70-40 pitch angle degree

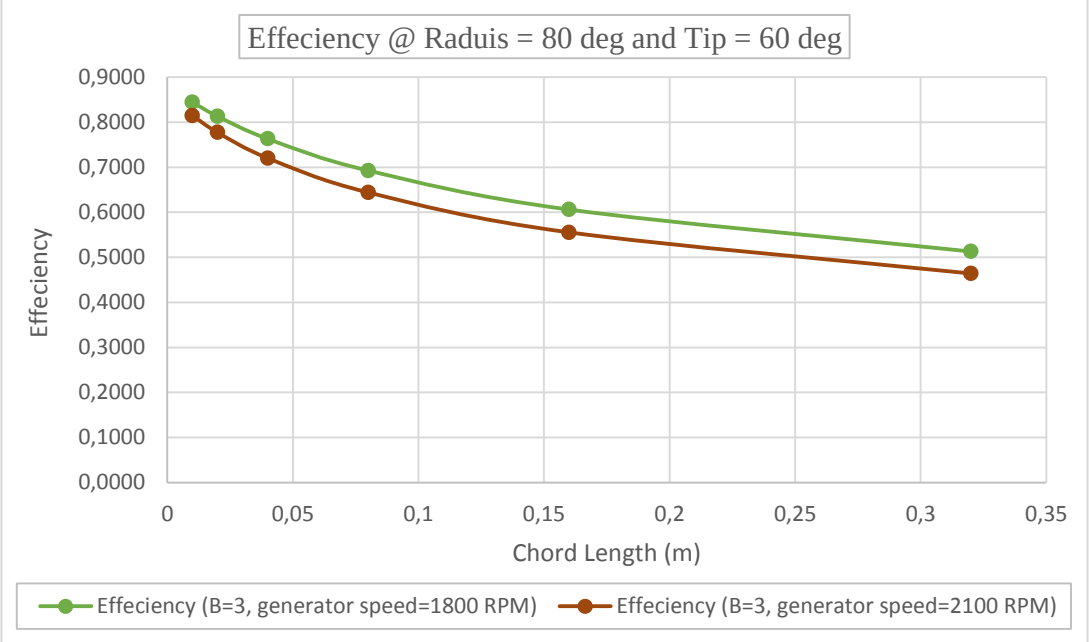

Fig. 6.25 Wind Turbine Efficiency at 80-60 pitch angle degree

Three unique types of results have been created in this segment with a given arrangement of factors. The general torque, thrust and productivity of the wind turbine have been figured as plot in the past areas. The principal set of results

demonstrate the general wind turbine torque rate at various chord lengths of the blade, and distinctive pitch angle rate, utilizing two generator speed (RPM) settings, being done 3 blades.

From Figure 6.19, it is evident that the torque values become greater as the chord length of the wind turbine blade is increased, within the different setting of generator speed RPM. This increase can be quantified to about 30% to 45% increase at each chord length increase.

On the other hand, when we take a gander at the torque rate with at a predefined chord length (0.32 m) and indicated blade number (3 blades) it can be watched that the effect the generator speed RPM variety from 1800 RPM to 2100 RPM has on the torque values is additionally at around 40% expansion. Observing the torque values by keeping all parameters as constant and varying the pitch angle at the wind turbine blade, it can be seen that the variety in pitch angle does not significantly affect the general torque estimations of the wind turbine. Keeping all parameters as consistent, the expansion in torque rate with various pitch points is under 1%. In any case, it ought to be said that the smaller the chord length of the blade is, the more prominent the expansion in torque rate would be.

Quite, when we take a gander at the general thrust comes about, the dialog introduced beforehand for the torque rate would likewise apply to the thrust comes about utilizing the comparable blend of the parameters. The primary distinction that can be seen between the torque comes about and the thrust comes about is that the expansion in thrust rate at various chord lengths is in the vicinity of 35% and 48%. Similarly, as the torque rate, the thrust rate increment would be decreased when the chord lengths are extending. Thus, the pitch angle variety does not affect incredibly the thrust rate. As while expanding the blade pitch edge, the thrust esteem would increment to under 1% at each pitch angle setting. With respect to the proficiency, it is obviously from Fig. 6.25, 6.26 and 6.27 that the productivity rate would diminish paying little heed to which parameter is being taken as a variable and which one as a consistent. Utilizing a similar perception rules from the torque and the thrust talk segment, the wind turbine effectiveness would diminish from a scope of 2.5% to 6.5% when the chord length is the main variable. The more prominent the chord length of the blade, the more effectiveness would diminish.

Then again, when the variable parameter is the generator speed (RPM), we can see that the proficiency would increment by roughly 1% when the generator speed (RPM) is shifted between 1800 RPM and 2100 RPM. The one recognizable perception in the turbine productivity is the point at which the pitch angle is set to 70° at 20% sweep and 40° at the tip of the blade. Fig. 6.25 demonstrates that the productivity truly does not change extraordinarily while going from generator speed 1800 RPM to 2100 RPM, while doing the examination on a turbine with a similar number of blades. It appears that after a specific scope of pitch angle variety, the generator speed (RPM) would should be to some degree expanded or diminished for the proficiency of the wind turbine to be affected altogether. Similarly, as how the proficiency isn't affected enormously with the parameter rate utilized as a part of this investigation, a few forecasts can be made to the torque and thrust rate. Despite the fact that more examination would be required, by freely expanding the chord length, generator speed (RPM) or some other variable, it can be expected that the torque and thrust rate would carry on comparatively. They would continue expanding as the distinctive factors utilized as a part of this investigation are expanded. The strategy in which these outcomes were ascertained was by taking the BEM theory and make an interpretation of it into a MAT LAB code.

Chapter Seven

CONCLUSIONS AND FUTURE WORK

7.1. Conclusions

The purpose of the study is to estimate the wind energy and wind assessment at El-Spiaa, Tripoli _Libya station at both heights of 10 and 40m. Then enforcement modified BEM analysis with and without different existing correction models using NACA 63(4)221 airfoil profile to know the efficiency of this theory to predicting the performance of wind turbine. Also, for validation the results it will be compared with experimental case which is (NLSE) Risoe wind turbine, because, they have the same airfoil type. The last purpose of this dissertation is to apply BEM theory to design the rotor blade and to predict its aerodynamic performance, also study the results of some important parameters related of blade design process.

The principal conclusions as result of this study as follows:

- This study shows that the wind energy is available in El-Spiaa, Tripoli _Libya, and it could be used to generate electricity, also wind energy may use for other applications like water sea desalination.
- The wind power density, E, (W/m²) can be expressed in terms of the Weibull shape and scale parameters, k and c, and it is found that the yearly wind power density of year 2013 at both heights of 10 and 40 m are (651.02 W/m²) and (814.61W/m²) respectively, also the yearly wind power density for year 2014 at 10 and 40 m are (715.85W/m²) and (980.41 W/m²) respectively.
- The present modeling is based on the iteration process for axial inflow factor (a) and the angular inflow factor (a') .
- Maximum theoretical power coefficient is obtained from rotor having optimum blade geometry and the minimum value obtained from a rotor has constant chord-optimum twist.
- Increase of solidity affects the aerodynamics of the turbine in two important ways. The first way for higher solidity delivers better of blade surface for the wind turbine. In addition, increases of aerodynamic torque. Nevertheless,

drag coefficient induces losses and increase with growth in the solidity. The results indicate that the maximum power coefficient increases as the number of blades increases, because the drag losses decrease as the solidity increases. Also for number of blades between 3 to 5 produces a narrow performance curve with a sharp peak making the turbine very sensitive to tip-speed ratio changes and, optimum solidity appears to be achieved with three blades.

- This study shows that the modified twist angle effects on power coefficient, while the optimum chord linearized twist angle reduced the power output by approximately 8.3 % compared with the power output of the optimum blade.
- Rotor having optimum chord linear twist geometry shows the minimum theoretical thrust force coefficient.
- Rotor having optimum blade geometry produces highly power compared with others cases.
- The effect of tip losses factor reduced of the power output around 2.23 % that for power output the case of optimum blade.

7.2. Recommendations for Future Works

This examination can be without a doubt utilized for additionally works. So the further works may be each specifically similar to the point of the postulation to include significant convenience level hub wind turbine for blade design. Identified with the investigations of the theory to broaden the examinations on flat hub of wind turbine as they some depicted in the accompanying sections.

- This work ought to be stretched out to ponder plausibility of extricating the accessible power in wind energy for producing power and ocean water desalination by utilizing HAWTs in various areas along the city seashore.
- The adjustment of a designed blade was done for direct decrease of chord-length conveyance and straight variety of turn point appropriation, other option strategies for alteration may likewise be attempted and their execution might be contrasted and their design of blades ones got in this investigation.
- Designed wind turbines can be analyzed with using other theories as Navier Stokes and Genetic Algorithm analyses apparatus for greatest guesses of higher wind speeds value.

- The airfoil database which are used it could be expanded for including of data for higher and lower value of Reynolds numbers. Moreover, many airfoils types can be additional to the database.

REFERENCES

[1] H. Borgheipour, N. Kargari and T. F. Hashemi, "Co2 Emission from Vegetable Oil Plants Using IPCC Guideline 2006: Iran's Experience," *EnviroInfo,* pp. 573-580, 2014.

[2] F. von Koenig, Wind energy in practicle use: Wheels, rotors, mills, wind power plants, Munich: Udo Pfriemer Verlag GmbH, 1976.

[3] E. Hau and H. von Renouard, "Wind Turbines: Fundamentals, Technologies, Application, Economics," *Windmills and Windwheels,* pp. 1-21, 2006.

[4] "Wikipedia, Windpump," October 2017 . [Online]. Available: https://en.wikipedia.org/wiki/Windpump. [Accessed October 2017].

[5] Millbrook Wind Farm, "History of Wind Power," Millbrook First Nation, 18 August 2012. [Online]. Available: http://www.millbrookwindfarm.ca/windinformation/history/. [Accessed 20 February 2017].

[6] A. P. Schaffarczyk, "Types of Wind Turbines," in *Introduction to Wind Turbine Aerodynamics*, Berlin, Springer Berlin Heidelberg, 2014, pp. 7-20.

[7] J. DeCoste, D. McKay, B. Robinson, S. Whitehead, S. Wright, M. Koksal and L. Hughes, Self-starting vertical axis wind turbine - Final Year Design Project, Mechanical Engineering, Halifax: Dalhousie University, 2006.

[8] "HAWT and VAWTs in operation medium," Wikimedia Commons, the free media repository, [Online]. Available: https://commons.wikimedia.org/wiki/File:HAWT_and_VAWTs_in_operation_medium.gif. [Accessed October 2017].

[9] H.-J. Wagner and J. Mathur, Introduction to wind energy systems: basics, technology and operation, Springer Science & Business Media, 2012.

[10] "Different Types and Parts of a Horizontal Axis Wind Turbines," Dolcera, Public Wiki, [Online]. Available: https://www.dolcera.com/wiki/index.php?title=Different_Types_and_Parts_of_a_Horizontal_Axis_Wind_Turbines&action=info. [Accessed October 2017].

[11] "Wind turbine size increase 1980-2010.png," Wikimedia Commons, the free media repository, [Online]. Available: https://commons.wikimedia.org/wiki/File:Wind_turbine_size_increase_1980-2010.png. [Accessed October 2017].

[12] "large turbine.gif," Wikimedia Commons, the free media repository, [Online]. Available: https://commons.wikimedia.org/wiki/File:EERE_illust_large_turbine.gif. [Accessed October 2017].

[13] O. Ceyhan, Aerodynamic design and optimization of horizontal axis wind turbines by using BEM theory and genetic algorithm, Ankara: Middle East Technical University, 2008.

[14] R. A. Kishore, Small-scale Wind Energy Portable Turbine (SWEPT) (PhD diss.), Blacksburg: Virginia Tech, 2013.

[15] T. Göçmen, Comouter-aided aerodynamic design of small scale horizontal axis wind turbine blades (Master's thesis), Izmir: İzmir Institute of Technology, 2012.

[16] M. S. Elmnefi and A. M. Bofares, "An Analysis of Wind Speed Distribution at Benina, Benghazi, Libya," *Trans Tech Publications - Applied Mechanics and Materials,* vol. 492, pp. 550-555, 2014.

[17] J. F. Manwell, J. G. McGowan and A. L. Rogers, Wind energy explained: theory, design and application, John Wiley & Sons, 2010.

[18] SEDA, Handbook, NSW Wind Energy, Australia: Sustainable Energy Development Authority of NSW, 2002.

[19] P. A. C. Rocha, R. C. de Sousa, C. F. de Andrade and M. E. V. da Silva,

"Comparison of seven numerical methods for determining Weibull parameters for wind energy generation in the northeast region of Brazil," *Applied Enervy*, vol. 89, no. 1, pp. 395-400, 2012.

[20] K. Y. Maalawi and M. T. S. Badawy, "A direct method for evaluating performance of horizontal axis wind turbines," *Renewable and Sustainable Energy Reviews*, vol. 5, no. 2, pp. 175-190, 2001.

[21] T. Lombardo, "Rooftop Wind Turbines: Are They Worthwhile?," engineering.com, [Online]. Available: https://www.engineering.com/ElectronicsDesign/ElectronicsDesignArticles/ArticleID/9556/Rooftop-Wind-Turbines-Are-They-Worthwhile.aspx. [Accessed October 2017].

[22] F. M. Kamal and M. Quamrul-Islam, "Aerodynamic characteristics of a stationary five bladed vertical axis vane wind turbine," *Journal of Mechanical Engineering*, vol. 39, no. 2, pp. 95-99, 2008.

[23] google earth. [Online].

[24] J. Gomez-Leon, Wind Turbine Blade Analysis Using Blade Element Momentum Theory (PhD diss.), New York: Rensselaer Polytechnic Institute, 2016.

[25] R. Mikkelsen, Actuator disc methods applied to wind turbines (PhD diss.), Lyngby: Technical University of Denmark, 2003.

[26] A. Rogers, Aerodynamics of Wind Turbines, 2009.

[27] A. M. Bufares and M. S. Elmnefi, "Design and performance of horizontal axis wind turbine using blade element momentum theory (BEMT)," *Applied Mechanics and Materials*, vol. 492, p. 106, 2014.

[28] H. JaGlauert, Windmills and Fans. Aerodynamic theory (ed. Durand, W. F.), Berlin, Germany: Julius Springer, 1935b.

[29] P. J. Moriarty and H. C. A, "AeroDyn Theory Manual," NREL EL/-500-

36881, USA, 2005.

[30] Brøndsted, Povl, and Rogier PL Nijssen, eds., "Advances in wind turbine blade design and materials," *Elsevier*, 2013.

[31] O. CEYHAN, "Aerodynamic design and optimization of horizontal axis wind turbines by using BEM theory and genetic algorithm," *Middle East Technical University*, 2008.

[32] "XFLR5," [Online]. Available: http://www.xflr5.com. [Accessed October 2017].

[33] "UIUC Airfoil coordinates database," UIUC Applied Aerodynamics Group , [Online]. Available: http://m-selig.ae.illinois.edu/ads/coord_database.html. [Accessed October 2017].

[34] M. A. ELFARRA, "Horizontal Axis Wind Turbine Rotor Blade: Winglet and Twist Aerodynamic Design and Optimization Using CFD," *PhD diss., MIDDLE EAST TECHNICAL UNIVERSITY*, 2011.

[35] Moriarty, Patrick J., and A. Craig Hansen, "AeroDyn theory manual," *Golden, CO: National Renewable Energy Laboratory*, 2005.

[36] "Airfoil," Wikipedia, [Online]. Available: https://en.wikipedia.org/wiki/Airfoil.

[37] A. M. Awin, "On the use of Taylor expansion in solving first order ordinary differential Equations," *International Journal of Mathematical Education in Science and Technology 20,* vol. no. 5, pp. 749-753, 1989.

[38] S. Mathew, "Wind energy: fundamentals, resource analysis and economics. Vol.1," *Heidelberg: Springer*, 2006.

[39] Pandey, M. M., K. P. Pandey, and T. P. Ojha, "An analytical approach to optimum design and peak performance prediction for horizontal axis wind turbines," *Journal of Wind Engineering and Industrial Aerodynamics 32,* vol. no. 3, pp. 247-262, 1989.

[40] Zhiquan, Ye, Cheng Zhaoxue, Chen Jingyi, and Bai Shibao, "Aerodynamics optimum design procedure and program for the rotor of a horizontal-axis wind turbine," *Journal of Wind Engineering and Industrial Aerodynamics 39,* Vols. no. 1-3, pp. 179-186, 1992.

[41] Handbook, NSW Wind Energy, Sustainable Energy Development Authority of NSW (SEDA).

[42] Munduate, X., and F. N. Coton, "An aerodynamic method for the preliminary design of horizontal axis wind turbines," *Acta Polytechnica 40,* vol. no. 1, 2000.

APPENDIX A

- **Calculation of Weibull Histogram**

The Statistics of wind data obtained from measurements for two years (24-month) period. From January 2013 to December 2014. The statistical wind data set was analyzed using Weibull distributions in order to investigate the Weibull shape and scale parameters at 10 m.

Table A.1 Frequency of wind speed in interval 1m/s of year 2013

Wind speed (m/s)	Frequency wind speed of year 2013	Percentage of frequency Wind speed of year 2013
0	1	0.000387898
1	4	0.00155159
2	156	0.060512025
3	143	0.055469356
4	156	0.060512025
5	426	0.165244375
6	284	0.110162917
7	87	0.033747091
8	358	0.138867339
9	156	0.060512025
10	320	0.12412723
11	58	0.022498061
12	187	0.07253685
13	41	0.015903801
14	34	0.013188518
15	82	0.031807603
16	8	0.003103181
17	2	0.000775795
18	36	0.013964313
19	0	0
20	17	0.006594259
21	1	0.000387898
22	5	0.001939488
23	0	0
24	2	0.000775795
25	6	0.002327386
26	3	0.001163693
27	0	0
28	1	0.000387898
29	0	0
30	3	0.001163693
31	0	0
32	0	0
33	0	0
34	0	0
35	1	0.000387898

Table A.2 Frequency of wind speed in interval 1m/s of year 2014

Wind speed (m/s)	Frequency wind speed of year 2014	Percentage of frequency Wind speed of year 2014
0	1	0.000404367
1	1	0.000404367
2	111	0.044884755
3	118	0.047715326
4	222	0.089769511
5	436	0.176304084
6	263	0.106348564
7	117	0.047310958
8	306	0.123736353
9	143	0.057824505
10	329	0.133036797
11	47	0.019005257
12	146	0.059037606
13	42	0.016983421
14	40	0.016174687
15	70	0.028305702
16	13	0.005256773
17	14	0.00566114
18	20	0.008087343
19	2	0.000808734
20	13	0.005256773
21	0	0
22	5	0.002021836
23	1	0.000404367
24	4	0.001617469
25	2	0.000808734
26	0	0
27	1	0.000404367
28	1	0.000404367
29	1	0.000404367
30	2	0.000808734
31	0	0
32	1	0.000404367
33	1	0.000404367
34	1	0.000404367
35	0	0

Table A.3 Determination of Weibull parameters for year 2013 and 2014 at 10m

Wind speed (m/s)	ln (U) of year 2013	ln(-ln(P(U))) of year 2013	ln (U) of year 2014	ln(-ln(P(U))) of year 2014
0	0	-7.813893646	0	-7.813893646
1	0.693147181	-6.236084554	0.693147181	-7.12008987
2	1.098612289	-2.741028383	1.098612289	-3.062513633
3	1.386294361	-2.075515145	1.386294361	-2.32214251
4	1.609437912	-1.626781155	1.609437912	-1.597835345
5	1.791759469	-0.864820406	1.791759469	-0.808607142
6	1.945910149	-0.502736545	1.945910149	-0.466741315
7	2.079441542	-0.402485097	2.079441542	-0.328807047
8	2.197224577	-0.01535846	2.197224577	0.012932205
9	2.302585093	0.149709653	2.302585093	0.170981092
10	2.397895273	0.510779805	2.397895273	0.564600936
11	2.48490665	0.584118297	2.48490665	0.628954555
12	2.564949357	0.861202037	2.564949357	0.859570069
13	2.63905733	0.93674837	2.63905733	0.940362307
14	2.708050201	1.00687119	2.708050201	1.028154565
15	2.772588722	1.227476346	2.772588722	1.229268231
16	2.833213344	1.256044158	2.833213344	1.27917291
17	2.890371758	1.263514878	2.890371758	1.34134574
18	2.944438979	1.433242953	2.944438979	1.455540543
19	2.995732274	1.433242953	2.995732274	1.469583253
20	3.044522438	1.561426683	3.044522438	1.582827064
21	3.091042453	1.571159652	3.091042453	1.582827064
22	3.135494216	1.626251436	3.135494216	1.643658663
23	3.17805383	1.626251436	3.17805383	1.657879076
24	3.218875825	1.652244765	3.218875825	1.725595059
25	3.258096538	1.7544954	3.258096538	1.769368555
26	3.295836866	1.833168224	3.295836866	1.769368555
27	3.33220451	1.833168224	3.33220451	1.795299276
28	3.36729583	1.868551831	3.36729583	1.825124574
29	3.401197382	1.868551831	3.401197382	1.860455886
30	3.433987204	2.066504141	3.433987204	1.962849604
31	3.465735903	2.066504141	3.465735903	1.962849604
32	3.496507561	2.066504141	3.496507561	2.055696814
33	3.526360525	2.066504141	3.526360525	2.695805773
34	3.555348061	2.066504141	3.555348061	2.695805773

APPENDIX B

➢ Coordinates of NACA 63(4)-221 airfoils

Table B.1 Coordinates of NACA 63(4)-221 airfoil

X/C	Y/C	X/C	Y/C
1	0	0	0
0.95018	0.00708	0.00633	-0.01527
0.90039	0.01629	0.009	-0.01861
0.85056	0.02693	0.01425	-0.02414
0.80067	0.03849	0.02708	-0.03385
0.75073	0.05054	0.05237	-0.04743
0.70071	0.06262	0.07747	-0.05753
0.65063	0.07426	0.15233	-0.07765
0.60048	0.08512	0.20208	-0.08612
0.55027	0.09485	0.25176	-0.09156
0.5	0.10309	0.3014	-0.09439
0.44969	0.10949	0.35103	-0.09469
0.39934	0.11369	0.40066	-0.09227
0.34897	0.11529	0.45031	-0.08759
0.2986	0.11383	0.5	-0.08103
0.24824	0.10946	0.54973	-0.07295
0.19792	0.10204	0.59952	-0.0637
0.14767	0.09111	0.64937	-0.05366
0.09753	0.07593	0.69929	-0.04318
0.07253	0.06601	0.74927	-0.03264
0.04763	0.05375	0.79933	-0.02257
0.02292	0.03757	0.84944	-0.01347
0.01075	0.02628	0.89961	-0.00595
0.006	0.02001	0.94982	-0.00076
0.00367	0.01627	1	0

➢ S809 Airfoil Coordinates and Aerodynamic Data

Table B.2 S809 airfoil coordinates

X/C	Y/C	X/C	Y/C
1	0	0.000213	-0.001794
0.996203	0.000487	0.001045	-0.003477
0.98519	0.002373	0.001208	-0.003724
0.967844	0.00596	0.002398	-0.005266
0.945073	0.011024	0.009313	-0.011499
0.917488	0.017033	0.02323	-0.020399
0.885293	0.023458	0.04232	-0.030269
0.848455	0.03028	0.065877	-0.040821
0.80747	0.037766	0.093426	-0.051923
0.763042	0.045974	0.124111	-0.063082
0.715952	0.054872	0.157653	-0.07373
0.667064	0.064353	0.193738	-0.083567
0.617331	0.074214	0.231914	-0.092442
0.56783	0.084095	0.271438	-0.099905
0.519832	0.093268	0.311968	-0.105281
0.474243	0.099392	0.35337	-0.108181
0.428461	0.10176	0.395329	-0.108011
0.382612	0.10184	0.438273	-0.104552
0.33726	0.10007	0.48192	-0.097347
0.29297	0.096703	0.527928	-0.086571
0.250247	0.091908	0.576211	-0.073979
0.209576	0.085851	0.626092	-0.060644
0.171409	0.078687	0.676744	-0.047441
0.136174	0.07058	0.727211	-0.0351
0.104263	0.061697	0.776432	-0.024204
0.076035	0.052224	0.823285	-0.015163
0.051823	0.042352	0.86663	-0.008204
0.03191	0.032299	0.905365	-0.003363
0.01659	0.02229	0.938474	-0.000487
0.006026	0.012615	0.965086	0.000743
0.000658	0.003723	0.984478	0.000775
0.000204	0.001942	0.996141	0.00029
0	-0.00002	1	0